

GSFC JPSS CMO
September 18, 2012
Released

Joint Polar Satellite System (JPSS) Ground Project
Code 474
474-00033

Joint Polar Satellite System (JPSS)
VIIRS Cloud Mask (VCM)
Algorithm Theoretical Basis Document
(ATBD)

For Public Release

The information provided herein does not contain technical data as defined in the International Traffic in Arms Regulations (ITAR) 22 CFC 120.10.
This document has been approved For Public Release.



Goddard Space Flight Center
Greenbelt, Maryland

Joint Polar Satellite System (JPSS) VIIRS Cloud Mask (VCM) Algorithm Theoretical Basis Document (ATBD)

JPSS Electronic Signature Page

Prepared By:

Neal Baker
JPSS Data Products and Algorithms, Senior Engineering Advisor
(Electronic Approvals available online at https://jpssmis.gsfc.nasa.gov/mainmenu_dsp.cfm)

Approved By:

Heather Kilcoyne
DPA Manager
(Electronic Approvals available online at https://jpssmis.gsfc.nasa.gov/mainmenu_dsp.cfm)

Preface

This document is under JPSS Ground AERB configuration control. Once this document is approved, JPSS approved changes are handled in accordance with Class I and Class II change control requirements as described in the JPSS Configuration Management Procedures, and changes to this document shall be made by complete revision.

Any questions should be addressed to:

JPSS Ground Project Configuration Management Office
NASA/GSFC
Code 474
Greenbelt, MD 20771

Change History Log

Revision	Effective Date	Description of Changes (Reference the CCR & CCB/ERB Approve Date)
Original	July 31, 2011	474-CCR-11-0048: This version baselines D43766, VIIRS Cloud Mask (VCM) Algorithm Theoretical Basis Document ATDB (REF Y2412), Rev J dated 12/22/2010 as a JPSS document, version Rev -. This is the version that was approved for NPP launch. Per NPOESS CDFCB - External, Volume V – Metadata, doc number D34862-05, this has been approved for Public Release into CLASS. This CCR was approved by the JPSS Algorithm ERB on July 31, 2011.
Revision A	July 25, 2012	474-CCR-11-0232 approved by JPSS Ground AERB on December 14, 2011 474-CCR-12-0400 approved by JPSS Ground AERB on May 11, 2012 474-CCR-12-0476 approved by JPSS Ground AERB on July 25, 2012

Northrop Grumman Space & Mission Systems Corp.
Space Technology
One Space Park
Redondo Beach, CA 90278



**Engineering & Manufacturing Development (EMD) Phase
Acquisition & Operations Contract**

CAGE NO. 11982

**VIIRS Cloud Mask (VCM)
Algorithm Theoretical Basis Document ATBD (ref Y2412)**

Document Number: D43766

Document Date: 12/22/2010

Revision: J

Point of Contact: K. D. Hutchison, J. Roskovensky, J. Jackson, B. Lisager, and R. Mahoney

ELECTRONIC APPROVAL SIGNATURES:

Roy K Tsugawa, A&DP IPT Lead

Prepared by
Northrop Grumman Space Technology
One Space Park
Redondo Beach, CA 90278

Prepared for
Department of the Air Force
NPOESS Integrated Program Office
C/O SMC/CIK
2420 Vela Way, Suite 1467-A8
Los Angeles AFB, CA 90245-4659

Under
Contract No. F04701-02-C-0502

COMMERCE DESTINATION CONTROL STATEMENT

The export of these commodities, technology or software is subject to U.S. Export Laws and Regulations in accordance with the Export Administration Regulations. Diversion contrary to U.S. law is prohibited.

Northrop Grumman Space & Mission Systems Corp. Space Technology One Space Park Redondo Beach, CA 90278		 	
Revision/Change Record			Document Number D43766
Revision	Document Date	Revision/Change Description	Pages Affected
---	01/26/2007	Initial PCIM Release to bring document into Matrix Accountability. Reference original document number: Y2412 delivered in 2004	All
A	06/22/2007	Revision A Release to bring document into Matrix Accountability. Contains revisions found in v5 r8 of the Raytheon document Y2412 delivered 30 Nov2005 as part of VIIRS 1.0.5 drop	All
B	07/25/2007	Revision B Reference ECR A131	All
C	09/18/2007	Revision C was initiated to correct document format and reference errors. No technical data was changed. ECR A131	All
D	03/12/2008	Revision D Reference ECR 142 Update to VCM Cloud Shadow Logic	All
E	12/17/2008	Revision E Release in response to CDA RFAs and bug fixes to improve performance of the M5 and M7 Reflectance tests. Update to Limitations Section.	All
F	12/09/2009	Revision F provides added details on the theoretical description of the VCM cloud phase algorithm, plus minor updates to the cloud shadow description, heavy aerosol logic, and references. ECR A-262B	13, 48-55, 61-70, 83
G	05/05/2010	Revision G corrects the equation used for the Binary Cloud Mask Error Rate and the equation used for the cloud top tropopause limit used in the cloud shadow detection algorithms, adds the equation for PCT along with minor punctuation and format corrections. It also relocates the discussion on Cloud Shadows to conform to the existing outline of the ATBD. ECR A-298	2, 12, 14, 74-77
H	09/16/2010	Revision H addresses RFAs raised during the Document Convergence review process; minor formatting and typo corrections. ECR A-326	All
J	12/22/10	Updates thresholds for cloud confidence tests based upon global synthetic data using final VIIRS pre-launch sensor characterizations. Note: these thresholds may be further updated during NPP CalVal and may not be reflected in the ATBD.	All

TABLE OF CONTENTS

	Page
LIST OF FIGURES	ix
LIST OF TABLES	xii
GLOSSARY OF ACRONYMS	xiii
ABSTRACT	xv
1.0 INTRODUCTION	1
1.1 PURPOSE	1
1.2 SCOPE	1
1.3 VIIRS DOCUMENTS	1
1.4 REVISIONS	1
2.0 EXPERIMENT OVERVIEW	2
2.1 OBJECTIVE OF VIIRS CLOUD MASK	2
2.2 INSTRUMENT CHARACTERISTICS	3
2.3 HISTORICAL PERSPECTIVE AND EVOLUTION OF THE VCM	4
3.0 ALGORITHM DESCRIPTION	6
3.1 PROCESSING OUTLINE	6
3.2 ALGORITHM INPUT	6
3.2.1 VIIRS Data	7
3.2.1.1 VIIRS 375m Earth View SDR File	7
3.2.1.2 VIIRS 750m Earth View SDR File	7
3.2.1.3 VIIRS Gridded Snow/Ice Cover IP	7
3.2.1.4 VIIRS Gridded TOC NDVI IP	7
3.2.1.5 VIIRS Active Fire IP	8
3.2.2 Non-VIIRS Data	8
3.2.2.1 Surface Type Database	8
3.2.2.2 Sea Surface Winds	8
3.2.2.3 Total Precipitable Water	8
3.2.2.4 Near Surface Temperature	8
3.3 ALGORITHM OUTPUT	9
3.3.1 Cloud Mask Quality	11
3.3.2 Cloud Detection Result and Confidence Indicator	11
3.3.3 Day/Night	11
3.3.4 Snow/Ice Surface	11

3.3.5 Land/Water Background	11
3.3.6 Sun Glint Flag	12
3.3.7 Shadow Detected.....	13
3.3.8 Non-cloud Obstruction.....	13
3.3.9 Fire Detected.....	13
3.3.10 Cloud Detection Tests.....	13
3.3.11 Cloud Adjacency.....	13
3.3.12 Cloud Phase.....	14
3.3.13 Imagery Resolution Tests - Deleted.....	14
3.3.14 Conifer Boreal Forest Flag.....	14
3.3.15 Spatial Uniformity Flag	15
3.3.16 Thin Cirrus Flag.....	15
3.3.17 Ephemeral Water Flag	16
3.3.18 Flag to Identify Degraded/Excluded Conditions.....	16
3.4 THEORETICAL DESCRIPTION OF THE VCM ALGORITHMS	17
3.4.1 Physics of the Problem.....	17
3.4.1.1 Overview of Cloud Detection Tests.....	17
3.4.1.2 Determination of Cloud Confidence	20
3.4.2 Determination of Background Conditions	24
3.4.3 Cloud Detection Tests.....	29
3.4.3.1 IR Threshold Cloud Test (BT _{M15}).....	29
3.4.3.2 Tri-Spectral Cloud Test (BT _{M14} – BT _{M15} & BT _{M15} – BT _{M16})	30
3.4.3.3 Cloud Test (BT _{M15} – BT _{M12}).....	32
3.4.3.4 Cloud Detection Test (BT _{M12} – BT _{M13}).....	35
3.4.3.5 Visible Reflectance (M1, M5 & M7).....	37
3.4.3.6 Visible Reflectance Ratio Test (M7/M5).....	39
3.4.3.7 Visible (Ref _{M9}).....	43
3.4.3.8 Infrared (BT _{M15} -BT _{M16}).....	44
3.4.3.9 High Cloud Test (BT _{M12} – BT _{M16}).....	45
3.4.3.10 Imagery Resolution Spatial Tests.....	47
3.4.4 The VCM Cloud Phase Algorithm.....	49
3.4.4.1 Initial Determination of Cloud Phase.....	49
3.4.4.2 Identification of Cloud Overlap	49
3.4.4.2.3 Additional Cloud Phase Logic	55

3.4.4.3 Implementation of the Cloud Phase Algorithm	55
3.4.5 Differentiating Between Heavy Aerosols and Clouds	63
3.4.5.1 Heavy Aerosols over Ocean Surfaces	65
3.4.5.2 Heavy Aerosols over Land Surfaces	69
3.4.5.3 Volcanic Ash	72
3.4.5.4 Impact of Cloud Phase Errors on Heavy Aerosols Identification	75
3.4.6 The Geometric-Based Cloud Shadow Algorithm	81
3.5 PRACTICAL CONSIDERATIONS	85
3.5.1 Numerical Computation Considerations	85
3.5.2 Programming and Procedural Considerations	85
3.5.3 Configuration of Retrievals	85
3.5.4 Quality Assessment and Diagnostics	85
3.5.5 Exception Handling	86
3.6 ALGORITHM VALIDATION	86
4.0 ASSUMPTIONS AND LIMITATIONS	87
4.1 ASSUMPTIONS	87
4.2 LIMITATIONS	87
5.0 REFERENCES	88

LIST OF FIGURES

	Page
Figure 1. VCM Conceptual Design.....	6
Figure 2. A graphical depiction of three thresholds used in cloud screening.	21
Figure 3. Five Groups of cloud tests used to make cloudy confidences in the VCM during daytime conditions over land backgrounds.	23
Figure 4. The five processing paths of the VIIRS Cloud Mask Algorithm for the analysis of data collected in daytime conditions.	24
Figure 5. Logic in the VCM to determine presence of snow/ice in each VIIRS pixel.	26
Figure 6. Results of snow/ice processing in current VCM algorithm. Upper left shows color composite imagery (snow is purple), upper right is NCEP database, lower left is VCM snow before corrections, and lower right is VCM snow field after corrections described above.	29
Figure 7. Brightness temperature differences between AVHRR channel 3 (3.75- μm) minus channel 5 (12.0- μm) and total precipitable water (path) for cloudy pixels (\blacktriangle) of cirrus clouds (left panel) and stratus clouds (right panel) along with cloud-free pixels (+) (from Hutchison et al., 1995).	29
Figure 8. Tri-spectral diagram for ocean scenes taken from MODIS data. The dark diamonds in the figure represents the dynamic threshold for the tri-spectral test and the dark blue circles are the observed values. Values to the upper right of the threshold indicate cloud and lower left of the threshold indicate clear.....	31
Figure 9. Distribution of cloudy (blue) and cloud-free (red) pixels as a function of M15-M12 BT difference and total precipitable water based upon global synthetic data.	34
Figure 10. Distribution of cloudy (red) and cloud-free (blue) pixels over land as a function of M12-M13 BT difference and solar zenith angle based upon global synthetic MODIS TOA SDRs.....	36
Figure 11. Distribution of cloudy (red) and cloud-free (blue) pixels over water as a function of M12-M13 BT difference and solar zenith angle based upon global synthetic MODIS TOA SDRs.....	36
Figure 12. Distribution of cloudy (red) and cloud-free (blue) pixels over snow/ice as a function of M12-M13 BT difference and solar zenith angle with global synthetic MODIS TOA SDRs.....	37
Figure 13. Dynamic thresholds for M5 reflectance test for 10 TOC NDVI bins as a function of scattering angle.....	39
Figure 14. Discrimination between clear (green) and cloudy (red) pixels over Sahael Africa as a function of NDVI for MODIS equivalent of VIIRS M5 band (left) and M1 band (right).....	39
Figure 15. Bispectral reflectance ratio in the forward (left panel) and non-forward (right panel) scattering directions for optically thick clouds (\blacktriangle) over ocean surfaces as a function of the cosine of solar zenith angle (from Hutchison and Hardy, 1995, Int. J. Rem. Sensing, 16, 3665-3680).....	40
Figure 16. Behavior of Dual Cloud Confidence Threshold Sets for M7/M5 Over Ocean	42
Figure 17. Histogram of the frequency of occurrence of the AVHRR reflectance ratio R0.86/R0.63 for a scene over the Arabian Peninsula and Arabian Sea.....	43

- Figure 18. Brightness temperature differences between AVHRR channel 4 (10.8- μm) minus channel 5 (12.0- μm) versus channel 4 brightness temperatures, as described by Saunders and Kriebel (1988), for cloud-free pixels (\blacktriangle) and cirrus cloudy pixels (+), (from Hutchison et al., 1995). 44
- Figure 19. Brightness temperature differences between AVHRR channel 3 (3.75- μm) minus channel 5 (12.0- μm) and total precipitable water (path) for cloud-free pixels (\blacktriangle) and cirrus cloudy pixels (+) shows detection threshold is highly sensitive to water vapor in the atmosphere (from Hutchison et al., 1995). 46
- Figure 20. Flow diagram describing the spatial uniformity testing effects on cloud confidence. 48
- Figure 21. RTM simulations of the 11- μm minus 12- μm brightness temperature differences as a function of cloud phase, optical depth, and visible reflectance in the 0.6- μm band. ... 50
- Figure 22. Results from RTM calculations of 0.65- μm reflectance and the brightness temperature difference between 11- and 12- μm for single-layer water clouds, single-layer ice cloud, and ice cloud overlapping a water cloud as a function of optical depth. The boldface line without symbols represents the function used to determine the split-window brightness temperature difference threshold used in the cloud overlap detection algorithm. (Figure 1 from Pavolonis & Heidinger, 2004). 51
- Figure 23. Results from RTM calculations of reflectances in the 1.65- μm and 1.38- μm bands for clouds of varying optical thickness values over ocean surfaces in Panel (a) and grassy land surfaces, shown in Panel (b) using a relative scattering angle of 31.4 degrees. (Figure 2 from Pavolonis & Heidinger, 2004) 53
- Figure 24. Results from RTM calculations support the relationship between a derived 3.75- μm emissivity and the $BT_{M15} - BT_{M16}$ feature. 54
- Figure 25. Flow diagram of the cloud phase algorithm. 57
- Figure 26. MODIS data collected 1 August 2001 from 1220 to 1225 UTC and the corresponding VCM Phase. Left: RGB composite; Cold clouds are white, warm clouds are yellow, land is green and ocean is black. Right: Clear pixels are dark blue, partly cloudy are in blue, water clouds are in light blue, opaque ice clouds are in yellow, cirrus clouds are in red, and overlapping clouds are in dark red. 63
- Figure 27. Analyses of MODIS granule MODA2001.213.1210 based upon the VCM using Tests 1-3 and the MODIS Collection 5 cloud mask algorithms. Panel (a) shows an RGB (0.65- μm , 1.6- μm , 0.412- μm) color composite of MODIS imagery and Panel (b) has a manually-generated cloud mask. VCM and MODIS results for cloud confidence are in Panels (c) and (d) respectively along with heavy aerosol flags in Panels (e) and (f)... 66
- Figure 28. Analyses of MODIS granule MODA2003.299.1840 based upon the VCM using Tests 1-3 and MCM Collection 5 algorithms. Panel (a) shows an RGB [0.412- μm , 1.6- μm , (11- μm - 12- μm)] color composite of MODIS imagery and Panel (b) has a manually-generated cloud mask. VCM and MODIS results for cloud confidence are in Panels (c) and (d) respectively along with heavy aerosol flags in Panels (e) and (f)..... 68
- Figure 29. Panel (a) shows the VIIRS AOT retrievals without using the VCM heavy aerosol flags due to the large number of false alarms shown in Panel (e) of Figure 3 with Tests 1-3. Panel (b) shows the MODIS Collection 5 AOT results form the MOD04 product, and Panel (c) the cloud confidence in the VIIRS aerosol module after combining the cloud

confidence and the heavy aerosol flag from the updated VCM procedures to identify heavy aerosols.....	69
Figure 30. Analyses of heavy aerosols and clouds with the EVCM algorithms for MODIS granule MODA2002.091.0240. Panel (a) shows a true-color composite of MODIS imagery while Panel (b) has the automated cloud confidence and Panel (c) the cloud phase analyses. Candidate heavy aerosols detected by the smoke test are shown in Panel (d) along with dust candidates in Panel (e). The final heavy aerosol results are in Panel (f) after the spatial test has been applied to candidate heavy aerosols.	71
Figure 31. Frequency of occurrence for false alarms using reverse absorption technique with threshold of zero based upon global MODIS data (from Pavolonis et al., 2006.....	73
Figure 32. Misclassifications of clouds using reverse absorption test with Scene 1210 and thresholds = 0.0 K.....	74
Figure 33. Misclassifications of clouds using reverse absorption test with Scene 1210 and thresholds = -0.25 K.	74
Figure 34. Misclassifications of clouds using reverse absorption test with Scene 1210 and thresholds = -0.5 K.	74
Figure 35. True color images of volcanic eruptions caught by MODIS Terra (0155 UTC in upper left) and Aqua (0450 UTC in upper right) granules on Julian day 268 in 2002. VCM cloud phases analyses shown in lower panels.	77
Figure 36. Heavy aerosol candidates identified by application of the new VCM smoke test (upper panels) and new dust test (lower panels) for granules shown in Figure 35.....	78
Figure 37. Results from the new VCM spatial test of heavy aerosol candidates (upper panels) and final heavy aerosol flags (lower panels) for granules shown in Figure 35.....	79
Figure 38. Color composites of MODIS data shown in Figure 35 reveal misclassifications by new heavy aerosol procedures occur because thin cirrus in misclassified as water clouds in the cloud phase analyses.	81
Figure 39. Cloud Shadow Algorithm Logic.....	83

LIST OF TABLES

Table 1. VIIRS bands used in the VCM algorithm.....	3
Table 2. Ancillary and Auxiliary data inputs for the VCM	6
Table 3. File specification for the 48-bit VCM.....	9
Table 4. Base thresholds used for the Ref _{M9} thin cirrus test in the VCM algorithm	15
Table 5. Cloud tests used in the VIIRS Daytime Cloud Mask Algorithm as a function of surface type.	19
Table 6. Cloud tests used in the VIIRS Nighttime Cloud Mask Algorithm as a function of surface type.....	20
Table 7. Classification of cloud confidence for M9 Reflectance Test in VCM over ocean	22
Table 8. Base mid-point thresholds used for BT _{M15} test for cloud in the VCM algorithm.....	30
Table 9. Thresholds used for BT _{M14} – BT _{M15} and BT _{M15} -BT _{M16} test for cloud in the VCM algorithm.....	32
Table 10. Thresholds used for BT _{M15} – BT _{M12} test for cloud in the VCM algorithm.....	34
Table 11. Thresholds used for BT _{M12} – BT _{M13} test for cloud in the VCM algorithm.....	35
Table 12. Minimum values of the variable thresholds used for Ref _{M1} test for low cloud in the VCM algorithm	38
Table 13. Minimum values of the variable thresholds used for Ref _{M5(M1)} test, correspond to TOC NDVI interval 0.9-1.0.....	38
Table 14. Minimum values of the variable thresholds used for Ref _{M7} test for cloud in the VCM algorithm.....	38
Table 15. Thresholds used for Ref _{M7} /Ref _{M5} test for cloud in the VCM algorithm.....	41
Table 16. Thresholds used for Ref _{M9} test for cirrus cloud in the VCM algorithm.....	44
Table 17. Clear/Cloudy temperature thresholds in Kelvin for BT _{M15} -BT _{M16} cloud detection test at mid-latitudes	45
Table 18. Thresholds used for BT _{M12} – BT _{M16} test for high cloud in the VCM algorithm.....	46
Table 19. Results from analyses of MODIS data in and outside sun glint regions with and without spatial tests.	48
Table 20. Initial cloud top phase classifications based upon M15 brightness temperatures.....	49
Table 21: The range in 11 μm minus 12 μm brightness temperature difference (SWBTD) and a derived emissivity at 3.75 μm (EMS[3.8]) that defines the spectral characteristics of cloud overlap.	55
Table 22. Cloud overlap criteria for cloud phase identification.....	58
Table 23. Cirrus cloud tests for cloud phase identification.....	61
Table 24. Cloud phase reclassification tests.	62

GLOSSARY OF ACRONYMS

APOLLO	AVHRR Processing Scheme Over cloud Land and Ocean
ATBD	Algorithm Theoretical Basis Document
AVHRR	Advanced Very High Resolution Radiometer
AVIRIS	Airborne Visible Infrared Imaging Spectrometer
BT	Brightness Temperature
BTD	Brightness Temperature Difference
CLAVR	Clouds from AVHRR
CMIS	Conical Scanning Microwave Imager/Sounder
CrIS	Cross-track Infrared Sounder
EDC	EROS Data Center
EDR	Environmental Data Record
EMS	Psuedo Emissivity
EROS	Earth Resources Observation System
FOV	Field of View
GAC	Global Area Coverage
HIRS	High Resolution Infrared Radiation Sounder
HSR	Horizontal Spatial Resolution
IR	Infrared
LAC	Local Area Coverage
LUT	Look-Up Table
MAS	MODIS Airborne Simulator
MCM	MODIS Cloud Mask
MODIS	Moderate Resolution Imaging Spectroradiometer
MODTRAN	Moderate Resolution Atmospheric Radiance and Transmission Model
NASA	National Aeronautics and Space Administration
NCEP	National Center for Environmental Prediction
NDVI	Normalized Difference Vegetation Index
NIR	Near Infrared
NOAA	National Oceanic and Atmospheric Administration
NPOESS	National Polar-orbiting Operational Environmental Satellite System
Ref	Reflectance
RGB	Red-Green-Blue
SDR	Sensor Data Record
SERCAA	Support of Environmental Requirements for Cloud Analysis and Archive

SRD	Sensor Requirements Document
SUCCESS	Subsonic Aircraft Contrail and Cloud Effects Special Study
TOA	Top-of-Atmosphere
TOC	Top-of-Canopy
TPW	Total Precipitable Water
TIWV	Total Integrated Water Vapor
USGS	United States Geological Survey
UV	Ultraviolet
UW	University of Wisconsin
VCM	VIIRS Cloud Mask
VIIRS	Visible/Infrared Imager/Radiometer Suite

ABSTRACT

Identifying pixels as either cloudy or clear is an essential component of the National Polar-orbiting Operational Environmental Satellite System (NPOESS) Visible/Infrared Imager Radiometer Suite (VIIRS). The VIIRS Cloud Mask (VCM) technique incorporates a number of cloud detection tests that determine whether a pixel is obstructed by a cloud and produces for each moderate-resolution VIIRS pixel a cloud confidence of confidently cloudy, probably cloudy, probably clear, or confidently clear. The VCM next identifies the phase of the cloud as water, supercooled water or mixed phase, opaque ice, non-opaque ice, or overlapping cloud based upon an algorithm developed by Pavolonis and Heidinger (2004). Cloud phase classes also include partly cloudy (i.e. probably clear) or (confidently) clear. Next, the VCM examines pixels classified as confidently cloudy and flags those found to contain heavy aerosols (Hutchison et al., 2008; 2010). In addition, it tests for volcanic ash in pixels classified as confidently cloudy using logic developed by Pavolonis et al., (2006). The internal fire tests in the original VCM had performed poorly and have now been replaced by the mask generated by the Active Fires Algorithm. Finally, the VCM tests for cloud shadows based on sun-cloud-earth line of sight geometry computations (Hutchison et al., 2009). In order to perform its cloud classification, the VCM algorithm first determines a processing path for each pixel. The processing paths include day/night, sun glint, land, desert, water (inland or sea), coastline, and (newly updated logic) to detect snow/ice backgrounds. Next, the VCM algorithm executes a series of tests, using one or more bands, to examine solar reflectances, during daytime conditions, along with Brightness Temperatures (BT). The threshold values for these tests depend upon the dominant regional classification, or surface type, of the pixel, viewing geometry, and atmospheric conditions. The tests applied to generate the VCM have a lengthy heritage in the tests originally developed by Saunders and Kriebel (1988) and updated in the CLAVR (CLOUDs from AVhrR) by Stowe *et al.* (1995) and MODIS (Ackerman *et al.*, 1997) and SERCCA (Support to Environmental Requirements for Cloud Analyses and Archive) by Gustafson et al., (1994) cloud mask algorithms. However, the VCM also employs additional cloud tests created to exploit the unique VIIRS design, including imagery-resolution spatial tests to detect sub-pixel clouds over ocean backgrounds (Hutchison et al., 2005) and similar tests to detect ephemeral water over land surfaces. Each cloud test returns a clear or cloudy result with an associated clear sky confidence level. Analogous to the MODIS Cloud Mask, the VCM groups its cloud confidence tests into five categories. The minimum clear sky confidence from individual members represents the clear sky confidence for that group and the product of all the group clear sky confidences is used to determine the overall clear sky confidence value. After the cloud confidence is determined, the VCM tests the pixel for aerosols, and fires, and then performs a spatial uniformity test. Algorithms to generate the VIIRS cloud, aerosol, land, ocean, surface temperature, and snow/ice Environmental Data Records (EDRs) use the VCM as auxiliary data.

1.0 INTRODUCTION

1.1 PURPOSE

This Algorithm Theoretical Basis Document (ATBD) describes the algorithm used to retrieve the Cloud Mask IP for the VIIRS instrument on the NPOESS. Specifically, this document identifies the sources of input data required for retrieval, provides the physical theory and mathematical background underlying the use of this information in the retrievals, includes implementation details, and describes assumptions and limitations of the proposed approach.

1.2 SCOPE

This document covers the algorithm theoretical basis for the cloud mask product of VIIRS on NPOESS.

Section 1 describes the purpose and scope of this document. Section 2 is an overview of the cloud mask. The theoretical description and implementation of the algorithm are described in Section 3, and the assumptions and limitations of the approach are summarized in Section 4. References for citations in the text are listed in Section 5.

1.3 VIIRS DOCUMENTS

This document contains references to other VIIRS documents. These are given in italicized brackets, e.g., [*Y2412*] CLOUD MASK. The VIIRS documents cited in this document are listed below:

[<i>PS154640-102</i>]	Performance Specification Algorithm Specification for the VIIRS
[<i>Y2388</i>]	VIIRS Software Development Plan
[<i>Y2469</i>]	VIIRS Context Software Architecture
[<i>Y2470</i>]	VIIRS Data Interface Control Document

1.4 REVISIONS

This document was formerly released under document number Y2412 dated September 1998. Due to the significant number of modifications made to the VIIRS Cloud Mask software and ATBD, this document is re-released under Northrop Grumman document number D43766.

2.0 EXPERIMENT OVERVIEW

2.1 OBJECTIVE OF VIIRS CLOUD MASK

The VCM is defined by pixel-level flags that indicate when a cloud intersects a line segment extending between the sensor and a given area of the Earth's surface. There are no requirements listed for a binary cloud mask in the Integrated Operational Requirements Document (IORD) – II, which requires cloud cover be specified to a 10% accuracy on a 6-km HCS. The IORD lists as an objective a goal of achieving 5% accuracy at a 1-km HCS, which might be considered the binary VCM product at VIIRS moderate (M-band) resolution.

The VCM was designed to form the beginning of the NPOESS processing chain for other VIIRS data products. Algorithms that use the VCM include seven cloud products (cloud optical thickness and effective particle size; cloud top pressure, height, and temperature; cloud base height; and cloud cover/layers), three ocean surface products (sea surface temperature, ocean color, and net heat flux), five land surface products (land surface temperature, normalized difference vegetation index and enhanced vegetation index, albedo, soil moisture, and surface type), three snow/ice products (a sub-pixel snow mask, ice surface temperature, and ice age), and three atmospheric aerosol products (optical thickness, particle size parameter, and suspended matter). Therefore, the VCM algorithm must accurately differentiate between clouds and cloud-free surfaces, and also between clouds and heavy aerosols in order to support the production of these surface, cloud, and atmospheric products.

Stringent requirements are stated for the VCM in terms of probability of correct typing (PCT), and the frequency of occurrence of false alarms and leakage. Definitions for these terms are as follows:

- The fraction of pixels classified "probably" is defined by the following equation. Probably clear/cloudy (PCPC) conditions should be minimized but not exceed 15%:

$$FPCPC = \frac{\#PCPC}{\#pixels\ in\ eac\ geograpic\ class'}$$

$$\text{where } PCPC = (VCM|_{prob\ clr}) OR (VCM|_{prob\ cldy})$$

- Probability of Correct Typing: has no direct impact on EDRs and is defined as

$$PCT = 1 - \text{Binary Cloud Mask Error}$$

$$= 1 - \frac{\#[(VCM|_{conf\ clr}\ AND\ Trut|_{cldy})\ OR\ (VCM|_{conf\ cldy}\ AND\ Trut|_{clr})]}{\#pixels\ in\ eac\ geograpic\ class - \#PCPC\ pixels}$$

- Leakage can severely impact ocean and land EDRs and is defined by this equation:

$$\frac{\#pixels\ w\ ere\ (VCM|_{conf\ clr}\ AND\ Trut|_{cldy})}{\#pixels\ in\ eac\ geograpic\ class}$$

- False alarms can severely impacts cloud EDRs:

$$\frac{\#pixels\ were\ (VCM|_{conf\ cldy}\ AND\ Trut|_{ctr})}{\#pixels\ in\ eac\ geograpic\ class}$$

- Binary Cloud Mask Error is one minus the PCT and defined as:

$$\frac{\#[(VCM|_{conf\ ctr}\ AND\ Trut|_{cldy})\ OR\ (VCM|_{conf\ cldy}\ AND\ Trut|_{ctr})]}{\#pixels\ in\ eac\ geograpic\ class - \#PCPC\ pixels}$$

These VCM requirements must be satisfied to support the creation of cloud, aerosol, land, ocean, and ice surface products without (1) classifying pixels as confidently clear pixels that are in fact cloud contaminated, (2) classifying pixels as confidently cloudy pixels that are in fact cloud-free, while (3) differentiating between pixels that are classified initially as cloudy but in fact contain heavy aerosols. For the efficiency of the operational NPOESS system, the VCM is tasked to generate other datasets used by downstream algorithms in the processing sequence, including cloud shadows, land classes (including, land snow/ice, coast, desert, ocean, inland and ephemeral water), and sun-glint regions.

2.2 INSTRUMENT CHARACTERISTICS

The VIIRS sensor collects data in five Imagery resolution (375-m) channels, called I-bands, and sixteen Moderate resolution (750-m) channels, called M-bands. VIIRS collects data at both resolutions in the visible, near-infrared, and thermal infrared wavelengths. The VIIRS bands used in the cloud mask algorithm are identified in Table 1. Additional details on the instrument design are provided in the VIIRS Experiment Overview [V-0].

Table 1. VIIRS bands used in the VCM algorithm

VIIRS Band	Wavelength (μm)
M1	0.412
M4	0.555
I1	0.64
M5	0.672
I2	0.865
M7	0.865
M9	1.378
M10	1.61
M11	2.25
I4	3.74
M12	3.7
M13	4.05
M14	8.55
M15	10.7625
I5	11.45

VIIRS Band	Wavelength (μm)
M16	12.0125

2.3 HISTORICAL PERSPECTIVE AND EVOLUTION OF THE VCM

The VCM was developed using an algorithm heritage initially established by Saunders and Kriebel (1988) which formed the theoretical basis for NASA's MODIS cloud mask (Ackerman et al., 1997), NOAA's CLAVR (Stowe et al., 1995), the Department of Defense SERCCA (Support to Environmental Requirements for Cloud Analyses and Archive; see Gustafson et al., 1994), and the APOLLO (AVHRR Processing scheme Over Land, cLOUDs, and Ocean; see Kriebel et al., 2003) cloud mask algorithms used at the Deutsches Zentrum für Luft- und Raumfahrt. (DLR). However, the VCM most closely follows the architecture of the MODIS cloud mask algorithm.

While the VCM algorithm has its basis in these heritage algorithms, its logic most closely follows the MODIS cloud mask by classifying each pixel as one of four possibly cloud confidences: confidently cloudy, confidently clear, probably cloudy, and probably clear. These cloud confidences support the development of all VIIRS products. For example, high quality sea surface temperatures are based upon pixels classified as confidently clear by the VCM. Therefore, it is important that pixels classified as confidently clear in reality contain no clouds, i.e. that VCM minimizes "leakage" of clouds into the SST analyses. Conversely, other cloud EDRs are based upon pixels classified as confidently cloudy by the VCM and it becomes important that the VCM not classify pixels as confidently cloudy that are in reality cloud-free, i.e. that VCM minimizes false alarms.

While the VCM has its heritage in other cloud mask algorithms, it continues to be enhanced to exploit the unique data characteristics of the VIIRS sensor. The VCM now uses cloud detection tests that vary with viewing geometry and surface classification, which are updated routinely to compensate for variations in surface conditions, e.g. produced in part by seasonal change in precipitation patterns (Hutchison et al., 2005). In addition, the VCM now exploits (1) unique VIIRS dual-gain bands to improve cloud detection over desert regions (Hutchison and Jackson, 2003) (2) data collected in the more narrow (15-nm) VIIRS M9 channel, when compared to the similar (30-nm) MODIS bandpass, (3) imagery resolution (I-band) cloud tests to detect sub-pixel cloud edges over ocean surfaces (Hutchison et al., 2005), and (4) new cloud phase logic that identifies, for the first time, pixels that contain multiple cloud layers of ice and water clouds (Pavolonis and Heidinger, 2004). In the release of D43766, Revision C, VCM now accurately differentiates between heavy aerosols and clouds to support the generation of aerosol products across the full range of conditions required by the NSS (Hutchison et al., 2008; 2010). Finally, a geometry based cloud shadow detection algorithm has been implemented (Hutchison et al., 2009).

The VCM has evolved to address the derived requirements for all algorithms that rely upon it. Performance of the key NPOESS SST EDR, other ocean, land, and atmospheric EDRs are based only on pixels classified as confidently clear by the VCM, while performance of the cloud EDRs are based only upon pixels classified as confidently cloudy. Therefore, rather than solely relying upon PCT, VCM performance is now measured by:

- Minimizing leakage (i.e. classifying a pixel confidently clear when it is in fact contains a cloud) for algorithms that retrieve land and ocean surface products. While no cloud mask algorithm is capable of achieving a 99% PCT for ocean, daytime conditions in the absence of sun glint, this was the requirement in the original NSS to support the SST EDR. A derived requirement to support the SST EDR is not in PCT but minimizing the leakage rate to 1% over ocean surfaces outside sun glint and in daytime. This requirement can be achieved with the current VCM algorithm.
- Minimizing false alarms (calling a cloud-free pixel to be confidently cloudy) for algorithms used to retrieve the remaining cloud products. Cloud products are only generated for pixels classified as confidently cloudy in the VCM IP. Therefore, it is important that false alarms, which have been problems for other cloud mask algorithms especially over land surfaces, be kept to a minimum. The current VCM produces fewer false alarms than heritage cloud mask algorithms and they will be further reduced when VIIRS data become available.
- In addition, the VCM must be able to discriminate between heavy aerosols and clouds to support the aerosol module. This derived requirement does not mean the VCM must detect or identify heavy aerosols but that aerosols with an optical depth in the $0 \leq \tau \leq 2$ range cannot be classified as clouds. This derived requirement is satisfied with the VCM heavy aerosol modifications introduced in Revision A of this document.

3.0 ALGORITHM DESCRIPTION

3.1 PROCESSING OUTLINE

The current processing outline (see Figure 1) is based on the MODIS current operational approaches. The VCM uses VIIRS data and ancillary data as input to produce a variety of output flags. The VCM output is used by many EDRs that are dependent on cloud masking. The VCM performs cloud tests at both the moderate resolution and at the higher imagery resolution.

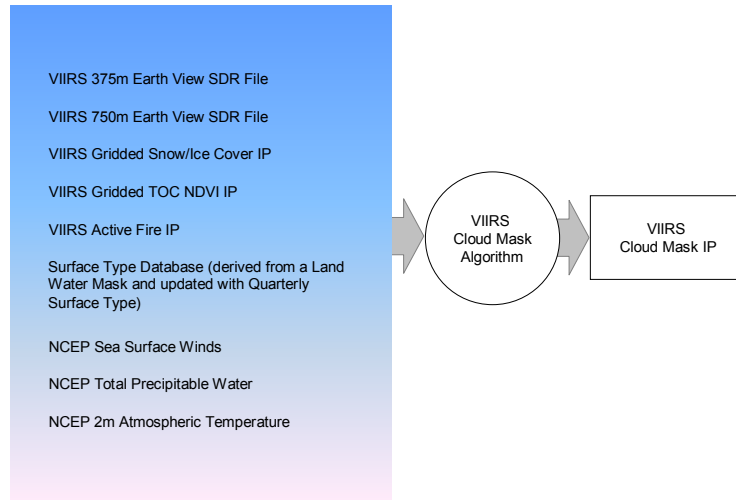


Figure 1. VCM Conceptual Design.

3.2 ALGORITHM INPUT

The algorithm requires auxiliary information from the VIIRS instrument and ancillary data from outside sources, as shown in Table 2. All input data are explained in greater detail in this section.

Table 2. Ancillary and Auxiliary data inputs for the VCM

Input Data	Source of Data
VIIRS 375m Earth View SDR File	VIIRS
VIIRS 750m Earth View SDR File	VIIRS
VIIRS Gridded Snow/Ice Cover IP	VIIRS
VIIRS Gridded TOC NDVI IP	VIIRS
VIIRS Active Fire IP	VIIRS
Surface Type Database	Land Water Mask updated with VIIRS Quarterly Surface Type
Sea Surface Winds	NCEP
Total Precipitable Water	NCEP

Input Data	Source of Data
Near Surface Temperature	NCEP

3.2.1 VIIRS Data

Input to the cloud mask algorithm is assumed to be calibrated and navigated VIIRS radiance data as well as geolocation, snow/ice data, and Top-of-Canopy Normalized Difference Vegetation Index (TOC NDVI) and near-surface temperature fields.

3.2.1.1 VIIRS 375m Earth View SDR File

The VCM performs cloud detection tests at the imagery pixel resolution and therefore requires data from the VIIRS 375m Earth View SDR File. The VCM uses reflectance information from bands I1 and I2 and BT information from bands I4 and I5. Imagery resolution geolocation parameters, terrain data, solar angles, and sensor angles are also obtained from this file.

3.2.1.2 VIIRS 750m Earth View SDR File

The VCM output is mainly based upon moderate pixel resolution tests and evaluations. Therefore, the VCM requires data from the VIIRS 750m Earth View SDR File. The VCM uses reflectance information from bands M1, M4, M5, M7, M9, M10, and M11, BT information from bands M12, M13, M14, M15, and M16 and radiance data from band M12. Moderate resolution geolocation parameters, VIIRS grid information, terrain data, solar angles, and sensor angles are also obtained from this file.

3.2.1.3 VIIRS Gridded Snow/Ice Cover IP

Spectrally, snow/ice and clouds have many similar features, therefore, the snow/ice map is needed to decide which cloud detection tests will be applied and to adjust thresholds of several tests (Hall et al., 1995; Hall et al., 1996). The VIIRS Gridded Snow Cover IP is granulated to produce a snow/ice database that will decrease the misclassification of snow/ice as clouds. During the daytime, this map is used in conjunction with tests based on the VIIRS SDRs to determine the presence or absence of snow/ice in order to select the correct processing path and cloud detection tests. During nighttime conditions, there are no SDR data available to detect snow/ice, so the snow/ice map is used directly to select the correct processing path and cloud detection tests. Direct use of this map degrades VCM nighttime cloud detection performance as compared to that of daytime since the map is granulated from a database that has a more coarse resolution than the VIIRS SDR data.

3.2.1.4 VIIRS Gridded TOC NDVI IP

Reflectance off the broad ensemble of land classes varies greatly due to the type and quantity of vegetation. Often a single reflectance threshold will be unable to distinctly separate clear sky from clouds. Therefore, a 17-day composite of VIIRS TOC NDVI is used to describe, in part, the current surface vegetation state. This database is used to (1) calculate dynamic thresholds for the

M5 reflectance cloud test, (2) switch between the M5 and M1 reflectance cloud test, (3) calculate dynamic thresholds for the M1 reflectance cloud test, (4) restrict the use of the BTM15 – BTM12 test and (5) restrict the use of the BTM12 – BTM13 test over non-desert, non-snow land and coastal regions.

3.2.1.5 VIIRS Active Fire IP

The VIIRS Active Fire IP provides a Fire Mask field representing a fire classification of each pixel in the granule. This field is used to set the fire bit of the Cloud Mask.

3.2.2 Non-VIIRS Data

The non-VIIRS data that the VCM uses is provided by several different sources and is described in the following subsections.

3.2.2.1 Surface Type Database

Various land types possess different reflective properties and these variations need to be considered when developing cloud detection thresholds. A global surface type database, derived from the MODIS Land/Water Mask (MLWM) and updated with a Quarterly Surface Type product is used to identify surface classes. This database includes classifications such as inland water, seawater, desert, land, forest, and coast, and will be used to determine the background land type of each pixel. Initially, the Quarterly Surface Type will come from MODIS. Once available, the VIIRS product can be used, although no decision has been made about the frequency of updates to this database.

3.2.2.2 Sea Surface Winds

Sea surface winds need to be analyzed when determining sun glint. Therefore, sea surface wind data is needed to determine if sun glint is present over a water surface. Sea surface wind data will be obtained from NCEP sea surface forecast.

3.2.2.3 Total Precipitable Water

Total precipitable water is needed to calculate total path integrated water vapor which is used to determine whether or not to perform the M9 thin cirrus test in daytime desert stratification and is also used to compute dynamic thresholds for the M15 – M12 brightness temperature difference test in daytime desert stratification with latitudes greater than 60°. Total precipitable water data will be obtained from the NCEP forecast.

3.2.2.4 Near Surface Temperature

A near surface, atmospheric temperature is needed to set nighttime BTM15 thresholds to detect multi-layered clouds during nighttime conditions. The NCEP 2-m Atmospheric Temperature data set will be used to create the ancillary data by re-mapping the gridded product to the pixel level swath space via bilinear interpolation of the 4 nearest grid points surrounding each pixel.

Temporal and spatial interpolations will be performed as described in the EDRPR. Therefore, valid NCEP data will be within 3 hours of the satellite overpass.

3.3 ALGORITHM OUTPUT

The output of the VCM algorithm will be 6 bytes (48 bits) for each moderate resolution pixel. The mask includes information about the processing path the algorithm took (e.g., land or ocean) and whether a view of the surface is obstructed. A potentially large number of applications will use the cloud mask and some algorithms will be more tolerant of cloud contamination than others. For example, some algorithms may apply a correction to account for the radiative effects of a thin cloud. In addition, certain algorithms may use spectral channels that are more sensitive to the presence of clouds than others.

To allow for the imprecise measurement of the real world and to accommodate a wide variety of applications, the mask is more than a simple yes/no decision. The cloud mask includes 4 levels of ‘confidence’ with regard to whether a pixel is thought to be clear as well as the results from different spectral tests. The bit structure of the cloud mask is described in Table 3 and a description of the bit fields follow.

Table 3. File specification for the 48-bit VCM

BYTE	Bit	Flag Description Key	Result
0	0-1	Cloud Mask Quality	00=Poor 01=Low 10=Medium 11=High
	2-3	Cloud Detection Result & Confidence Indicator	00 = Confident Clear 01 = Probably Clear 10 = Probably Cloudy 11 = Confident Cloudy
	4	Day / Night	0 = Night 1 = Day
	5	Snow / Ice Surface	1 = Snow/Ice 0 = No Snow/Ice
	6-7	Sun Glint	00 = None 01 = Geometry Based 10 = Wind Speed Based 11 = Geometry & Wind
1	0-2	Land / Water Background	000 = Land & Desert 001 = Land no Desert 010 = Inland Water 011 = Sea Water (Oceans) 101 = Coastal
	3	Shadow Detected	1 = Yes 0 = No
	4	Non Cloud Obstruction (Heavy Aerosol)	1 = Yes 0 = No
	5	Fire Detected	1 = Yes 0 = No
	6	Cirrus Detection (Solar) (RM9)	1 = Cloud 0 = No Cloud
	7	Cirrus Detection (IR) (BTM15-BTM16)	1 = Cloud 0 = No Cloud

BYTE	Bit	Flag Description Key	Result
2	0	IR Threshold Cloud Test (BTM15)	1 = Cloud 0 = No Cloud
	1	High Cloud (BTM12 - BTM16) Test	1 = Cloud 0 = No Cloud
	2	IR Temperature Difference Test (BTM14 - BTM15 & BTM15 - BTM16)	1 = Cloud 0 = No Cloud
	3	Temperature Difference Test (BTM15 - BTM12)	1 = Cloud 0 = No Cloud
	4	Temperature Difference Test (BTM12 - BTM13)	1 = Cloud 0 = No Cloud
	5	Visible Reflectance Test (RM5)	1 = Cloud 0 = No Cloud
	6	Visible Reflectance Test (RM7), also used for Visible Reflectance Test (RM1)	1 = Cloud 0 = No Cloud
	7	Visible Ratio Test (RM7/RM5)	1 = Cloud 0 = No Cloud
3	0-1	Adjacent Pixel Cloud Confident Value	00 = Confident Clear 01 = Probably Clear 10 = Probably Cloudy 11 = Confident Cloudy
	2	Conifer Boreal Forest	1 = Yes 0 = No
	3	Spatial Uniformity Test	1 = Yes 0 = No
	4	Dust candidate	1 = Yes 0 = No
	5	Smoke candidate	1 = Yes 0 = No
	6	Dust/Volcanic Ash	1 = Yes 0 = No
	7	SPARE	
	4	0-7	SPARE
5	0-2	Cloud Phase	000 = Not Executed 001 = Clear 010 = Partly Cloudy 011 = Water 100 = Mixed Phase 101 = Opaque Ice 110 = Cirrus 111 = Cloud Overlap
	3	Thin Cirrus Flag	1 = Thin Cirrus 0 = None
	4	Ephemeral Water Flag	1 = Yes 0 = No
	5	Degraded TOC NDVI Flag	1 = Yes 0 = No
	6	Degraded Sun Glint Flag	1 = Yes 0 = No
	7	Degraded Polar Night Flag	1 = Yes 0 = No

3.3.1 Cloud Mask Quality

Since VIIRS produces a cloud mask in any situation, a quality flag is attached to the final cloud mask. This flag reflects the number of tests executed for a given processing path. The quality definitions listed in Table 3 represent the following:

- Poor means that exactly no tests were executed,
- Low means that less than 50% of the tests were executed,
- Medium means that 50% or more of the tests were executed, and
- High means that exactly all of the tests were executed.

3.3.2 Cloud Detection Result and Confidence Indicator

The VCM provides an overall confidence that clouds exist in each VIIRS moderate resolution pixel. The possible cloud confidences are: confident cloudy, probably cloudy, probably clear, confident clear. These cloud confidence flags do not convey strength of conviction in the outcome of each individual cloud detection test for a given pixel, as discussed in Section 3.4.1.1 Overview of Cloud Detection Tests. This final or overall determination is a combination of the individual confidences of all applied tests as described in Section 3.4.1.2 Determination of Cloud Confidence.

3.3.3 Day/Night

The solar zenith angle at the pixel latitude and longitude is used to determine if a daytime or nighttime cloud masking algorithm should be applied. Daytime algorithms, which include solar reflectance data, are constrained to solar zenith angles less than 85°.

3.3.4 Snow/Ice Surface

Certain cloud detection tests (e.g., visible reflectance tests) are applied differently in the presence of snow or ice. This bit indicates a processing path and, if set, it should not be interpreted that snow/ice is on the ground. In daytime conditions, the VCM will use the VIIRS Gridded Snow Cover IP in conjunction with a reflectance based snow detection algorithm to check for snow surfaces. During the night, the VCM will use only the VIIRS Gridded Snow Cover IP to identify snow covered pixels. More information about the processing logic is given in Section 3.4.2 Determination of Background Conditions.

3.3.5 Land/Water Background

The surface type flag contains information concerning the processing path taken through the algorithm. There are five possible surface types: inland water, seawater, coast, desert land, and non-desert land. The VCM will read a geolocated surface type product, derived from a global MODIS Land/Water Mask-Quarterly Surface Type database, to directly determine the land/water background for each pixel.

Thresholds for the spectral tests are a function of surface background, land and water being the two most obvious. The specific processing path can be determined partially from this flag with snow or ice surface information available in the preceding flag. The snow/ice flag takes

precedence over the Land/water background flag, and the both inland water and sea water pixels are treated the same by the VCM. More information about the particular processing paths is given in Section 3.4.2 Determination of Background Conditions.

Note that the surface type database is limited to water features of 1 km resolution or larger, and therefore does not always support the identification of pixels that might contain surface water. This limitation can cause problems for downstream products (e.g., land surface temperature, aerosols) that rely on VCM for proper land/water identification. For this reason, an imagery-resolution ephemeral water detection test is used to supplement the VCM Land/water background flag from non-desert land to inland water. The ephemeral water detection test is discussed in Section 3.3.17 Ephemeral Water Flag.

3.3.6 Sun Glint Flag

There is a justifiable concern that cloud detection will not be as reliable in glitter-contaminated regions. A classification as clear is probably correct, but a classification as cloudy may actually be due to the glitter effect as opposed to a cloud. Sun glint will be considered over both land and water areas. Land regions are included because spatially unresolved water bodies, snow, or recent rainfall can also cause sun glint. Sun glint will not prohibit the generation of a cloud mask, however solar channel threshold values need to be adjusted for sun glint contaminated pixels.

Sun glint is tested for if the solar zenith angle is less than or equal to 89° . This extends slightly into the defined nighttime regime that is defined by solar zenith angle less than or equal to 85° . The first sun glint test checks the value of the reflected sun angle θ_r . If θ_r is between 0° and 36° , the sun glint flag will be set. Below is the formula for the reflected sun angle:

$$\cos \theta_r = \sin \theta \sin \theta_o \cos(180 - \phi_r) + \cos \theta \cos \theta_o$$

where

$$\theta = \text{SatelliteZenithAngle}$$

$$\theta_o = \text{SolarZenithAngle}$$

$$\phi = \text{SatelliteAzimuthAngle}$$

$$\phi_o = \text{SolarAzimuthAngle}$$

$$\phi_r = \phi_o - \phi = \text{RelativeAzimuthAngle}$$

The second sun glint test evaluates the sea surface winds and the solar geometry. Knowledge of sea surface winds is included in the sun glint test because surface winds can narrow the region in which sun glint may occur. Sun glint is identified when the slope of the water reflects the sun towards the satellite. If the water surface is disturbed by wind the sun is reflected from multiple spots on the surface. As the wind-rippled surface moves, so do individual glints of reflected sun. Therefore, the ensemble of glints produces a glitter pattern whose shape and size can be related to sea surface wind speed and the satellite viewing geometry. In the equation below, P represents the probability that the pixel is contaminated by sun glint due to sea surface wind speed (McClain and Yeh, 1994). Sun glint is identified when $P > 1.5$, where P is defined as

$$P = (1 / \pi \sigma^2) \exp[-\tan^2 \theta_N / \sigma^2]$$

$$\sigma^2 = 0.003 + 0.00512(\text{windspeed}(m / s))$$

$$\cos 2\omega = \cos \theta \cos \theta_o + \sin \theta \sin \theta_o \cos(\phi - \phi_o)$$

$$\theta_N = \cos^{-1}[(\cos \theta + \cos \theta_o) / 2 \cos \omega]$$

3.3.7 Shadow Detected

This flag identifies cloud-free pixels that contain shadows cast from adjacent pixels. The clouds that project shadows may be from nearby scans or adjacent granules. This flag is critically important to many algorithms that use the VCM as ancillary data. For example, failure to identify cloud shadows will result in aerosol optical thickness values being abnormally low while many land products, e.g, NDVI and surface albedo, will be corrupted. The VCM algorithm incorporates a geometric-based cloud shadow, using an approach developed for the NASA MOD09 products. However, the algorithm was re-engineered for use in the VCM to reduce processing requirements by an order of magnitude while maintaining similar performance characteristics. The algorithm is fully described in Section 3.4.6 The Geometric-Based Cloud Shadow Algorithm.

3.3.8 Non-cloud Obstruction

It is common for pixels that contain heavy aerosols, i.e. with optical depths that exceed ~ 0.6 , to be classified as confidently cloudy by VCM and heritage cloud algorithms (Brennan et al., 2005). Therefore, additional tests are performed to identify and differentiate between pixels that contain these heavy aerosols and clouds (Hutchison et al., 2008; 2010). The results are flagged in the VCM to show (1) results of all heavy aerosol tests and (2) results of the volcanic ash test for potential use by the aerosol algorithms. The heavy aerosol restoral tests are discussed in Section 3.4.5 Differentiating Between Heavy Aerosols and Clouds.

3.3.9 Fire Detected

The fire detection bit was originally modeled after the fire detection algorithm within the MCM. The procedure has been replaced with the fire mask generated with the VIIRS Active Fire algorithm. (The latter algorithm employs a small set of cloud tests to accurately differentiate between clouds and fire while the fire tests within the VCM were found to be unable to accurately detect fires.)

3.3.10 Cloud Detection Tests

These bits represent the results of individual cloud detection tests. Each individual test is discussed in Section 3.4 3 Cloud Detection Tests.

3.3.11 Cloud Adjacency

The cloud confidence value of all eight adjacent pixels will be searched and the furthest value from confidently clear reported. For boundary, e.g. edge of scan pixels, all available surrounding

pixels will be searched. (Originally cloud adjacency was reported for pixels classified as confidently cloudy; however, it was changed to include all pixels as required by the aerosol module.)

3.3.12 Cloud Phase

If the cloud confidence is confident cloudy or probably cloudy, the VCM will determine the cloud phase, which determines the processing paths for all of the VIIRS Cloud EDRs. Possible VCM cloud phase outcomes include one of the following five categories: water, mixed phase, opaque ice, cirrus, or overlap. The following definitions are given for each category.

- Water: Single cloud layer composed completely of water droplets.
- Mixed Phase: Single cloud layer composed of a mixture of water and ice particles or of supercooled water.
- Opaque Ice: Optically thick cloud with cloud top composed of ice crystals as determined by low M15 brightness temperature and lack of cloud overlap signature.
- Cirrus: Non-opaque, single-layer ice cloud.
- Overlap: At least two distinctive cloud layers defined as an ice cloud above a cloud predominantly of water phase.

In addition, pixels that possess a confidence of probably clear are given the partly cloudy label and phase is not determined. Those of confident clear status are labeled as clear. The “not executed” category is reserved for pixels in which the cloud phase algorithm could not be executed due to bad or missing data. Further information is provided in Section 3.4.4 The VCM Cloud Phase Algorithm.

3.3.13 Imagery Resolution Tests - Deleted

These tests were deleted because the results were inaccurate and the tests could not be made sufficiently reliable to perform cloud confidence classifications. The tests were originally implemented to support the Ice EDRs, which were shown by NGST to perform better with the results from the VCM at M-band resolution than with these imagery resolution tests. Imagery bands continue to be used as a means of detecting possible cloud edges in moderate resolution data to ensure sub-pixel clouds do not impact ocean surface products, e.g. sea surface temperature EDRs. These imagery resolution tests are discussed in Section **Error! Reference source not found.** and Section 3.4.3.10 Imagery Resolution Spatial Tests.

3.3.14 Conifer Boreal Forest Flag

The Conifer Boreal Forest flag indicates whether a land pixel is of Conifer Boreal Forest type or not. This information is read from the MODIS Land/Water Mask – Quarterly Surface Type database and passed on to the Snow/Ice Module. The VCM classifies the Conifer Boreal Forest surface type as land no desert.

3.3.15 Spatial Uniformity Flag

I-band spatial uniformity tests are performed on confident clear and probably clear pixels over water surfaces that do not contain sea ice using the four imagery resolution pixels that are imbedded in a single moderate resolution pixel. These tests have proven to be useful in detecting small-scale cloud structures over a uniform background, which aid in the accurate identification of confident clear pixels necessary for surface remote sensing over the ocean. If a moderate resolution pixel's cloud confidence is changed by the spatial uniformity tests, then a value of 1 will be assigned to the Spatial Uniformity Test bit. Otherwise, its value is 0.

3.3.16 Thin Cirrus Flag

This flag outputs the results of a daytime or nighttime thin cirrus test for every pixel under any environmental stratification. Results of the tests performed are not used for cloud confidence determination so that they may attempt to detect as much thin cirrus as possible without overclouding and adversely affecting the cloud confidence levels. During the day, the Ref_{M9} (1.38 μm) test is used while, at night, the $BT_{M15} - BT_{M16}$ (11 $\mu\text{m} - 12 \mu\text{m}$) is run. (See Sections, 3.4.3.7 Visible (Ref_{M9}) and 3.4.3.8 Infrared ($BT_{M15}-BT_{M16}$) respectively.) Both of these tests are used to detect cirrus and their results are used in the production of the VCM cloud confidence. The thin cirrus versions of these tests possess greater sensitivity to thin cirrus than the standard versions in that they employ lower thresholds necessary to detect the more optically thin cloud. They also complement the standard versions by using the standard version threshold as an upper limit so that it is not possible that cirrus can be detected by both the thin cirrus and standard versions of these tests. On the other hand, the thin cirrus flag may detect a cloud when other cloud tests, and the cloud confidence as well, indicates a cloud. This will be common if thin cirrus overrides a lower cloud.

During the night, thin cirrus is detected if $BT_{M15} - BT_{M16}$ is less than the $BT_{M15} - BT_{M16}$ mid-point (Clear/Cloudy Threshold), which is a dynamic threshold described in the following sections, and greater than the $BT_{M15} - BT_{M16}$ mid-point $- 0.25$ K. During the day, thin cirrus is detected if Ref_{M9} is less than the Ref_{M9} mid-point (Clear/Cloudy Threshold), also presented in the following sections, and greater than a Thin Cirrus Threshold. The Thin Cirrus Threshold is dependent on the surface type and, in some cases, atmospheric water vapor concentration. Table 4 shows the base Thin Cirrus Thresholds according to surface type.

Table 4. Base thresholds used for the Ref_{M9} thin cirrus test in the VCM algorithm

Ref_{M9}	
Surface	Base Ref_{M9} Thin Cirrus Threshold
Water	0.0125
Land	0.0125
Coast	0.0125
Desert	0.03
Snow/Ice	0.03

The Ref_{M9} thin cirrus test is not performed if total path integrated water vapor (TPIWV) is less than or equal to 0.25 cm. For land and coastal pixels, the base thin cirrus threshold is linearly increased between the particular land or coast thin cirrus threshold and the desert thin cirrus threshold when TPIWV decreases from 3 cm to 0.25 cm.

3.3.17 Ephemeral Water Flag

The relatively coarse definition of inland water provided by the global surface type map (resolutions of 1 km or larger) is considered inadequate to support identification of pixels that might contain surface water. Since the presence of surface water can impact all land algorithms (e.g., aerosols, surface reflectance and surface temperatures), an ephemeral water detection test is applied to overcome the deficiency. The test is performed for confidently clear moderate resolution pixels over land containing no snow and under daytime illumination only. It is based upon imagery resolution TOA NDVI values calculated using Bands I1 and I2 by the equation

$$TOA\ NDVI = \frac{Ref_{I2} - Ref_{I1}}{Ref_{I2} + Ref_{I1}},$$

where Ref_{I1} and Ref_{I2} are the reflectances of the I1 and I2 bands, respectively. Ephemeral water is assumed present if any of the imagery resolution pixels have a TOA NDVI threshold less than 0.01. When found, the ephemeral water flag is set to “Yes” and the VCM Land/Water Background Flag is reset to “Inland Water”. The threshold, which is identical to that used by the MODIS aerosol team to detect water contamination, will be evaluated and may be moved toward zero if warranted.

It should be noted that since clouds normally generate a very low NDVI (I1 and I2 reflectances are very similar for clouds), any cloud leakage will be falsely identified as inland water.

It should also be noted that the TOA NDVI will reduce but not eliminate surface water from land algorithms. Algae or other vegetation within water boundaries can produce NDVI values that exceed this threshold, even though the pixel is 100% water. However, the test will greatly aid attempts to flag poorer quality products collected in mixed land/water conditions.

3.3.18 Flag to Identify Degraded/Excluded Conditions

Quality flags have been added to identify degraded conditions as identified in NPOESS System Specification, Rev N dated September 12, 2008. Conditions flagged as degraded include (a) over land, $0.2 < TOC\ NDVI < 0.4$, (b) sunglint present (over land or ocean backgrounds), and (c) poleward of 60 degrees latitude and nighttime conditions. The System Specification also notes clouds with optical thickness < 1.0 as a degraded condition but this cannot be flagged in the VCM since the optical thickness EDR is generated after the VCM execution is complete.

3.4 THEORETICAL DESCRIPTION OF THE VCM ALGORITHMS

3.4.1 Physics of the Problem

The VCM algorithm actually consists of several different sets of logic or algorithms, each designed to complete part of the overall requirements for the VCM IP. Those algorithms include:

- Algorithms to determine the background conditions in VIIRS data to determine processing paths
- Algorithms to detect or identify clouds over various background conditions and establish confidences that a pixel is cloudy,
- Algorithms to classify the phase of pixels classified as confidently or probably cloudy,
- Algorithms to project geometric cloud shadows, and
- Algorithms to identify pixels that were originally classified as confidently cloudy but actually contain heavy aerosols. (Note: the VCM attempts to detect all volcanic ash, regardless of cloud confidence, as added information for the aerosol module.)

In this section, an overview is provided of the theoretical basis of algorithms used in the VCM to accomplish each of these functions, including the dependency of each function to the final VCM product. It is noteworthy that the logic for individual VCM cloud tests could be perfect, given a particular background conditions, but the VCM could fail if the logic fails to accurately categorize the diverse global backgrounds conditions into the proper VCM processing path. Additionally, cloud cover/layers algorithms fail to meet EDR requirements if the VCM classifies incorrectly water clouds as ice clouds. Thus, all errors in the VCM, from the determination of background conditions, propagate into the final VIIRS EDRs. As a result, NGST has emphasized the VCM algorithm(s) in an attempt to provide a state-of-the-science cloud mask for NPOESS.

3.4.1.1 Overview of Cloud Detection Tests

Multispectral cloud detection algorithms, like the VCM, start with the assumption that each pixel is cloud-free, then a series of cloud tests are applied to detect different types of clouds that might be present in VIIRS data. These tests are designed to exploit the different signatures of clouds and surrounding backgrounds in multispectral data or to compare reflectances or brightness temperatures in one band against some expected values for cloud-free conditions. Thus, multispectral algorithms used to detect clouds normally employ numerous cloud tests and the confidence that a pixel contains a cloud increases with the number of tests that predict a cloud to be present.

Summaries of tests applied in the VCM as a function of background conditions and solar illumination, i.e. daytime and nighttime, are shown in Table 5 and Table 6 respectively. Note that the table consists of two types of cloud tests. The moderate resolution tests (M-band tests) are spectral tests whose results determine overall cloud confidence, as discussed in the next section. The imagery resolution tests (I-band tests) are spatial tests that are applied over ocean surfaces to detect sub-pixel clouds, not detectible with spectral tests, which could impact ocean products such as the sea surface temperature and ocean color products. The results of these spatial tests may change the overall cloud confidence over water surfaces from confidently clear to probably clear

or probably cloudy. An overview of the logic used in the VCM to determine these backgrounds is found in the next section and the theoretical basis for each test is presented in the Section 3.4.3 Cloud Detection Tests. (Note: this table does not include tests to identify heavy aerosols, cloud shadows or ephemeral water.)

Table 5. Cloud tests used in the VIIRS Daytime Cloud Mask Algorithm as a function of surface type.

Cloud Spectral Tests Used to Determine Cloud Confidence	Water	Land	Desert	Coast	Snow
1. M9 (1.38 μm) Reflectance Test	X	X	X (if TPW > 0.25 cm)	X	X
2. M15-M16 (10.76 μm – 12.01 μm) Brightness Temperature Difference (BTD)	X	X	X	X	
3. Tri-Spectral M14, M15, M16 (8.55, 10.76, 12.01 μm) BTD Test	X				
4. M15-M12 (10.76 μm -3.70 μm) BTD Test	X (if no sun glint)	X (if TOC NDVI > 0.2)	X (if Lat > 60° or < -60°)	X (if no sun glint and if TOC NDVI > 0.2)	X
5. M12-M13 (3.70 μm -4.05 μm) BTD Test	X (if -60° < Lat < 60°) and no sun glint	X (if -60° < Lat < 60°) and TOC NDVI > 0.2			X (if -60° < Lat < 60°)
6. M1 (0.412 μm) Reflectance Test			X (if -60° < Lat < 60°)		
7. M5 (0.672 μm), M1 (0.412 μm) Reflectance Tests		X (M5 if TOC NDVI \geq 0.2; M1 otherwise)		X (M5 if TOC NDVI \geq 0.2; M1 otherwise)	
8. M7 (0.865 μm) Reflectance Test	X				
9. M7/M5 (0.865 μm / 0.672 μm) Reflectance Ratio Test	X	X (if RefM5 \geq LD_M5_Gemi Thresh)			
Cloud Spatial Tests Used to Modify the Final Cloud Confidence Classification	Water	Land	Desert	Coast	Snow
10. I5 (11.45 μm) Spatial Test	X				
11. I2 (0.865 μm) Reflectance Test	X				

Table 6. Cloud tests used in the VIIRS Nighttime Cloud Mask Algorithm as a function of surface type.

Cloud Tests	Water	Land	Desert	Coast	Snow
1. M15-M16 (10.76 μm – 12.01 μm) Brightness Temperature Difference (BTD)	X	X	X	X	
2. M15 (10.8 μm) Brightness Temperature (BT) Test	X	X	X	X	X
3. M12-M16 (3.70 μm – 10.76 μm) BTD Test		X M12 > BTM12 limit and Elev < Elev Thresh			
4. Tri-Spectral M14, M15, M16 (8.55, 10.76, 12.01 μm) BTD Test	X				
5. M15-M12 (10.76 μm -3.70 μm) BTD Test	X	X if TOC NDVI > 0.25 & M12 > 230 K	X if TOC NDVI > 0.25 & M12 > 230 K	X if TOC NDVI > 0.25 & M12 > 230 K	X
Cloud Spatial Tests Used to Modify the Final Cloud Confidence Classification	Water	Land	Desert	Coast	Snow
6. I4 (3.74 μm) Spatial Test	X				
7. I5 (11.45 μm) Spatial Test	X				

3.4.1.2 Determination of Cloud Confidence

Thresholds are needed to establish the value or range of values where each test, shown in Table 5 and Table 6, transitions from cloud-free to cloud conditions and these thresholds are necessarily a function of the backgrounds since a pixel is defined as cloudy if it contains > 50% cloud cover. Each cloud test used in the VCM algorithm employs at least three thresholds, (i.e. a highest threshold, midpoint threshold, and lowest threshold), to predict cloud-free confidence for a given test as originally developed for the MODIS cloud mask algorithm.

Figure 2 is a graphical representation of how a confidence level is assigned for a spectral test. The abscissa represents the observation and the ordinate the clear-sky confidence level. In this test, an observation greater than a value of γ is determined to be a high confidence clear scene and assigned a value of 1. An observation with a value less than α is cloudy and assigned a confidence level of 0. These confident clear and confident cloudy thresholds, γ and α respectively, are determined from observations and/or theoretical simulations. Values between α and γ are assigned a value between 0 and 1 (or 1 and 0). Assignment is based on a linear function. The β value in Figure 2 is the pass/fail threshold that indicates whether a pixel is

considered clear or cloudy by a given test. Each test therefore has a minimum of three thresholds values: confident cloudy/probably cloudy, clear/cloudy, and confident clear/probably clear which are used to determine the four levels of confidence; i.e. confident clear, probably clear, probably cloudy, and confident cloudy. Some tests, such as the visible ratio test, identify cloud if the observations fall within a given range (e.g., $0.9 < \text{Ref}_{M7}/\text{Ref}_{M5} < 1.1$). For these range tests there are six thresholds, three for each end.

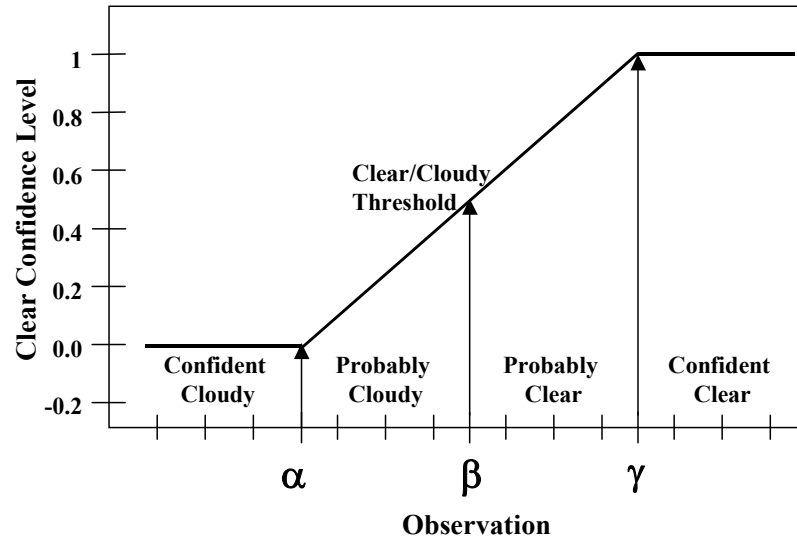


Figure 2. A graphical depiction of three thresholds used in cloud screening.

As an illustration,

Table 7 shows the highest threshold, midpoint threshold, and lowest threshold for the VIIRS M9 Reflectance test, #1 in Table 5, for non-sun glint water regions to be 2.5%, 2.0%, and 1.5% respectively. (Note: this example applies to a single test while the final cloud confidence is a rollup of all of the cloud detection tests applied to the pixel.) If the VIIRS M9 reflectance over a water background equals or exceeds the highest threshold, i.e. 2.5%, there is zero confidence that the pixel is cloud-free and the pixel is considered to be confidently cloudy by this test. If the VIIRS M9 reflectance equals or is less than the lowest threshold, i.e. 1.5%, the test predicts confidently clear and “1.0” is assigned as the cloud-free confidence. The midpoint threshold is used to distinguish between cloudy and cloud-free with a cloud confidence of 50% for VIIRS pixels with an M9 reflectance of 2.0%. If the VIIRS M9 reflectance value lies between the midpoint and highest threshold, the pixel is classified as probably cloudy while those between the midpoint and lowest thresholds are classified as probably clear. Thus, the result of each test applied in Table 5 and Table 6 returns a confidence level ranging from 0 (high confidence that the pixel is cloudy) to 1 (high confidence that the pixel is clear).

Table 7. Classification of cloud confidence for M9 Reflectance Test in VCM over ocean

VIIRS M9 Reflectance Test	Cloud Detection Threshold (%)	VIIRS Cloud Confidence	Remarks
M9 equals or greater	2.5	Confidently Cloudy, 0	Low Cloud-free Confidence Threshold
$2.0 < M9 < 2.5$		Probably Cloudy, Linearly interpolated between 0 and 0.5	
M9	29.0	0.5	Midpoint Threshold
$1.5 < M9 < 2.0$		Probably Clear, Linearly interpolated between 0.5 and 1	
M9 equals or less than	1.5	Confidently Clear, 1	High Cloud-free Confidence Threshold

The individual confidence levels for all cloud tests applied, as a function of background conditions shown in Table 5 and Table 6, must be combined to determine a final decision on cloud confidence for each pixel. The confidence level of an individual test is denoted as F_i and the final quality flag as Q .

The VIIRS Cloud Mask is a clear-sky conservative case. A test with a confident clear result sets the bit to clear. Several tests are not independent of one another. For example, consider daytime over oceans in regions without sun glint (See Table 5). If stratocumulus clouds are present, they will likely be detected by the visible reflectance test (#7), the reflectance ratio test (#8), and $BT_{M15}-BT_{M12}$ (#4). These same tests will likely miss the presence of thin uniform cirrus clouds, which would probably be detected by the tri-spectral M14, M15, and M16 (#3). Very thin cirrus clouds would best be detected by the M9 test (#1), which may have difficulty detecting low-level clouds. Because of this overlap in the type of clouds different tests detect, each test is considered in one of five groups, as illustrated in Figure 3, which applies to daytime land conditions. These five groups are:

Group I (Emission Threshold)

$$BT_{M15}$$

Group II (Emission Difference)

$$BT_{M12}-BT_{M13}$$

$$BT_{M15}-BT_{M12}$$

$$BT_{M14}-BT_{M15} \text{ \& } BT_{M15}-BT_{M16}$$

Group III (Reflectance Threshold)

$$Ref_{M1}$$

$$Ref_{M5}$$

$$Ref_{M7}$$

$$Ref_{M7}/Ref_{M5}$$

Group IV (Reflectance Thin Cirrus)

Ref_{M9}

Group V (Emission Thin Cirrus)

BT_{M15}-BT_{M16}

BT_{M12}-BT_{M16}

A minimum confidence is determined for each group,

$$G_{i=1,N} = \min[F_i],$$

where N is the number of groups in which cloud tests could be performed. This is determined by the processing path (see below) and N has a maximum of 5. The final cloud mask is then determined from the product of the results from each group;

$$Q = \sqrt[N]{\prod_{i=1}^N G_i}.$$

This approach is considered clear-sky conservative. If any test is highly confident that the scene is cloudy ($F_i = 0$), the final cloud mask is $Q = 00$, which is confident cloudy. Thus, the final determination of cloud confidence is based on a combination of the confidences for all tests applied to a given pixel, which is a function of the background, i.e. snow/ice, land, desert, ocean (inland water), and coast. Therefore, it is imperative that no cloud tests generate an unacceptable number of false alarms.

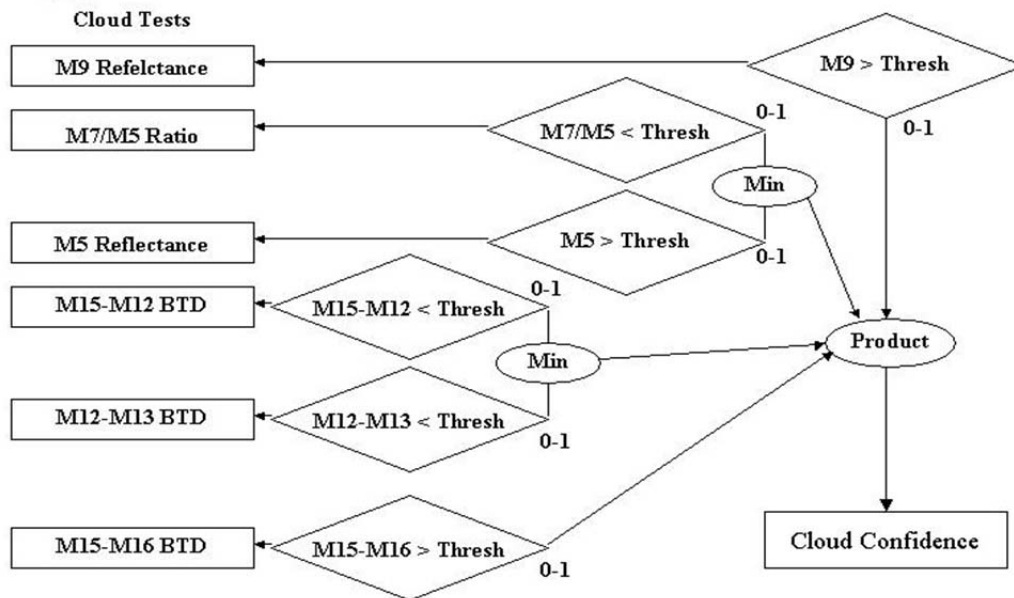


Figure 3. Five Groups of cloud tests used to make cloudy confidences in the VCM during daytime conditions over land backgrounds.

3.4.2 Determination of Background Conditions

The architecture of the VCM requires that background conditions be determined for each pixel prior to applying the cloud detection tests shown in Table 5 and Table 6. The algorithm is divided into eight conceptual domains according to surface type and solar illumination:

1. Daytime land
2. Daytime coast
3. Daytime water
4. Daytime desert
5. Daytime snow/ice covered regions
6. Nighttime land, desert, and coast
7. Nighttime water
8. Nighttime snow/ice covered regions.

“Daytime” is defined as a solar zenith angle $\theta_0 < 85^\circ$ and possible processing paths are shown in Figure 4. The “desert” classification is based on the IGBP Land Type classification of “Barren” which is carried over into the merged MODIS Land/Water Mask – Quarterly Surface Type database. For all observations within a given domain, it is generally expected that: (i) the same tests may be performed, and (ii) threshold values for each of these tests will not change. It is possible that more domains may be established in the future.

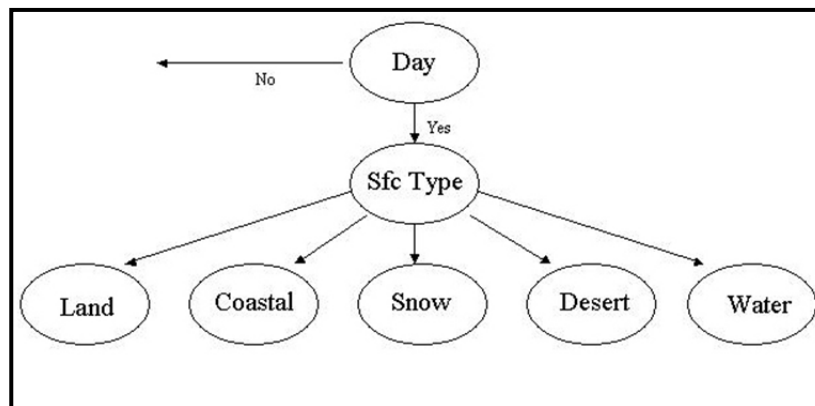


Figure 4. The five processing paths of the VIIRS Cloud Mask Algorithm for the analysis of data collected in daytime conditions.

Pixels found to be over land must be evaluated to determine if snow is present, since few of the land cloud tests can be applied when snow is present to avoid false alarms. The process currently uses gridded snow fields from NCEP but will ultimately use the VIIRS gridded snow IP. Logic exists in the VCM algorithm to use these background fields of snow data, which for daytime conditions, are then updated with logic in the VCM based upon the data being processed. These background snow/ice fields cannot be updated with real-time VIIRS data collected from the 1730 orbit or during nighttime conditions.

Testing of the VCM algorithm at NGST led to the discovery that the logic used in the original VCM to make snow versus land decisions were grossly in error. All logic errors have been corrected and the VCM algorithm now successfully uses these ancillary data.

The logic used to determine the snow/ice processing path is discussed in detail to ensure it is understood by users of the VCM products. It is also presented in the ATBD, rather than only the Operational Algorithm Description to assist those preparing for cal/val activities, since the logic may require adjustment with VIIRS on-orbit data. If adjustments are warranted, VCM performance could be significantly degraded until they are made.

The logic to evaluate the presence of snow in each pixel begins by reading the initial snow/ice flag from the ancillary database, which is created by granulating the 1x1 degree NCEP snow field to VIIRS M-band resolution to produce the "snow_ice_flag" which has a value of either YES or NO. This initial estimate serves as the fallback value of the snow/ice flag to a second evaluation performed by VCM. This second evaluation uses spectral tests based upon the VIIRS SDR data and is indicated by the "Perform VCM snow ice flag tests" box shown in the leftmost flowchart of Figure 5. The logic represented by this box is expanded upon in the remaining flowcharts of the figure and describes the tests made with the VIIRS SDR to determine this secondary snow/ice flag. This secondary snow/ice flag overrides the initial estimate when a definitive decision, YES or NO, can be made.

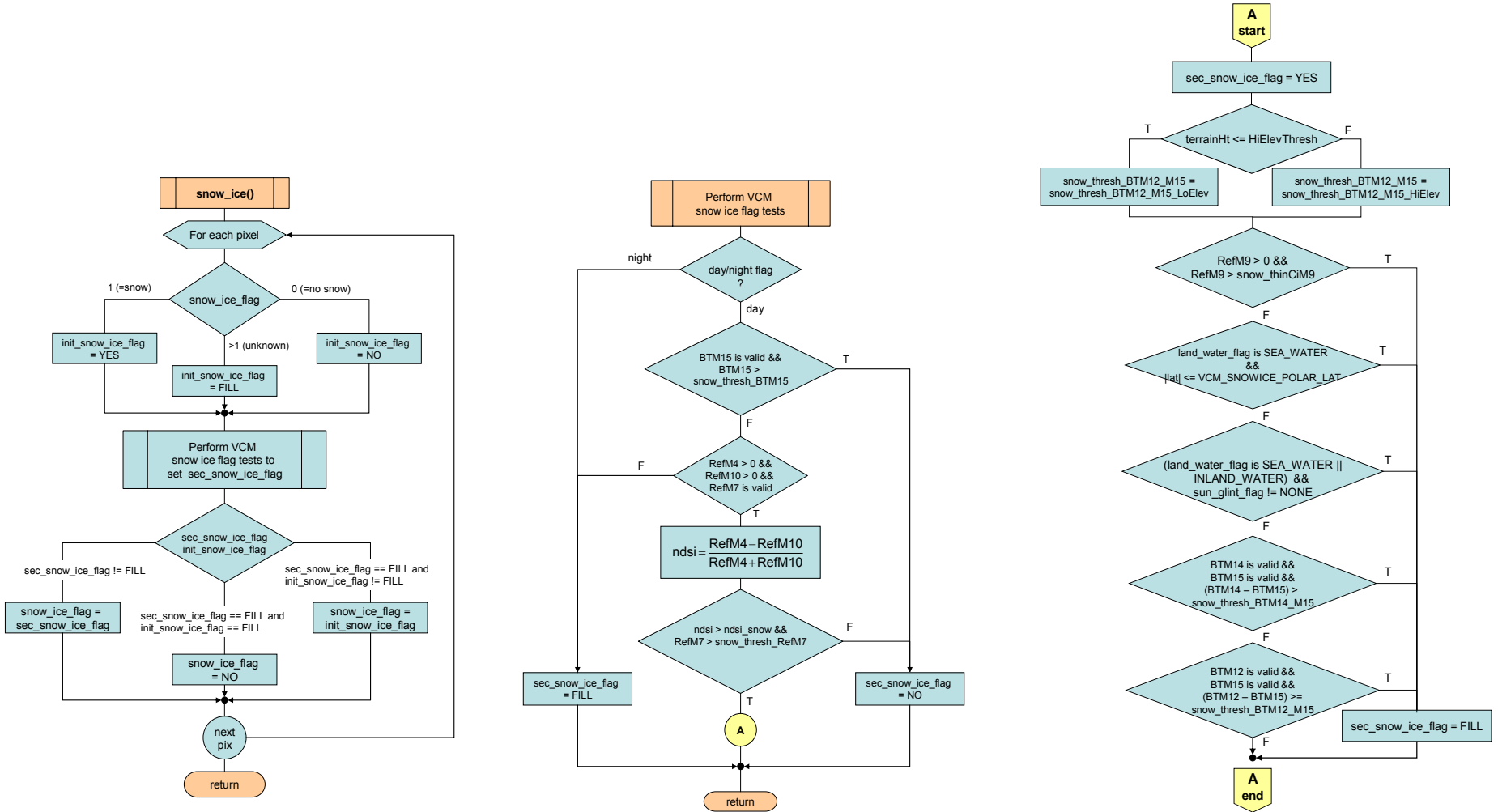


Figure 5. Logic in the VCM to determine presence of snow/ice in each VIIRS pixel.

For the secondary snow/ice evaluation, the M15 BT is first examined to determine if the surface temperature is too warm to support the presence of snow. In the original VCM, the procedure erroneously entered a “fill” value if this brightness temperature was greater than the threshold, which is currently set at 280 K. In the updated logic, the VCM correctly enters “no snow” if the M15 BT is too warm to support the presence of snow and the snow_ice_flag is set to the value of the sec_snow_ice_flag, i.e. NO. (In the early logic, the snow_ice_flag would have defaulted to the initial snow/ice flag, init_snow_ice_flag, or more specifically, the NCEP ancillary snow ice database.)

If the M15 BT is less than or equal to 280 K, the normalized difference snow index (NDSI) test is performed to determine the potential presence of snow, after verifying that actual SDR data are available in the bands needed to perform this test.

- If the NDSI test is not satisfied, the secondary snow/ice flag, sec_snow_ice_flag, is set to NO, and VCM continues processing for land without snow/ice. The original logic performed additional tests which normally resulted in this second flag being set again to “fill” and processing would be based upon the setting of the initial snow/ice flag (i.e., the NCEP ancillary snow ice database).
- If the NDSI test is satisfied, additional spectral tests are performed to ensure other features are not misclassified as snow, e.g. cloud edges of thin cirrus.

Most of the modifications made to the original VCM snow/ice logic concerned the portion of logic dealing with pixels that passed the NDSI test and might contain snow. Modifications to the original VCM snow/ice logic include the following corrections:

- Changes to determine if thin cirrus is present. The M15 BT test has been removed and now only the reflectance in the M9 band is examined. The current threshold is 5.25% for processing MODIS data if terrain is < 2-km. If the M9 reflectance exceeds this threshold, cirrus clouds are assumed. (Note: It is expected that this threshold will be reduced for VIIRS since the VIIRS instrument has a 15-nm bandpass for this band while MODIS has a 30-nm bandpass. The threshold should be checked early during cal/val activity.)
- Changes to the M14-M15 BTD threshold for thin cirrus. The threshold was lowered from 0.9-K to 0.5-K based upon the experience of the MODIS cloud team. This threshold is not expected to change when changing from MODIS to VIIRS data.
- An additional modification was made to this module post-launch after it was observed that low-level clouds found in regions behind a cold front over ocean backgrounds can become glaciated which makes these clouds be misclassified as snow/ice surfaces. Since this phenomenon occurs mostly over regions equatorward of 60° latitude, the logic was modified to return a “fill” value when the pixel lies in the latitudinal range of 60N – 60S. The net effect of this change is to increase the importance of the snow/ice ancillary database for snow/ice decisions within this large latitude band over ocean surfaces.

Again, if spectral tests with the SDR return a “fill” value, the pixel takes the value of the ancillary snow database, i.e. init_snow_ice_flag. However, if tests with the SDR return a “non-fill” value, then the pixel is assigned the value of the sec_snow_ice_flag. The impact of the snow

ice logic on VCM performance is demonstrated by the analyses of a MODIS granule using the original (erroneous) and updated procedures.

Figure 6 shows the ancillary data for MODIS proxy data, performance of the VCM with the daytime data SDR before corrections to this module, and performance after corrections noted above were implemented. The results are typical of those expected during nighttime conditions when the ancillary data cannot be updated with SDR tests for snow/ice. The figure shows, in the upper left panel, a color composite of MODIS imagery collected over the Intermountain West of the U.S. for MODIS granule MOD2002.032.1750. The color composite was constructed so snow/ice appear purple, thin cirrus clouds are blue, low-level water clouds are yellow. Dense cirrus clouds also have a purplish hue but are readily differentiated from snow by texture. Upper right panel shows the 1x1 degree snow (red) - no snow (blue) data in the NCEP database and the blockiness of these data are evident. The lower left contains the snow field generated by the logic in the uncorrected VCM and the blockiness artifacts of the NCEP snow fields are obvious. In the lower right panel are shown the results generated by the VCM algorithm after the corrections, noted above, were implemented. Not shown are the errors in VCM performance based upon misclassifications of the snow/ice in the VCM. VCM performance, compared to manually-generated cloud masks at NGST, showed a 7.6% larger error with the snow/ice mask in the lower-left panel compared to the analyses generated from the lower-right panel. Thus, it is apparent that choosing the incorrect snow/ice versus land processing path can have a major impact on VCM probability of correct typing (PCT) performance.

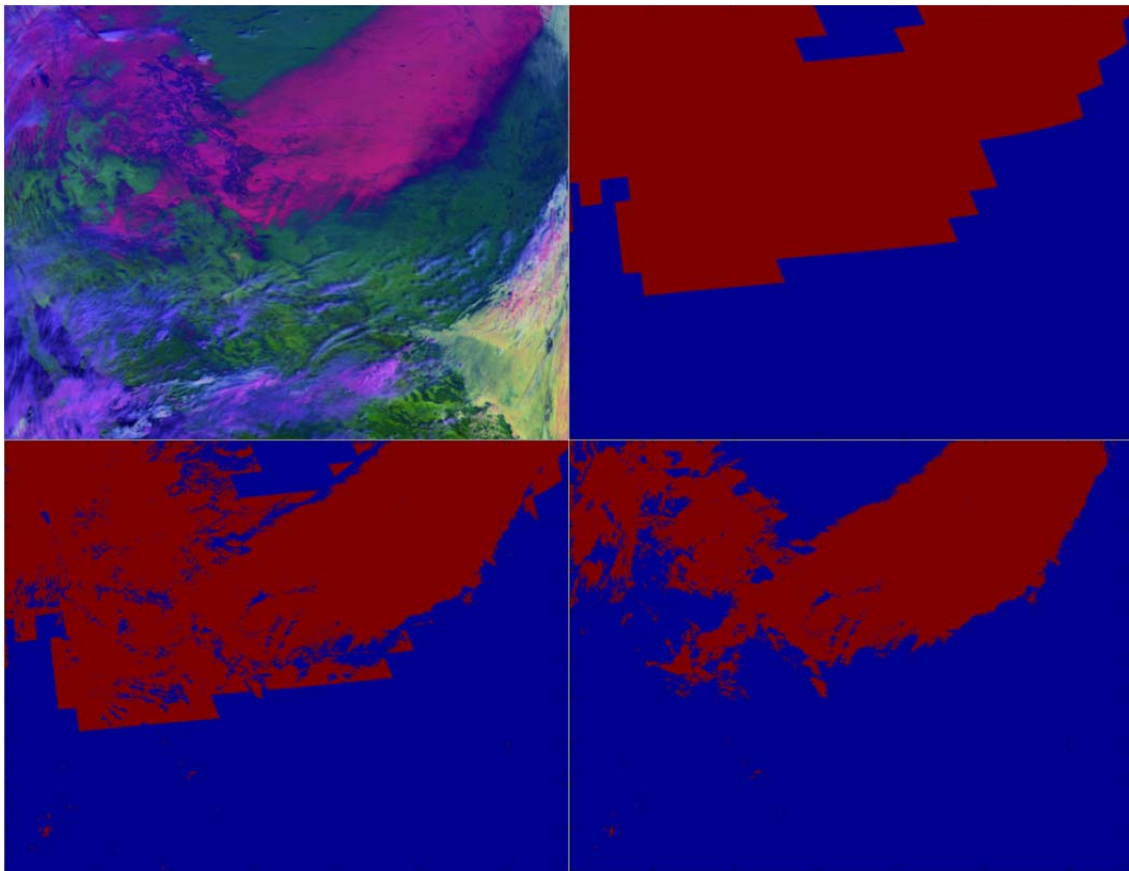


Figure 6. Results of snow/ice processing in current VCM algorithm. Upper left shows color composite imagery (snow is purple), upper right is NCEP database, lower left is VCM snow before corrections, and lower right is VCM snow field after corrections described above.

3.4.3 Cloud Detection Tests

Several infrared window threshold and temperature difference techniques have been developed for cloud detection. These algorithms are described below.

3.4.3.1 IR Threshold Cloud Test (BT_{M15})

The first infrared test to apply over all surface types during nighttime is a simple threshold test. The $11\ \mu\text{m}$ brightness temperature (BT_{M15}) is compared to ancillary surface temperature to determine the existence of clouds. This test is needed to detect a variety of clouds, especially cloud overlap conditions, i.e. ice clouds overlie water clouds in a single VIIRS FOV. The infrared spectral signatures of overlap clouds tend to be small because individual signatures of ice and water clouds are opposite; thus, when combined, the brightness temperature differences in overlap often fall below the detection threshold of either the ice or water clouds, as shown in Figure 7 (Hutchison et al., 1995). A simple IR cloud test is needed to detect overlap based upon, what Saunders and Kriebel originally called the “gross IR test.” Since the brightness temperature observed in overlap conditions is normally much colder than the surface, the test does not need to have an accurate measure of the surface temperature.

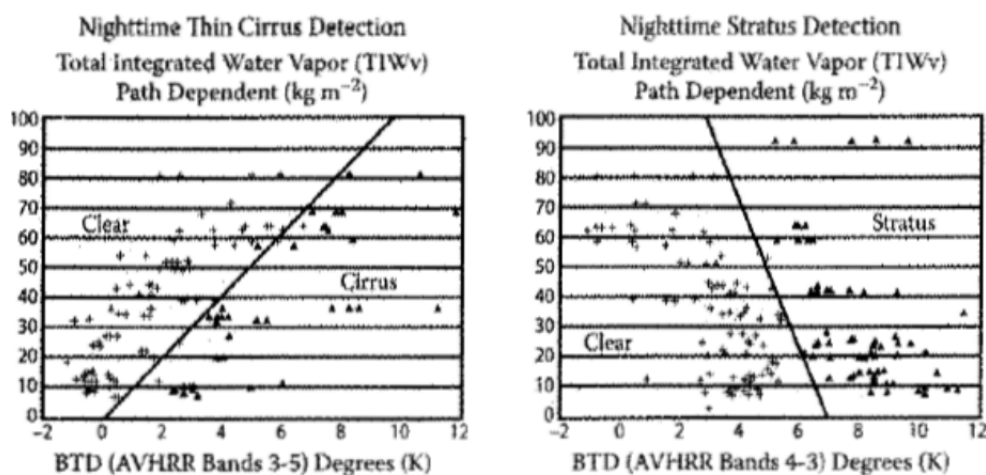


Figure 7. Brightness temperature differences between AVHRR channel 3 ($3.75\text{-}\mu\text{m}$) minus channel 5 ($12.0\text{-}\mu\text{m}$) and total precipitable water (path) for cloudy pixels (\blacktriangle) of cirrus clouds (left panel) and stratus clouds (right panel) along with cloud-free pixels (+) (from Hutchison et al., 1995).

Thus, if the difference between the surface temperature (T_s) and BT_{M15} is larger than a particular threshold, then cloud is assumed. Base (midpoint) thresholds for this difference, $T_s - BT_{M15}$, are given in Table 8.

Table 8. Base mid-point thresholds used for BT_{M15} test for cloud in the VCM algorithm

BT_{M15}	
Surface	Base mid-point $T_s - BT_{M15}$ Thresholds
Night Ocean	6.5 K
Night Inland Water	7.5 K
Night Land and Coast	8.4 K
Night Desert	14 K
Night Snow/Ice	8.4 K

The thresholds for this tests are varied by the total water vapor present in the atmosphere using standard procedures, i.e. the $T_s - BT_{M15}$ thresholds are adjusted for water vapor concentration using 11 $\mu\text{m} - 12 \mu\text{m}$ brightness temperature difference ($BT_{M15} - BT_{M16}$) by the following rules:

1. if $BT_{M15} - BT_{M16}$ is greater than 1 K then
threshold = threshold + 2*integer($BT_{M15} - BT_{M16}$)
2. threshold = threshold + 3a⁴,
where the parameter a = Sensor Zenith/Maximum Sensor Zenith (70°) in radians.

Final $T_s - BT_{M15}$ thresholds are calculated via

$$\begin{aligned} \text{Low_Confidence Clear} &= \text{threshold} + 2 \text{ K} \\ \text{Mid_Point} &= \text{threshold} \\ \text{High Confidence Clear} &= \text{threshold} - 2\text{K} \end{aligned}$$

3.4.3.2 Tri-Spectral Cloud Test ($BT_{M14} - BT_{M15}$ & $BT_{M15} - BT_{M16}$)

As a result of the relative spectral uniformity of surface emittance in the IR, spectral tests within various atmospheric windows (such as bands M14, M15, and M16 at 8.55- μm , 10.76- μm , and 12.01- μm , respectively) can be used to detect the presence of cloud. Differences between BT_{M15} and BT_{M16} are widely used for cloud screening with AVHRR measurements, and this technique is often referred to as the split window technique. Saunders and Kriebel (1988) used $BT_{M15} - BT_{M16}$ differences to detect cirrus clouds. Brightness temperature differences are greater over thin clouds than over clear or overcast conditions. Cloud thresholds are set as a function of satellite zenith angle and BT_{M15} .

A drawback of the bi-spectral technique at these wavelengths is that the brightness temperature generally decreases between 10- μm and 12- μm , whether a pixel is cloud-free or cloud-contaminated. Ackerman et al. (1990) first suggested using a combination of observations in the 8-13 μm region to improve the detection of cirrus clouds. The optimum bandset consisted of observations collected in the 8, 10, and 11- μm bandpasses, similar to those from MODIS Channels 29, 31, and 32 in addition to VIIRS bands M14, M15 and M16.

The basis of the tri-spectral technique for cloud detection lies in the differential absorption of both water vapor and ice particles that exists between different bandpasses in this region. The effect of the water-vapor continuum in clear spectra is that the equivalent blackbody temperatures decrease with increasing wavelength across the 10-13 μm region. A similar trend is observed with cirrus clouds, which is consistent with the absorption coefficient of ice. The technique exploits the fact that ice and water vapor absorption peak in opposite halves of the 8-13 μm window region. As a result, cloud-free regions tend to have negative differences in the BT_{M14}-BT_{M15} feature due to increased absorption by water vapor in the longer bandpass while positive M14-M15 brightness temperature differences suggest the presence of clouds. As the atmospheric moisture increases, BT_{M14} - BT_{M15} decreases while BT_{M15} - BT_{M16} increases.

Strabala et al. (1994) expanded the use of the tri-spectral combination of observations to include cloud phase determination while Baum et al. (2000) further explored this technique by utilizing very high spatial-resolution data from MODIS Airborne Simulator (MAS) data (King et al., 1996). The tri-spectral test has been applied to cloud phase determinations since the BT_{M14}-BT_{M15} feature for liquid water clouds is expected to be less than the BT_{M15}-BT_{M16} feature while it is expected to be larger for ice clouds (Ackerman et al., 1990). The relationship between the two brightness temperature differences and clear-sky has also been examined using collocated HIRS and AVHRR GAC global ocean data sets.

Figure 8 demonstrates a relationship between BT_{M15} - BT_{M16} and BT_{M14} - BT_{M15} using MODIS observations over the Atlantic Ocean. Given a value of BT_{M15} - BT_{M16}, to be clear, a pixel requires BT_{M14} - BT_{M15} to fall within a certain range of values. The threshold for this test is based on the value of BT_{M15} - BT_{M16} which varies for each pixel.

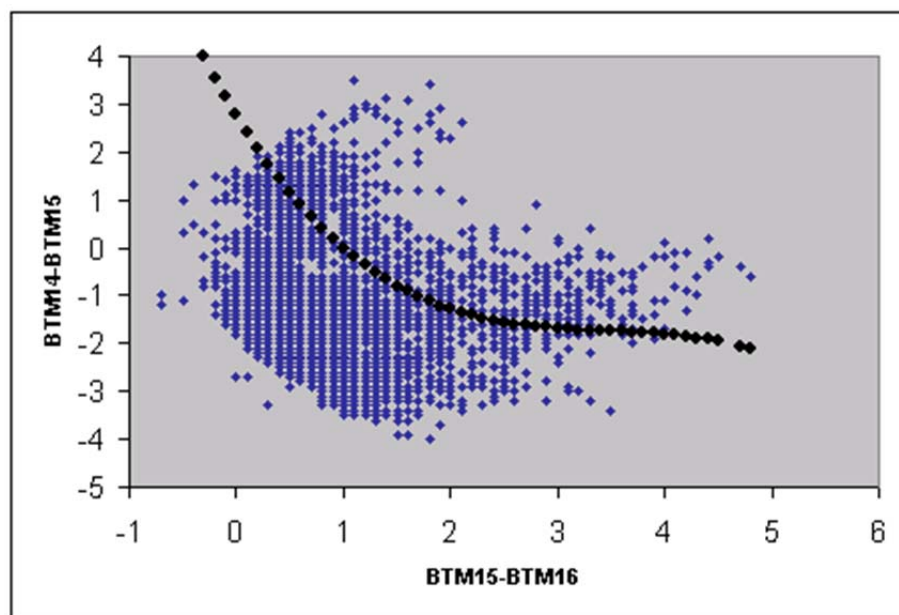


Figure 8. Tri-spectral diagram for ocean scenes taken from MODIS data. The dark diamonds in the figure represents the dynamic threshold for the tri-spectral test and the dark blue circles are the observed values. Values to the upper right of the threshold indicate cloud and lower left of the threshold indicate clear.

Brightness temperature difference testing can also be applied over land with careful consideration of variation in spectral emittance. For example, $BT_{M15} - BT_{M16}$ has large negative values over daytime desert and is driven to positive differences in the presence of cirrus. Some land regions have an advantage over ocean regions because of the larger number of surface observations, including air temperature and vertical profiles of moisture and temperature. Thus, far, this tri-spectral IR window brightness temperature difference test is only applied to water surfaces as indicated by the list of thresholds in Table 9.

Table 9. Thresholds used for $BT_{M14} - BT_{M15}$ and $BT_{M15} - BT_{M16}$ test for cloud in the VCM algorithm

$BT_{M14} - BT_{M15}$ & $BT_{M15} - BT_{M16}$			
Surface	Confident Cloudy	Clear/Cloudy Threshold	Confident Clear
Day Ocean		Dynamic	
Night Ocean		Dynamic	

3.4.3.3 Cloud Test ($BT_{M15} - BT_{M12}$)

The difference between BT_{M15} and BT_{M12} can be used to detect the presence of clouds. Due to the differential absorption of water vapor in the 3.7- μm and 10.76- μm channels, the clear sky brightness temperature difference is a function of total path integrated water vapor as well as background type.

At night the difference between the brightness temperatures measured in the longwave (10.76 μm) and in the shortwave (3.7 μm) window regions can be used to detect partial cloud or thin cloud within the VIIRS FOV. Large positive differences are observed only for the case where an opaque scene (such as thick cloud or the surface) fills the FOV of the sensor. Large positive differences occur at night over low-level water clouds due to the lower cloud emissivity at 3.7 μm , as shown in Section 3.4.3.1 above. However, large positive differences can often result from clear, arid surfaces due to different spectral surface emissivities. As a result, this test is run over land at night only if the TOC NDVI is greater than 0.25, indicative of a moderate to high amount of vegetation. The test is also run over the desert and in coastal regions using the same thresholds used for land.

A piece-wise linear function with a steep slope for low values of total integrated water vapor and a gentle slope for high values of total integrated water vapor has been selected as a reasonable approximation for use in the daytime desert regime and for polar deserts defined as poleward of 60°. During the night over land (non-snow) desert and coastal (land/water) surfaces the following thresholds are used for high, medium, and low clear sky confidence associated with total path Total Precipitable Water (TPW) of 0 cm.

$$\begin{aligned} Hi_conf &= +0.5 \text{ K} \\ Mid_pt &= 1.4 \text{ K} \\ Lo_conf &= 2.0 \text{ K}. \end{aligned}$$

All thresholds are adjusted by TPW calculated in the actual path by sensor zenith (vz) using a multiplicative factor of 0.1, in the following manner:

If $((TPW/\cos(vz)) \leq 5 \text{ cm})$ then

$$Hi_conf = Hi_conf - ((TPW/\cos(vz)) * 0.1)$$

$$Mid_pt = Mid_pt - ((TPW/\cos(vz)) * 0.1)$$

$$Lo_conf = Lo_conf - ((TPW/\cos(vz)) * 0.1)$$

If $((TPW/\cos(vz)) > 5 \text{ cm})$ then the values are:

$$Hi_conf = 0.0 \text{ K}$$

$$Mid_pt = 0.9 \text{ K}$$

$$Lo_conf = 1.5 \text{ K}$$

Over ocean and inland water surfaces, for $TPW/\cos(vz) \leq 5 \text{ cm}$, these thresholds values are: - 0.5K, 0.0K, and 1.0K respectively for the Hi_conf , mid_pt , and Lo_conf thresholds and are adjusted for TPW using multiplicative factors of 0.15. For $TPW/\cos(Vz) > 5 \text{ cm}$, these values are: -1.25K, -0.75K, and +0.25 respectively.

During the daylight hours the difference between BT_{M15} and BT_{M12} is large and negative because of reflection of solar energy at M12, as shown in Figure 11, which was generated at NGST with synthetic data. This technique is very successful at detecting low-level water clouds. Thresholds will vary for ecosystem type. Moderate to large differences between BT_{M15} and BT_{M12} result are observed in a non-uniform scene (e.g., broken cloud). The different spectral responses to a scene of non-uniform temperature are a result of Planck's law. The brightness temperature test is dependent on the temperature in the warmer portion of the scene increasing with decreasing wavelength (the shortwave window Plank radiance is proportional to the temperature to the thirteenth power, while the longwave dependence is to the fourth power). Differences in the brightness temperatures of the longwave and shortwave channels are small when viewing mostly clear or mostly cloudy scenes; however, for intermediate situations the differences become large (greater than 3 degrees). Figure 9 shows the distribution of cloudy (blue) and cloud-free (red) pixels in global synthetic data. The original VCM threshold for this test was set at -14C; however, based upon these synthetic data, the threshold was increased to -18C, which was found later to be more in agreement with heritage algorithms. Also note that at total precipitable water values below about 2 cm, the separation between clear and cloudy pixels becomes much less distinct. Thus, the synthetic data suggest that this test will not be effective in cloud detection over dry regions, such as arid land surfaces.

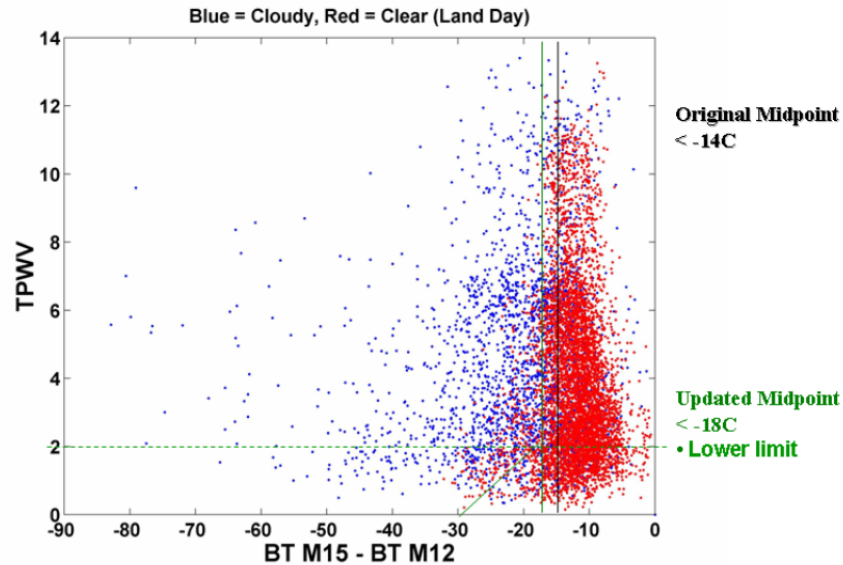


Figure 9. Distribution of cloudy (blue) and cloud-free (red) pixels as a function of M15-M12 BT difference and total precipitable water based upon global synthetic data.

This test is performed for all processing paths with certain exceptions. For example, at night, if BT_{M12} is less than 230 K, the test is not run due to calibration uncertainties in the M12 band. Table 10 lists the thresholds used. The effectiveness of this test can be maximized by replacing the static threshold with dynamic thresholds that are a function of total integrated water vapor.

Table 10. Thresholds used for $BT_{M15} - BT_{M12}$ test for cloud in the VCM algorithm

$BT_{M15} - BT_{M12}$			
Surface	Confident Cloudy	Clear/Cloudy Threshold	Confident Clear
Day Land	-20.0	-18.0	-16.0
Day Coast	-14.0	-12.0	-10.0
Day Ocean (no sun glint)	-12.0	-10.0	-8.0
Day Desert (polar)	Dynamic	Dynamic	Dynamic
Night Land & Desert & Coast	Dynamic	Dynamic	Dynamic
Night Ocean	Dynamic	Dynamic	Dynamic
Day Snow (high elevation)*	14.0	10.0	6.0
Day Snow (low elevation)*	10.0	7.0	4.0
Night Snow (low elevation)	+2.0	+1.0	0.0

*This test is $BT_{M12} - BT_{M15}$.

Infrared window tests at high latitudes are difficult. Distinguishing clear and cloud regions from satellite IR radiances is a challenging problem due to the cold surface temperatures. Yamanouchi et al. (1987) describes a nighttime polar (Antarctic) cloud/surface discrimination algorithm based upon brightness temperature differences between the AVHRR 3.7 and 11 μm channels and between the 11 and 12 μm channels. Their cloud/surface discrimination algorithm was more effective over water surfaces than over inland snow-covered surfaces. A number of problems arose over inland snow-covered surfaces. First, the temperature contrast between the cloud and snow surface became especially small, leading to a small brightness temperature difference between the two infrared channels. Second, the AVHRR channels are not well calibrated at extremely cold temperatures (< 200 K). As a result, this test is only applied in nighttime for snow/ice surfaces when the terrain height is lower than 2000 m.

Due to the increase in reflected 3.7 μm radiance under sun glint conditions, this test is not performed for ocean and coastal stratifications when sun glint is predicted. Bright land surfaces also cause enhancement in 3.7 μm radiance so that the clear sky $BT_{M15} - BT_{M12}$ values exceed their cloud thresholds. As a result, this test will only be performed over non-snow/non-desert land and coastal surfaces if the TOC NDVI is greater than 0.2.

3.4.3.4 Cloud Detection Test ($BT_{M12} - BT_{M13}$)

Performing this BT difference test is another method of separating the solar and thermal contributions of M12. Due to the small wavelength differences between these two bands the thermal contribution due to temperatures within a pixel are relatively close. The largest difference between these two bands is the solar component in the 3.7 μm channel. The difference removes the thermal emission, resulting in the solar component of 3.7 μm alone. Due to both the low reflectance of most surface types and the relative high reflectance of clouds in the 3.7 μm channel this test has demonstrated much promise in MAS data. Table 11 lists the thresholds used in the $BT_{M12}-BT_{M13}$ test.

This test is not performed in areas with bright surfaces such as polar regions, land and coastal areas, where TOC NDVI is less than 0.2, and under conditions of sun glint.

Table 11. Thresholds used for $BT_{M12} - BT_{M13}$ test for cloud in the VCM algorithm

$BT_{M12}-BT_{M13}$			
Surface (60° S – 60° N)	Confident Cloudy	Clear/Cloudy Threshold	Confident Clear
Day Land	15.5	13.75	12.0
Day Ocean (no sun glint)	11.0	10.5	10.0
Day Snow	14.5	12.5	10.5

Figure 10, Figure 11, and Figure 12 show results of the M12-M13 BT differences for synthetic truth cloud data over land, water, and snow/ice respectively for a “perfect” MODIS SDR as a function of solar zenith angle. (The MODIS SDR is from TOA radiances in the MODIS Terra

bandpasses.) The results show the current VCM cloud detection thresholds in solid lines and possible enhancements to these thresholds in dashed lines. It appears that improved detection could be achieved with this test over most land and water surfaces by lowering the corresponding thresholds and making the land threshold a function of solar zenith angle. Additionally, synthetic data suggests that the test should not be applied over snow/ice fields.

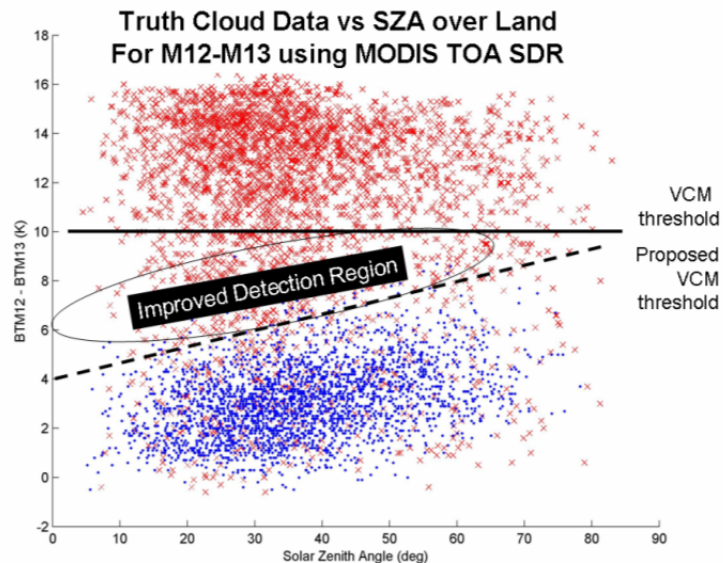


Figure 10. Distribution of cloudy (red) and cloud-free (blue) pixels over land as a function of M12-M13 BT difference and solar zenith angle based upon global synthetic MODIS TOA SDRs.

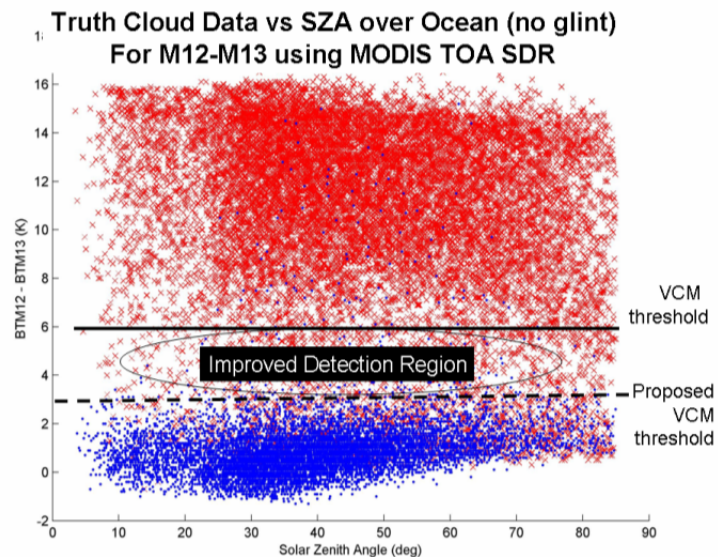


Figure 11. Distribution of cloudy (red) and cloud-free (blue) pixels over water as a function of M12-M13 BT difference and solar zenith angle based upon global synthetic MODIS TOA SDRs

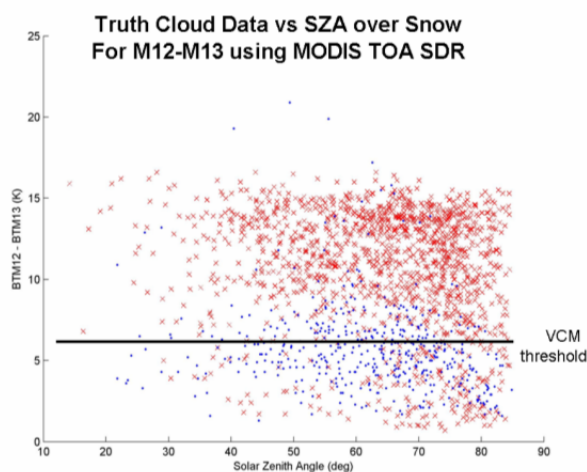


Figure 12. Distribution of cloudy (red) and cloud-free (blue) pixels over snow/ice as a function of M12-M13 BT difference and solar zenith angle with global synthetic MODIS TOA SDRs

3.4.3.5 Visible Reflectance (M1, M5 & M7)

The visible reflectance test is a single channel test whose strength is discriminating bright clouds over low reflective surfaces and weakness is trying to detect clouds over more highly reflective surfaces. Three different channels are used in this test depending on the ecosystem. Band M1 is used for non-polar desert (Hutchison and Jackson, 2003) and semi-arid ecosystems in conjunction with the M5 (0.67- μm) band for all other non-water cases under which the visible reflectance test is executed (Hutchison et al., 2005). The M7 (0.87- μm) reflectance test is applied over oceans with separate thresholds applied to sun glint and no sun glint regions. The M7 test is also applied to inland water surfaces using the threshold for sun-glint regions since inland water features may be shallow and more highly reflective. In addition, a TOA NDVI criterion is used to determine if the inland water surface, based upon the land/water mask, does indeed contain water or is contaminated with land. If the TOA NDVI exceeds a small value, currently taken as 0.2 (tunable), the M7 test is not applied since false alarms will occur over cloud-free vegetation regions.

The M1, M5, and M7 Reflectance tests employ dynamic thresholds that vary with the sun-Earth-satellite scattering geometry. The minimum value of these thresholds are listed in Table 12, Table 13, and Table 14. Over non-desert, non-snow land surfaces and coasts, M5 thresholds are derived using the scattering angle and TOC NDVI as shown in Figure 13 for the 10, 0.1 TOC NDVI bins. Over high NDVI (> 0.65) land surfaces the thresholds are applicable for scattering angles greater than 90 degrees. However, when TOC NDVIs are low (typically, TOC NDVIs < 0.20), improved contrast between the cloud and background is achieved using the M1 band, as shown in Figure 14. Therefore, the VCM uses the M1 reflectance rather than M5 values for TOC NDVI in the 0-0.2 range; however, these thresholds are currently based upon the M5, not the M1 band.

The M7, M5 and M1 thresholds, including high, medium and low clear sky confidence thresholds are calculated using a three-degree polynomial as a function of scattering angle. Over

land, the coefficients of the polynomial are a function of TOC NDVI and tuned for the specific band, M1 or M5. The number of coefficient sets required is driven by the quantization of the TOC NDVI range of 0.0 to 1.0. In application, TOC NDVI bin widths of 0.1 appear to be sufficient. Over ocean and inland water surfaces, the coefficients of the polynomial vary with the presence or absence of sunglint. Thresholds for inland water are the same as ocean sunglint. A determination of the RM5 thresholds for the 0.2 – 0.3 TOC NDVI bin is shown below:

$$\text{RM5 Low Cloud-free Confidence (Cloudy) Threshold} = 142.66293706 - 2.57860528x + 0.01773252x^2 - 0.00003685x^3$$

$$\text{RM5 Clear/Cloudy Threshold} = 122.19090909 - 2.32652292x + 0.01659848x^2 - 0.00003681x^3$$

$$\text{RM5 High Cloud-free Confidence (Clear) Threshold} = 99.13076923 - 2.00907925x + 0.01492075x^2 - 0.0000353135x^3,$$

where x is the scattering angle in degrees. Final thresholds are determined by linearly interpolating between values from the nearest two TOC NDVI bins.

Table 12. Minimum values of the variable thresholds used for Ref_{M1} test for low cloud in the VCM algorithm

Ref _{M1}			
Surface	Confident Cloudy	Clear/Cloudy Threshold	Confident Clear
Desert (non-polar)	0.40	0.35	0.30

Table 13. Minimum values of the variable thresholds used for Ref_{M5(M1)} test, correspond to TOC NDVI interval 0.9-1.0

Ref _{M5(M1)}			
Surface	Confident Cloudy	Clear/Cloudy Threshold	Confident Clear
Day Land & Coast	Dynamic	Dynamic	Dynamic

Table 14. Minimum values of the variable thresholds used for Ref_{M7} test for cloud in the VCM algorithm

Ref _{M7}			
Surface	Confident Cloudy	Clear/Cloudy Threshold	Confident Clear
Day Ocean (no sun glint)	0.11	0.09	0.07
Day Ocean (sun glint); Inland Water	0.30	0.27	0.24

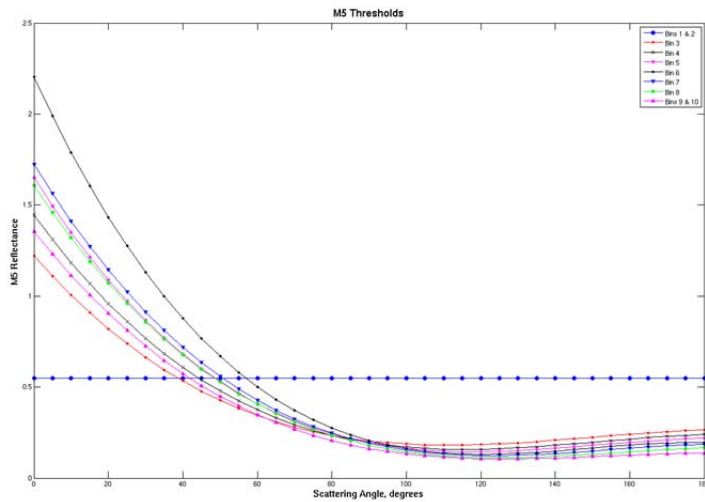


Figure 13. Dynamic thresholds for M5 reflectance test for 10 TOC NDVI bins as a function of scattering angle.

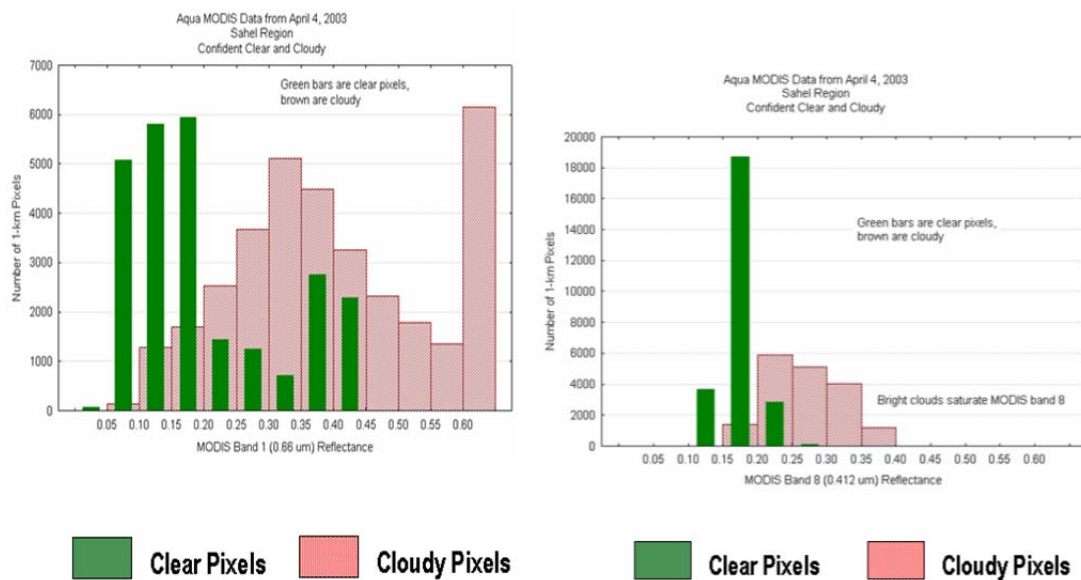


Figure 14. Discrimination between clear (green) and cloudy (red) pixels over Sahael Africa as a function of NDVI for MODIS equivalent of VIIRS M5 band (left) and M1 band (right).

3.4.3.6 Visible Reflectance Ratio Test (M7/M5)

The reflectance ratio test uses channel M7 divided by channel M5 ($Ref_{0.865\mu m} / Ref_{0.672\mu m}$) over ocean. This test makes use of the fact that the spectral reflectance at these two wavelengths is similar over clouds (ratio is near 1) and decreases markedly over cloud-free ocean surfaces due to the increased affect of Rayleigh scattering on the M5 band. Using AVHRR data this ratio has been found to be between 0.9 and 1.1 in cloudy regions over ocean but can become lower with decreases in solar illumination as shown in Figure 15.

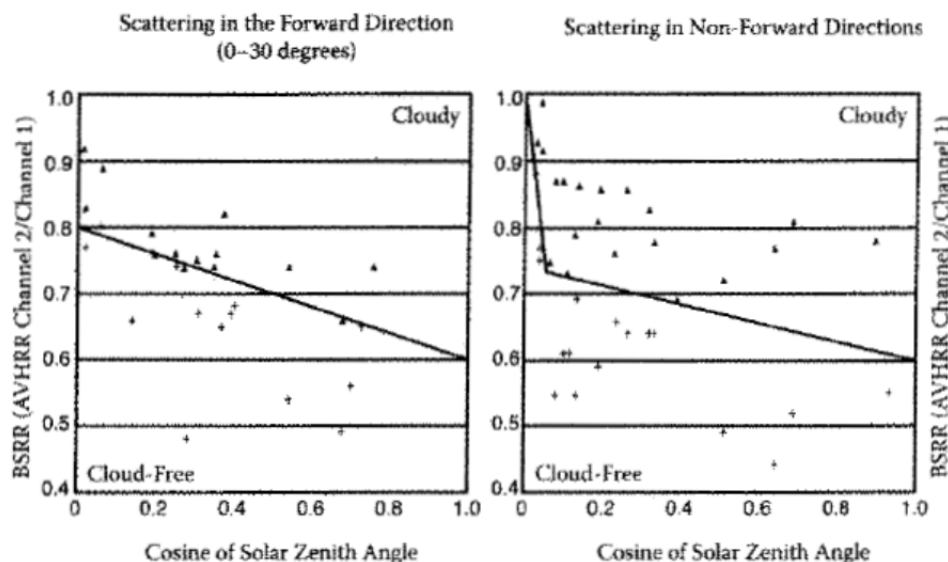


Figure 15. Bispectral reflectance ratio in the forward (left panel) and non-forward (right panel) scattering directions for optically thick clouds (\blacktriangle) over ocean surfaces as a function of the cosine of solar zenith angle (from Hutchison and Hardy, 1995, *Int. J. Rem. Sensing*, 16, 3665-3680).

In the absence of clouds, this test can produce false alarms over pixels classified as ocean but containing a mixture of ocean and vegetated land (i.e., sub-pixel islands). Therefore, two sets of clear/cloudy, high clear-sky confidence and low clear-sky confidence thresholds are used – one for “all ocean” and one for “partial land”. As shown in Table 15, this scenario is further divided into threshold sets for glint/no glint conditions. Cloud-free is indicated if the ratio is less than the “all ocean” confidently clear threshold or greater than the “partial land” confidently clear threshold. For overlapping confidently cloudy thresholds (i.e., the “all ocean” confidently cloudy threshold is greater than the “partial land” confidently cloudy threshold), a cloud is indicated if the ratio is between the clear/cloudy threshold and the confidently cloudy threshold. Figure 16 shows the effect of the threshold settings on the cloud confidence classification. For this example, the first index represents the “all ocean” case while the second index represents the “partial land” case.

Over land, a pseudo GEMI Index is used in place of the M7/M5 ratio, where reflectance values range from 0-1. This pseudo GEMI Index is defined by the equation:

$$\text{GEMI} = G * (1.0 - 0.25 * G) - \frac{100 * \text{Ref}_{M5} - 0.125}{1.0 - 100 * \text{Ref}_{M5}}$$

where

$$G = \frac{200 * (\text{Ref}_{M7} - \text{Ref}_{M5}) + 150 * \text{Ref}_{M7} + 50 * \text{Ref}_{M5}}{100 * \text{Ref}_{M7} + 100 * \text{Ref}_{M5} + 0.50}$$

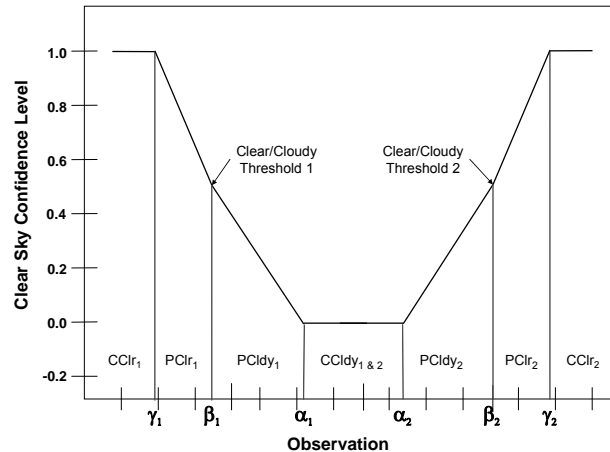
The GEMI test was developed for use in semi-arid environments where the straight ratio often fails (Pinty and Verstraete, 1992) as discussed below. This pseudo GEMI test was developed for the MODIS Airborne Simulator (MAS) and the thresholds listed on the “Day Land” line of Table 15 are appropriate for this version of the test. To eliminate false alarms which can occur over cloud-free pixels of mixed land and water, this test is not used unless the M5 reflectance exceeds

0.1. Future work will include the revision of this test to the true GEMI Index which is expected to provide more consistent cloud detection results from nadir to limb and between wet and/or aerosol-laden atmospheres vs. dry and/or clean atmospheres.

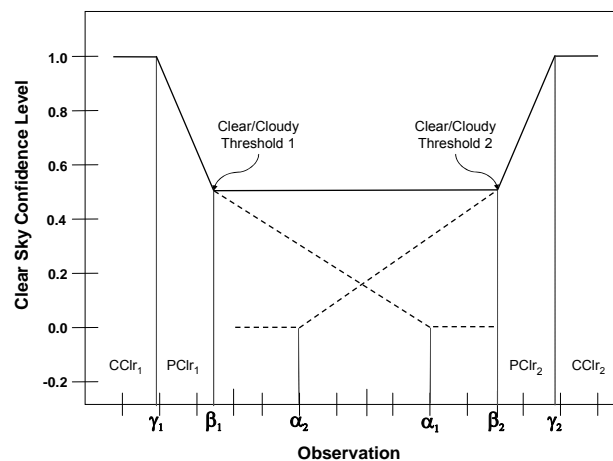
Table 15. Thresholds used for Ref_{M7}/Ref_{M5} test for cloud in the VCM algorithm

Ref_{M7}/Ref_{M5}			
Surface	Confident Cloudy	Clear/Cloudy Threshold	Confident Clear
Day Land*	1.78	1.82	1.87
<i>No Glint</i>			
Day Ocean (partial land, no sun glint)	1.00	1.05	1.10
Day Ocean (all ocean, no sun glint)	1.05	0.99	0.94
<i>Glnt</i>			
Day Ocean (partial land, sun glint)	1.02	1.06	1.10
Day Ocean (all ocean, sun glint)	1.05	1.00	0.95

*This test uses the GEMI Index.



a) No overlap between Confident Cloudy Thresholds ($\alpha_2 \geq \alpha_1$)



b) Overlap between threshold ranges ($\alpha_2 < \alpha_1$ and $\beta_2 > \beta_1$)

Figure 16. Behavior of Dual Cloud Confidence Threshold Sets for M7/M5 Over Ocean

Figure 17 illustrates some of the complexities of desert ecosystems as demonstrated by the visible reflectance ratio. The observations are from the AVHRR on the NOAA-9 and are over the Arabian Sea, the Arabian Peninsula, and surrounding regions. The figure shows histograms of reflectance ratio values for coastal/water scenes, as well as desert and more densely vegetated areas in the Persian Gulf region from approximately 15-25° N latitude and 50-70° E longitude. Almost all of the observations recorded in the histograms were from clear-sky conditions, as determined by inspection of visible and IR imagery. As suggested by the histograms of $\text{Ref}_{M7}/\text{Ref}_{M5}$, clear-sky ocean scenes have a ratio of less than 0.75. The surface type classifications are from the Olson World Ecosystems data set. One can immediately see that clear-sky desert values of the visible reflectance ratio cover a large range of values, including values one might normally associate with cloudy skies over vegetated surfaces. Also, note the large amount of overlap between the desert and shrub/grassland categories. This figure shows that clear-sky spectral threshold tests need to be applied very carefully in arid regions and also points out the need for high-resolution ecosystem maps. This test will not be performed over

desert, semi-desert, snow/ice, or some agricultural ecosystems. In addition to land, this reflectance ratio test may be performed over water during the daytime. These thresholds are based on analysis of AVHRR LAC and GAC data and the APOLLO algorithm.

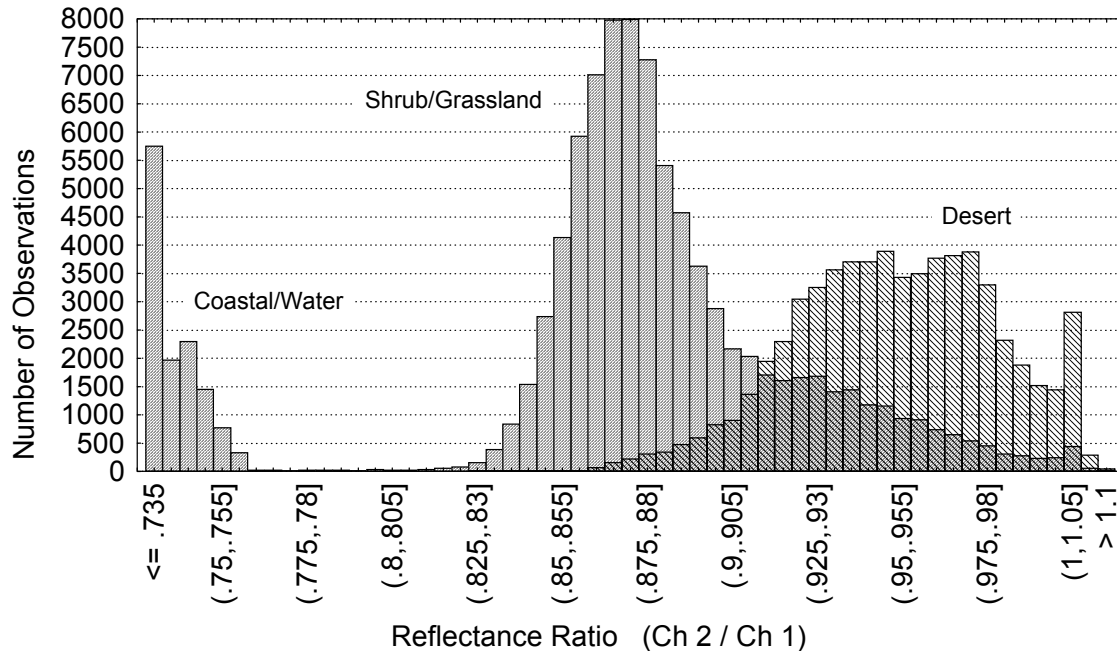


Figure 17. Histogram of the frequency of occurrence of the AVHRR reflectance ratio $R_{0.86}/R_{0.63}$ for a scene over the Arabian Peninsula and Arabian Sea

3.4.3.7 Visible (Ref_{M9})

VIIRS band M9 ($1.38 \mu\text{m}$) will use reflectance thresholds on a per pixel basis to detect the presence of thin cirrus cloud in the upper troposphere under daytime viewing conditions as well as mid-tropospheric level water clouds. The strength of this cloud detection channel lies in the strong water vapor absorption in the $1.38 \mu\text{m}$ region; however, this water vapor absorption band is very narrow (Valvoci, 1978; Gao et al., 1993). Thus, the VIIRS sensor is designed with a bandpass of 15-nm, compared to 30-nm of MODIS, to ensure contamination from surfaces does not impact this test. However, out-of-band responses in the VIIRS sensor, if they occur, can degrade the value of this test to the VCM. With sufficient atmospheric water vapor present (estimated to be about 0.4 cm precipitable water) in the beam path, no upwelling reflected radiance from the Earth's surface reaches the satellite (Hutchison and Choe, 1996). Since 0.4 cm is a small atmospheric water content, most of the earth's surface will indeed be obscured in this channel. With relatively little of the atmosphere's moisture located high in the troposphere, high clouds appear bright; reflectance from low and mid level clouds is partially attenuated by water vapor absorption. Ben-Dor (1994) analyzed a scene from the Airborne Visible Infrared Imaging Spectrometer (AVIRIS) to demonstrate that thin cirrus detection using $1.38 \mu\text{m}$ observations may be more difficult for elevated surfaces, dry atmospheric conditions, and high albedo

surfaces in this band. New injections of volcanic aerosols into the stratosphere may also impact this test.

The addition of the total integrated water vapor calculation to the algorithm allows this test to be bypassed for low values of TPIWV (less than or equal to 0.25 cm). Currently this enhancement has only been implemented for the daytime desert stratification processing path. Given the sensitivity to thin high clouds, the VIIRS 1.38 μm channel may detect much larger cloud coverage than previous satellite algorithms have indicated. Table 16 lists the thresholds used for the Ref_{M9} test.

Table 16. Thresholds used for Ref_{M9} test for cirrus cloud in the VCM algorithm

Ref _{M9}			
Surface	Confident Cloudy	Clear/Cloudy Threshold	Confident Clear
Day Land, Coastal, Ocean, Desert, Snow	0.040	0.035	0.030

3.4.3.8 Infrared (BT_{M15}-BT_{M16})

This BT difference test is used to detect cirrus clouds during the day and night over all surface types except that of snow/ice. (It also detects edge of water clouds, i.e. sub-pixel clouds.) The thresholds are dependent on the satellite zenith angle and BT_{M15} (Saunders and Kriebel, 1988). Table 17 lists the clear/cloudy look-up table for this test, which was developed using a radiative transfer model (Berk et al., 1989) for mid-latitude atmospheric conditions. Results of this test for manually-generated cloud fields of thin cirrus and adjacent cloud-free regions, coincident with radiosonde observations, are shown in Figure 18 (Hutchison et al., 1995).

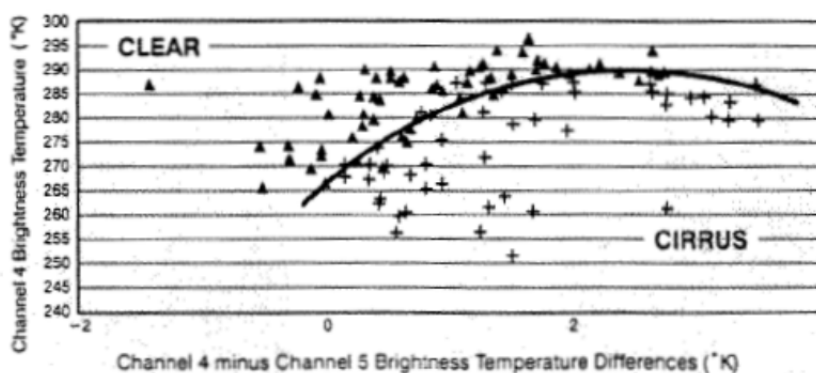


Figure 18. Brightness temperature differences between AVHRR channel 4 (10.8- μm) minus channel 5 (12.0- μm) versus channel 4 brightness temperatures, as described by Saunders and Kriebel (1988), for cloud-free pixels (\blacktriangle) and cirrus cloudy pixels (+), (from Hutchison et al., 1995).

To obtain the clear/cloudy threshold for this test, a bi-dimensional linear interpolation of values in Table 17 must be performed. (Currently, if the BT_{M15} exceeds the range of values shown in the table, the BT_{M15} is set to the minimum or maximum range value. In addition, if the secant of the satellite zenith angle is outside the range shown in the table, it too will be set to the lower

or upper limit of the range.) The confident cloudy threshold can be found by adding an incremental quantity to the clear/cloudy threshold, and the confident clear threshold can be found by subtracting the incremental quantity from the clear/cloudy threshold.

Table 17. Clear/Cloudy temperature thresholds in Kelvin for BT_{M15} - BT_{M16} cloud detection test at mid-latitudes

BT_{M15}	secant(satellite zenith angle)				
	1.0	1.25	1.50	1.75	2.0
260K	0.55	0.60	0.65	0.90	1.10
270K	0.58	0.63	0.81	1.03	1.13
280K	1.30	1.61	1.88	2.14	2.30
290K	3.06	3.72	3.95	4.27	4.73
300K	5.77	6.92	7.00	7.42	8.43
310K	9.41	10.74	11.03	11.60	13.39

The Saunders and Kriebel Thin Cirrus test has been successfully applied with many satellite sensors under global conditions. Since water vapor has a spectral signature similar to ice clouds, as shown in Figure 7, this test can create false alarms in more humid atmospheres and allows leakage in drier conditions. Thus, possible future enhancements to this test are using corrections applied as a function of total precipitable water (TPW). It is unclear at this time if current numerical models can forecast TPW with sufficient accuracy to use as a correction to this test.

3.4.3.9 High Cloud Test ($BT_{M12} - BT_{M16}$)

This window brightness temperature difference test is currently applied during the nighttime over all surface types except water. It is not applied if BT_{M12} is less than 230 K due to calibration uncertainties in the M12 band.

The original implementation of this cloud test stated that the test is useful for separating thin cirrus from cloud free condition and is insensitive to the amount of water vapor in the atmosphere. Thus, the current implementation of the test employs the single set of thresholds listed in Table 18.

Table 18. Thresholds used for $BT_{M12} - BT_{M16}$ test for high cloud in the VCM algorithm

$BT_{M12}-BT_{M16}$			
Surface	Confident Cloudy	Clear/Cloudy Threshold	Confident Clear
Night Land & Desert & Coast	4.50	4.00	3.50
Night Snow	4.50	4.00	3.50

The current implementation of this cloud test is incorrect based upon the results from (Hutchison et al., 1995) shown in Figure 19. With the current implementation, false alarms are expected in nighttime data collected over the more humid region, like the tropics, while leakage should occur in more dry regions such as the polar regions or lower-latitude areas experiencing the winter season. Improved detection of clouds in nighttime data should be achievable using the function shown in Figure 19 as the midpoint of a threshold that varies with precipitable water. In addition, the test should be highly useful over water backgrounds, not just land surfaces since the figure shows a brightness temperature difference of zero at the lowest level of precipitable water, indicative of a black-body surface in these bands.

The pre-launch tuning of the VCM algorithm using global synthetic data, during August 2011, confirmed that the M12-M16 brightness temperature differences varied by almost 10K for TPW values between the range of 10-100 kg m⁻² of moisture as indicated in this figure. As a result, no attempt was made to tune the thresholds for this test and it was recommended that the test be modified so the thresholds vary with path corrected TPW values. It is also recommended that the test be used over ocean backgrounds, which is not currently the case.

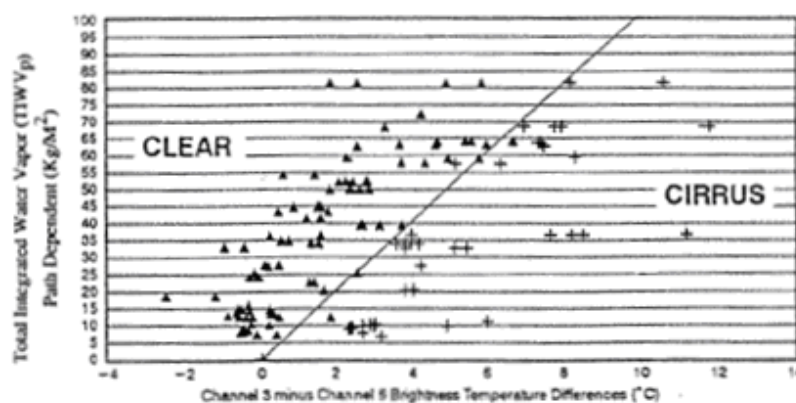


Figure 19. Brightness temperature differences between AVHRR channel 3 (3.75- μm) minus channel 5 (12.0- μm) and total precipitable water (path) for cloud-free pixels (\blacktriangle) and cirrus cloudy pixels (+) shows detection threshold is highly sensitive to water vapor in the atmosphere (from Hutchison et al., 1995).

3.4.3.10 Imagery Resolution Spatial Tests

Spatial tests based upon imagery channels provide a straightforward approach to reduce leakage in the VCM over ocean surfaces. These tests are applied both in daytime and night-time conditions using high (375-m) resolution imagery data in the 0.865-, 3.74- and 11.45- μm band passes. Spatial tests with the I2 channel (0.865- μm band) and I4 channel (3.74- μm band) are used to detect water clouds during the daytime and night-time conditions respectively, while the I5 channel (11.45- μm band), is used to detect edges of cirrus clouds. Due to calibration uncertainty, the I4 is not used if $BT_{I4} < 270 \text{ K}$.

The water (I2 or I4) cloud and ice (I5) cloud tests are performed in succession and referred to as the Max/Min test and the Mean test. The flow diagram in Figure 20 shows how the spatial uniformity tests can affect the final cloud confidence classification. The primary spatial uniformity test is the Max/Min test and all confident clear (solid arrows in Figure 20) and probably clear pixels (dashed arrows) over water are subjected to it. If the difference between the maximum and minimum of either the I-band reflectance or brightness temperature values is greater than a predetermined threshold, the moderate resolution pixel is considered to possess substantial variance likely to be the result of the presence of a cloud in the moderate resolution field-of-view. The I4 and I5 brightness temperature thresholds are both 0.5-K and the I2 reflectance threshold varies with viewing geometry. It is important to note that all confident clear pixels that pass the Max/Min test are relabeled as either probably clear or probably cloudy. The Mean test is only performed on pixels that pass the Max/Min test as defined by showing high imagery resolution reflectance or brightness temperature variance. Pixels that do not pass the Max/Min tests do not have their cloud confidence altered. The Mean test compares the mean of the four imbedded imagery resolution reflectance or brightness temperatures ($Mn4$) to the mean of the two imbedded imagery resolution pixels that have been identified as the maximum and minimum reflectances or brightness temperatures ($Mn2$). If the I2 reflectance (I4 or I5 brightness temperature) $Mn4$ value is greater (less than) than the $Mn2$ value, clouds are suspected to be present in the majority of the four imagery resolution pixels and the probably cloudy classification is assigned to that moderate resolution pixel. Otherwise, the probably clear assignment is made. This Mean test is important for determining the binary cloud mask in which the clear and cloudy distinction is made between the probably clear and probably cloudy cloud confidences. It must be noted that no addition of confident cloudy pixels can occur due to the results of the spatial uniformity tests.

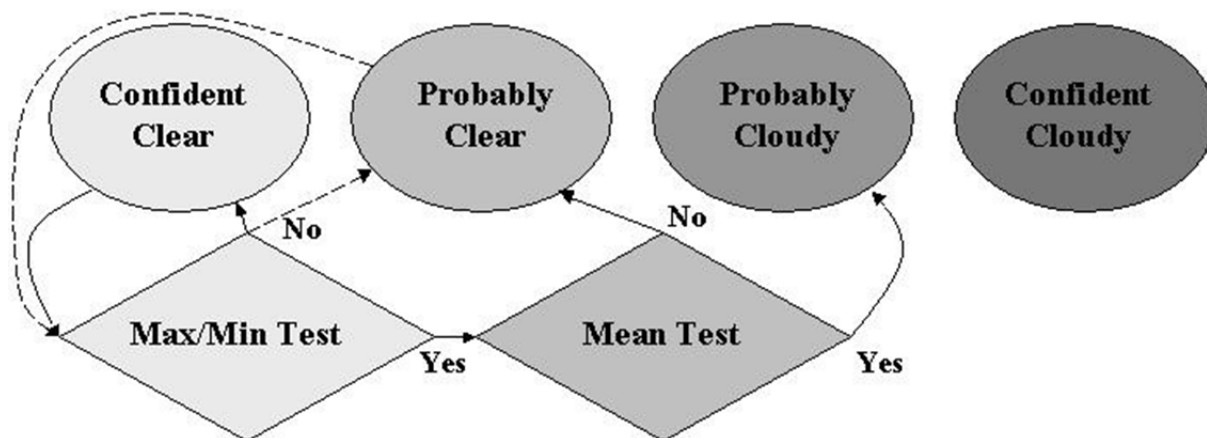


Figure 20. Flow diagram describing the spatial uniformity testing effects on cloud confidence.

The concept of using a spatial test to detect cloudy pixels over all ocean conditions, including sun glint regions, was prototyped and results compared against a subset of the MODIS granules. The prototype used the MODIS M13 band (0.667- μm) in daytime conditions since its 500m resolution nests within the 1 km MODIS channels in a manner similar to that planned for use with the VIIRS imagery and radiometry bands. Spatial tests based upon the 1 km resolution 3.74- μm and 11.45- μm bands were also prototyped for use in night-time conditions; however, results obtained from applying these tests are biased strongly toward false alarms, since a large area is affected by the tests. These thresholds will be updated pre-launch using global synthetic data. Once VIIRS imagery data become available with the NPP launch, all spatial tests will be applied with the same logic.

Results from the analysis of the three scenes consisting primarily of ocean surfaces, both without (original VCM) and with the spatial tests, are presented in **Error! Reference source not found.** These statistics show that leakage is reduced with the spatial tests, especially in sun glint regions (Hutchison et al., 2005).

Table 19. Results from analyses of MODIS data in and outside sun glint regions with and without spatial tests.

MODIS Scenes/Sun Conditions	Leakage Rate Without (With) Spatial Tests
Scene 20012131210 (All Pixels)	0.313 (0.0003)
Water Day Sun Glint	0.519 (0.0006)
Water Day No Sun Glint	0.033 (0.0000)
Scene 20012131210 (All Pixels)	0.0904 (0.0118)
Water Day Sun Glint	0.1974 (0.0122)
Water Day No Sun Glint	0.0360 (0.0116)
Scene 20012131210 (All Pixels)	0.1793 (0.0064)
Water Day Sun Glint	0.2991 (0.0083)
Water Day No Sun Glint	0.0656 (0.0028)

3.4.4 The VCM Cloud Phase Algorithm

Cloud phase is determined for all pixels that have a cloud confidence of Confidently Cloudy or Probably Cloudy. If the cloud confidence is classified as Probably Clear, the cloud phase is set to Partly Cloudy. An initial cloud phase analysis is based solely upon the cloud top temperature of each pixel. Next, a series of spectral tests are used to identify the presence of overlap, i.e. thin cirrus over lower-level water clouds in a single VIIRS pixel. Knowledge about cloud overlap is critical to other downstream cloud algorithms, since radiative transfer theory for the retrieval of these cloud properties is based upon an assumption that only a single cloud layer exists within any given pixel. Thus, the existence of overlap conditions suggests a degradation in the downstream cloud products. Finally, rules are applied to correct for known errors in this existing logic. The discussion starts with the initial cloud phase classification that is made from the observed cloud top temperature.

3.4.4.1 Initial Determination of Cloud Phase

The process by which water droplets or ice crystals form on nuclei is called heterogeneous nucleation while their formation in a pure (sterile) environment is referred to as homogeneous nucleation. Theoretical calculations and experimental measurements show that small water droplets freeze spontaneously in a sterile environment as the temperature drops to about -40C or about 233K. However, in the less sterile atmosphere, ice crystals usually begin to form as cloud temperatures reach about 258K, although natural clouds have been observed to contain some liquid droplets at temperatures approaching -40C (Rogers, 1976). Thus, the cloud phase algorithm uses cloud top temperatures to make initial classifications of cloud phase based upon M15 brightness temperatures. This initial cloud phase classification is made using the thresholds shown in Table 20.

Table 20. Initial cloud top phase classifications based upon M15 brightness temperatures.

M15 Brightness Temperature	Initially Cloud Top Phase
$BT_{M15} \leq 233.16 \text{ K}$	Opaque Ice (certain)
$233.16 \text{ K} < BT_{M15} \leq 253.16 \text{ K}$	Opaque Ice
$253.16 \text{ K} < BT_{M15} \leq 273.16 \text{ K}$	Mixed
$273.16 \text{ K} < BT_{M15}$	Water

Next, the cloud phase algorithm assesses the possibility that multiple clouds exist within a single field of view, i.e. overlap conditions are present. Different approaches are used with daytime and nighttime data. The methodology used during daytime conditions is described in Pavolonis and Heidinger (2004) while the nighttime approach is described by Pavolonis and Heidinger (2005). Both are highlighted in this document.

3.4.4.2 Identification of Cloud Overlap

The VIIRS cloud phase algorithm applies a series of tests to predict if overlap is present. If a given pixel passes any of these test groups, it is assumed that cloud overlap is present.

3.4.4.2.1 Split Window Longwave IR Test for Cloud Overlap

The Split Window Longwave IR Test uses the 11- μm (M15) minus the 12- μm (M16) brightness temperature difference ($BT_{M15}-BT_{M16}$) along with the visible reflectance in the M5 (0.6- μm) band to identify cloud overlap in daytime conditions.

Radiative transfer model (RTM) calculations (Pavolonis and Heidinger, 2004) have shown that, for optically-thin, single layered ice clouds, the $BT_{M15}-BT_{M16}$ feature has a maximum at cloud optical depths of about 2 and then decreases abruptly with increases in optical depth before it approaches some asymptotic value, as shown in Panel (a) of Figure 21. On the other hand, this brightness temperature difference decreases slowly and continuously for water clouds. Multi-layer clouds have been observed to exhibit a relationship that cannot be modeled using single layer clouds, as shown by the solid black line in Panel (a). Thus, the presence of overlap clouds can be determined using this Split Window Longwave IR Test. The actual implementation of this test in the VCM algorithm relies on the visible reflectance in the M5 (0.6- μm) band, as a surrogate for cloud optical depth. In this implementation, the test classifies a pixel as “overlap” if the $BT_{M15}-BT_{M16}$ feature is above the threshold shown in Panel (b) of Figure 21, implying the presence of thin cirrus, when the visible reflectance is greater than 30%, which indicates the presence of a lower-level water cloud.

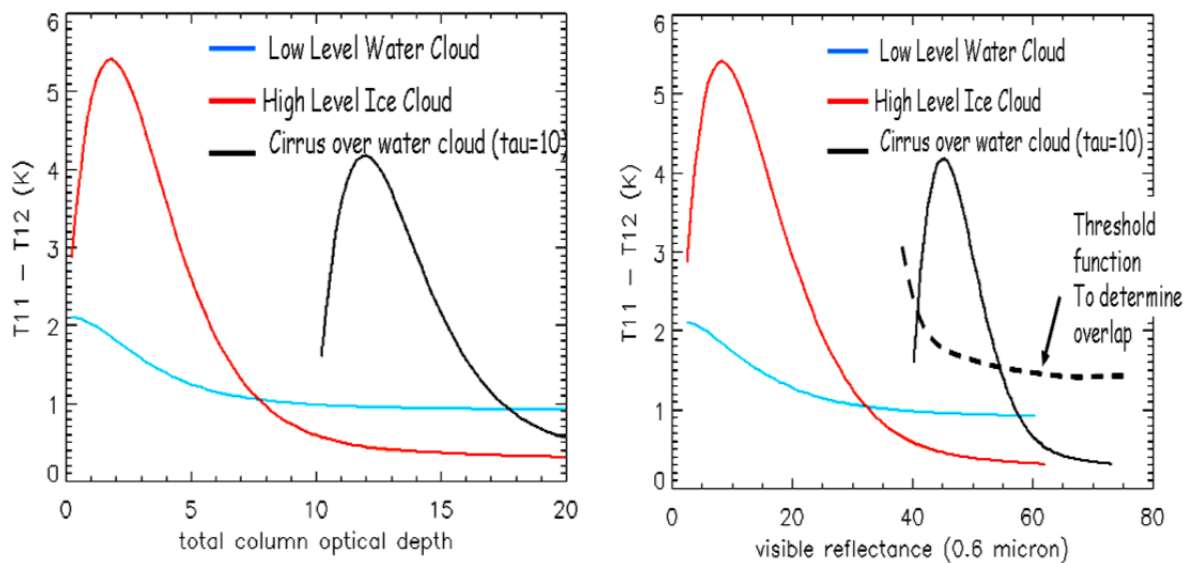


Figure 21. RTM simulations of the 11- μm minus 12- μm brightness temperature differences as a function of cloud phase, optical depth, and visible reflectance in the 0.6- μm band.

Actual thresholds vary with several parameters (solar zenith angle, viewing angle) and are depicted in Figure 22, which shows the results of radiative transfer model simulations for a single atmospheric profile (typical of the mid-latitude summer), solar zenith angle of 30-degrees, and viewing zenith angle of 11-degrees. Calculations were made of 0.65- μm reflectance and the brightness temperature difference between 11- and 12- μm as a function of visible cloud optical depth for several cloud types. One was a single-layer water cloud, another a single-layer ice cloud, and finally an ice cloud overlapping a water cloud. The optical depth of the single-layer water cloud and the water cloud used in the cloud overlap simulations ranges from 1.0 to 20.0.

The optical depth of the single-layer ice cloud ranges from 0.1 to 20.0. The boldface line without symbols represents the function used to determine the split-window brightness temperature difference threshold used in the cloud overlap detection algorithm. It was determined by fitting a fourth-degree polynomial to model output.

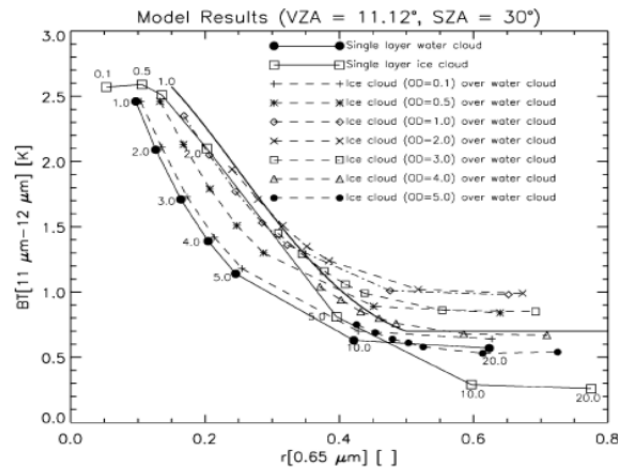


Figure 22. Results from RTM calculations of 0.65- μm reflectance and the brightness temperature difference between 11- and 12- μm for single-layer water clouds, single-layer ice cloud, and ice cloud overlapping a water cloud as a function of optical depth. The boldface line without symbols represents the function used to determine the split-window brightness temperature difference threshold used in the cloud overlap detection algorithm. (Figure 1 from Pavolonis & Heidinger, 2004).

The following are limitations to the successful detection of overlap conditions with this spectral test.

- Cloud optical depths out of range. Overlap is most evident from single-layered clouds when the visible optical depth of the high ice cloud is equal to 1 or 2 and the optical depth of the lower water cloud is 5 or greater, as shown in Figure 21. According to Wylie and Menzel (1999), most of the clouds located above 6-km in the tropics and mid-latitudes have a visible optical depth between 0.5 and 1.8. In addition, most lower-level clouds have a visible optical depth greater than 6. Thus, this test should be effective at detecting overlap under a wide range of conditions. However, if the visible optical depth of the ice cloud is less than about 0.5 or greater than about 3, the distinction between the cloud overlap and either of the single-layered cases is reduced, regardless of the optical depth of the lower water cloud. As a result, more optically thick ice clouds will be classified as opaque cirrus.
- Thin cirrus clouds that overlie a bright land surface, e.g. desert, could be misclassified as cloud overlap. As a result, the M5 reflectance must be at least 0.30 (30%) to help avoid these misclassifications.
- A single layer of broken water clouds or the edge of a water cloud often will have a large split-window brightness temperature difference (Hutchison et al., 1995) and a visible reflectance greater than 0.30 (30%). However, sub-pixel water clouds will have a M15 brightness temperature that is greater than 270 K. Thus, cloud overlap

is not allowed unless the TB_{M15} is less than 270 K. This condition may sometimes cause high thin cirrus overlying low water cloud to be missed.

- Another problem occurs when a thin cirrus cloud overlies a snow or ice surface. Both the visible reflectance and the split-window brightness temperature differences can be large enough to pass the cloud overlap test. Thus, this test cannot be applied over pixels that are classified as snow/ice by the VCM.

3.4.4.2.2 Near-IR Test for Cloud Overlap

The Near-IR Test uses reflectance values in the 1.65- μm (M10), 1.38- μm (M9), and 0.65- μm (M5) bands to identify overlap conditions. The test is only applied with data collected during Daytime conditions.

In the 1.65- μm region of the spectrum, ice particles absorb radiation much more strongly than water particles (Pilewskie and Twomey 1987). Thus, the radiation reflected back to the satellite in the M10 band will be greater when an optically thick water cloud is present compared to an optically thick ice cloud. Furthermore, in the 1.38- μm region, water vapor is a strong absorber of radiation, and so the radiation detected by a satellite at this wavelength will mainly be from the upper troposphere, unless the atmosphere is very dry. Because of this fact, the M9 band is very effective at detecting thin cirrus clouds (Gao et al. 1993). Thus, if both the reflectances in the M10 and M9 bands exceed some specified thresholds, there is a good possibility that both a high ice cloud and a lower water cloud are present in a given satellite field of view.

Model simulations were again performed (Pavolonis and Heidinger, 2004) in order to determine the difference in the relationship between reflectances in the M10 and M9 for a single-layer water cloud, a single-layer ice cloud, and an ice cloud overlapping a water cloud. The results are shown in Figure 23 for clouds of varying optical thickness values over ocean surfaces [Panel (a)] and grassy land surfaces [Panel (b)]. In this figure, the solar zenith angle is 30-degrees, the viewing zenith angle is 10-degrees, and the relative azimuth angle is 90-degrees. Calculations were performed for many different combinations of viewing and illumination angles so that the M10 and M9 thresholds that define cloud overlap conditions are grouped by scattering angle. Bins of 10-degree were chosen, and so there are 18 different functions that determine the M10 reflectance threshold with respect to the M9 reflectance value.

The M9 reflectance threshold was set to a constant value of 0.025 (2.5%) for all scattering angles over a water surface. The threshold functions were determined in the same manner as for the SWBTD test. A somewhat conservative approach was used to determine the 1.38- μm threshold to help to prevent the false detection of cloud overlap. For instance, upon analyzing several MODIS scenes it was found that the 1.38- μm reflectance of many single-layer midlevel clouds will often fall in the 2.0%–2.5% range. Also, even low clouds can have a 1.38- μm reflectance of 2.0% or greater if the overlying atmosphere is sufficiently dry. This especially occurs at higher latitudes.

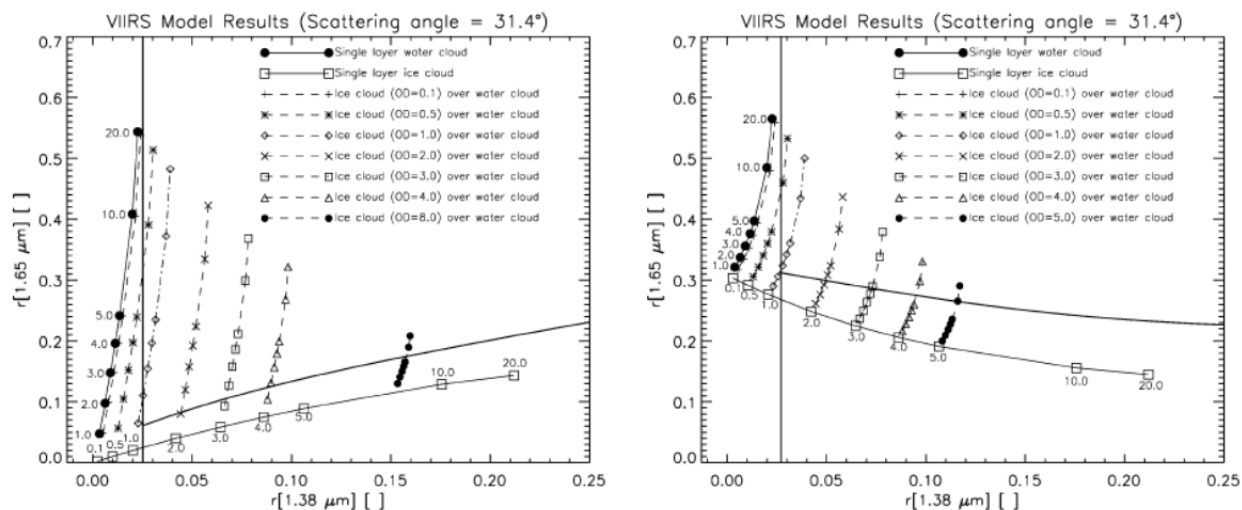


Figure 23. Results from RTM calculations of reflectances in the 1.65- μm and 1.38- μm bands for clouds of varying optical thickness values over ocean surfaces in Panel (a) and grassy land surfaces, shown in Panel (b) using a relative scattering angle of 31.4 degrees. (Figure 2 from Pavolonis & Heidinger, 2004)

The following are limitations to the successful detection of overlap conditions with this spectral test:

- RTM simulations indicate that this test should be effective at detecting cloud overlap when the visible optical depth (τ) of the ice cloud is within the range $1 < \tau < 8$. More optically-thin ice clouds may go undetected. Additionally, if the lower water cloud has an optical depth of 10 or greater, cloud overlap may be detected even if the ice cloud has an optical depth greater than 8.
- It is more difficult to distinguish between cloud overlap and a single layer ice cloud for some optical depth combinations when the underlying land surface has a high M10 reflectance since the surface and the water cloud may have similar reflectance values in this band. As a consequence, the M10/M5 ratio is used to ensure the surface is not bright in the M10 band. Pixels analyzed with this test must have a ratio of less than one.

3.4.4.2.3 MW- LW-IR Test for Cloud Overlap

The MW- LW-IR Test uses the Split Window Longwave IR approach, involving the $BT_{M15} - BT_{M16}$ feature with a derived or pseudo-emissivity (EMS in the 3.75- μm band, to identify cloud overlap at night. This 3.75- μm pseudo-emissivity or EMS[3.8] is calculated using the radiance in this band in a ratio to the radiances that would be generated by a blackbody at temperature equivalent to the 11- μm brightness temperature, in a manner described in Section 3.4.4.3 Implementation of the Cloud Phase Algorithm.

This cloud overlap test is applied only with nighttime data. Water clouds with an optical depth of 5 or greater generally have a 3.75- μm emissivity less than unity. Semitransparent clouds (such as cirrus) have an apparent emissivity much greater than unity because the emissivity computation

does not properly account for transmission. Therefore, this derived emissivity can be used with the $BT_{M15} - BT_{M16}$ feature to identify overlap conditions in a manner similar to that described by the Split Window Longwave IR Test.

Figure 24 shows results of simulations between the $BT_{M15} - BT_{M16}$ feature the derived $3.75\text{-}\mu\text{m}$ emissivity, i.e. $EMS[3.8]$. The simulations results vary with atmospheric profile and viewing geometry. Those shown below apply to a viewing angle of 11.12 degrees and a temperature profile characteristic of a tropical atmosphere with a total column precipitable water of 7 cm. Single layer water and ice clouds of varying optical depths and ice clouds of varying optical depths overlapping water clouds of various optical depths are shown. All ice (water) clouds have a cloud top pressure of 200 (800) hPa. The $BT_{M15} - BT_{M16}$ feature generally decreases with increasing cloud optical depth for all clouds shown. The $EMS[3.8]$ feature is less than unity for water clouds and has a maximum for a single layer ice cloud of optical depth 4.0 . The cloud overlap results have reduced $BT_{M15} - BT_{M16}$ and $EMS[3.8]$ values compared to single layered ice clouds. The overlap results also have a distinctly higher $EMS[3.8]$ than water clouds, except when the overlying ice cloud is very thin (e.g. optical depth of 0.1 or less). The distinction between single layer clouds and multilayered clouds is greatest when the optical depth of the lower liquid water cloud is 20.0 or greater. While the overlap results are similar to single layer results when the overlying ice cloud optical depth is 0.1 or less or 5.0 or greater, these simulations indicate that certain multilayered cloud systems should be identifiable at night using a technique that combines the use of $BT_{M15} - BT_{M16}$ and $EMS[3.8]$ values.

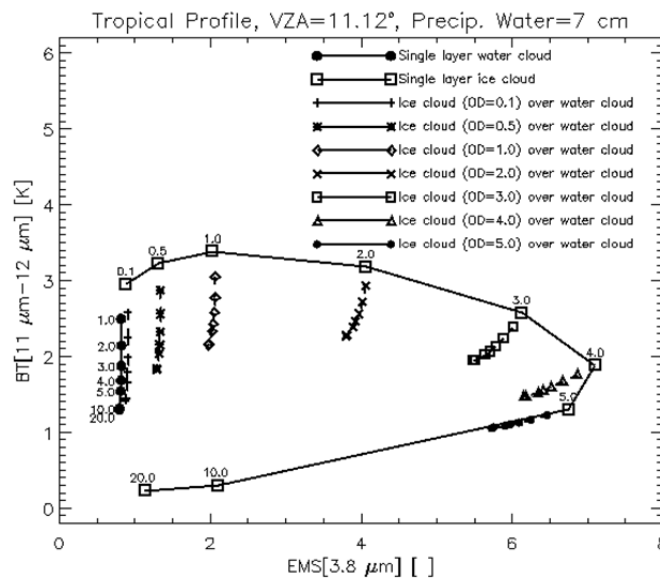


Figure 24. Results from RTM calculations support the relationship between a derived $3.75\text{-}\mu\text{m}$ emissivity and the $BT_{M15} - BT_{M16}$ feature.

Since RTM simulations show that cloud overlap signatures vary as a function of the atmospheric profile, a universal threshold approach would not be the most effective way to detect multi-layered cloud systems using this approach. Instead thresholds are used that represent, at least

broadly, the atmospheric profile encountered in global satellite observations. Thresholds are specified for tropical conditions (defined as 30°S to 30°N), middle-high latitude conditions over water, and middle-high latitude conditions over land. Thresholds are established so that any pixel that falls into a box defined by minimum and maximum values of the $BT_{M15} - BT_{M16}$ feature for the EMS[3.8] is considered cloud overlap, as long as the BT_{M15} is less than 290.0 K. (Note: Sub-pixel clouds or cloud edges can have a $BT_{M15} - BT_{M16}$ feature and a EMS[3.8] that falls within the overlap box. The restriction that BT_{M15} is less than 290.0 K is used to help minimize cloud edges from being falsely identified as cloud overlap.) The threshold values are shown in Table 21.

Table 21: The range in 11 μm minus 12 μm brightness temperature difference (SWBTD) and a derived emissivity at 3.75 μm (EMS[3.8]) that defines the spectral characteristics of cloud overlap.

Region	Min	Max	Min	Max
	EMS[3.8]	EMS[3.8]	SWBTD [K]	SWBTD [K]
30°S – 30°N	1.10	5.0	0.78	2.5
30°S – 90°S and 30°N – 90°N (water)	1.05	2.5	0.58	2.0
30°S – 90°S and 30°N – 90°N (land)	1.00	2.0	0.58	2.0

3.4.4.2.3 Additional Cloud Phase Logic

The cloud phase algorithm concludes with a series of tests to correct known deficiencies in the logic. These tests are called cloud phase reclassification tests in the next section. When specific conditions are present, the final cloud phase results can be changed. Changes in cloud phase occur if the following conditions are observed:

- Water clouds are changed to cirrus clouds if the tri-spectral test uniquely detects clouds in a pixel or if the M14-M15 BTD > cloud detection threshold and M9 > thin cirrus threshold.
- Mixed-phase clouds are changed to opaque ice clouds if the M14-M15 BTD > threshold and both the M15 BT < M15 opaque ice cloud threshold and M10/M5 < opaque ice cloud threshold.
- Mixed-phase clouds are changed to cirrus if M14-M15 BTD > cloud detection threshold and both M9 > cirrus threshold while M12 < cirrus threshold.
- Opaque Ice clouds are changed to mixed phase clouds if the M14-M15 BTD < cloud detection threshold and M10/M5 > opaque ice cloud threshold.

3.4.4.3 Implementation of the Cloud Phase Algorithm

Figure 25 shows the flow of this algorithm. Different spectral tests are performed to detect, first, cloud overlap and then non-opaque cirrus clouds. These tests and their individual thresholds are based on day versus night as well as surface type and are presented in Table 22 and Table 23. The band number prefix “R” represents reflectance, “BT” represents brightness temperature, and

“EMS”, the pseudo-emissivity. The pseudo-emissivity for the M12 band (EMS_{M12}) is used to detect cirrus clouds during the nighttime. This is defined as follows:

$$EMS_{M12} = \frac{L_T M12}{L_E M12},$$

where L_{TM12} is the M12 radiance calculated using the BT_{M12} and L_{EM12} is the M12 radiance calculated using BT_{M15} . Since M12 radiance during the daytime is made up of a solar and a thermal component, a pseudo M12 reflectance ($RM12$), useful for cirrus detection, is calculated as follows:

$$RM12 = \frac{\pi(L_T M12 - L_E M12)}{\left(SM12 * \frac{\mu_o}{r_o^2} - \pi * L_E M12 \right)},$$

where S_{M12} is the solar radiance for the M12 band (taken to be a constant equal to 10.725412 W/m²/μm), μ_o is the cosine of the solar zenith angle, and r_o is the Earth-to-Sun ratio (taken to be a constant of 1). The term “threshold” is stated when a variable threshold is implemented which is determined from various pre-defined functions. Daytime cloud overlap detection generally relies on the lower to modest R_{M10}/R_{M5} ratio values along with R_{M9} and $BT_{M15} - BT_{M16}$ cirrus levels. Cloud overlap detection during nighttime employs the M12 pseudo-emissivity as well as the brightness temperature difference of $BT_{M15} - BT_{M16}$.

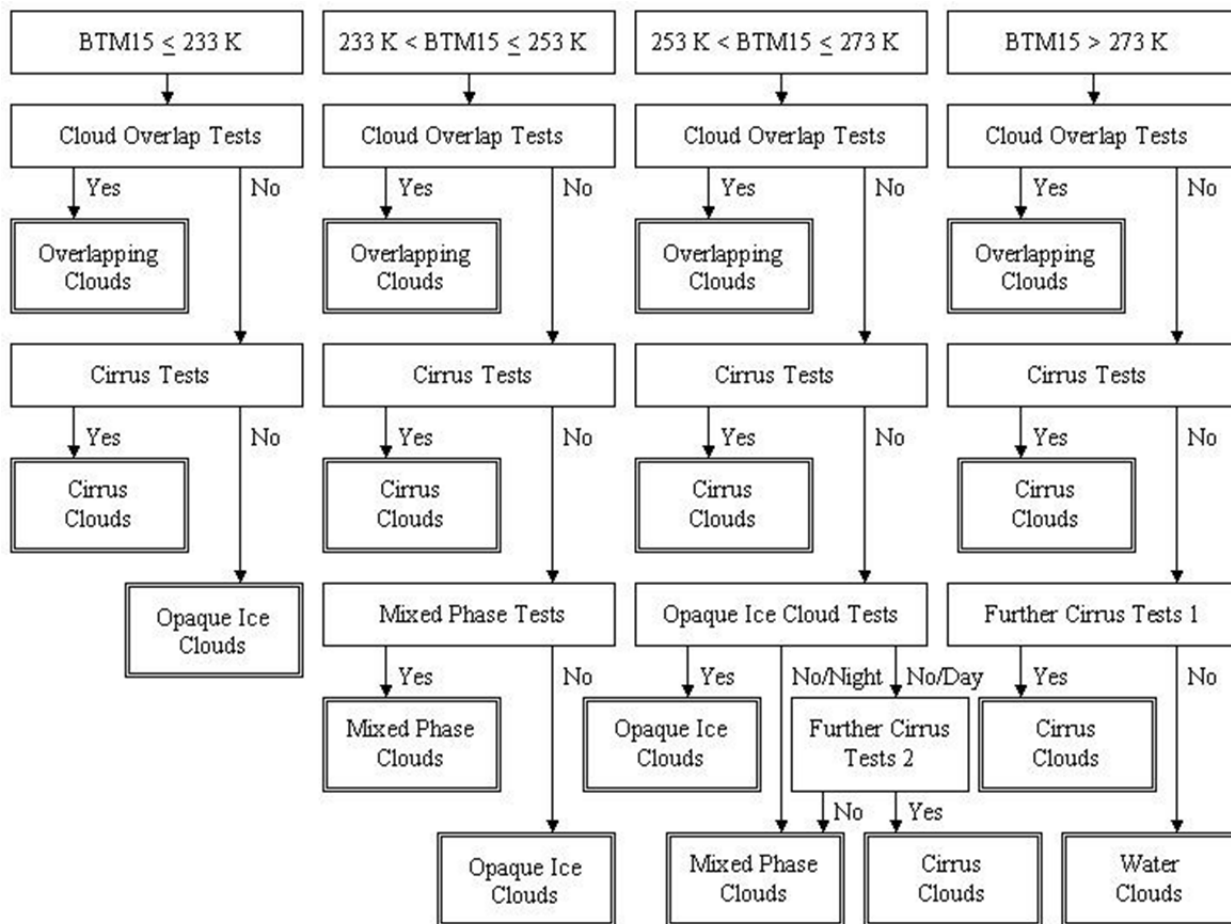


Figure 25. Flow diagram of the cloud phase algorithm.

Table 22. Cloud overlap criteria for cloud phase identification.

Condition	Logic
<p>Day Conditions Water background</p>	<p>Latitude between 50° N – 50° S and $0.025 < R_{M9} < 0.40$ (moist atmosphere) Or Latitude poleward of 50° and $0.10 < R_{M9} < 0.40$ TEST 1 – NIR Test: $RM10 >$ threshold function (cloud overlap possible.) Note: Threshold is a function of the M9 reflectances and scattering geometry AND $RM10/RM5 < 1.0$ (eliminates cirrus over bright backgrounds) AND $BTM15 < 280$ K (eliminates water clouds in dry atmospheres) IF ($RM9 < 0.08$), then application of test 2 is required to confirm overlap clouds: TEST 2 – SWBTD Test: $M15 - M16 >$ threshold function (Note: Threshold is a function of the M5 reflectances and scattering geometry) AND ($RM5 > 0.35$) (eliminates thin cirrus over desert backgrounds) AND $BTM15 < 270$ K (eliminates pixels partially filled by water clouds that may also have M5 reflectance values > 0.35) $RM10 > (0.10 (-50 < lat < 50) OR 0.30 (elsewhere))$</p>

Condition	Logic
Day/Land or Snow	<p>(0.027 (-40 < lat < 40) OR 0.10 (elsewhere)) < RM9 < 0.40 AND</p> <p>RM10 > threshold AND</p> <p>RM10/RM5 < 1.0 AND</p> <p>BTM15 < 280 K AND</p> <p>IF ((RM9 < 0.12) AND</p> <p>(RM5 > 0.35)) AND</p> <p>BTM15 - BTM16 > threshold</p> <p>OR</p> <p>RM5 > 0.35 AND</p> <p>BTM15 - BTM16 > threshold AND</p> <p>BTM15 > 270 K AND</p> <p>RM10 > (0.10 (-50 < lat < 50) OR 0.30 (elsewhere))</p>
Day/Desert	<p>M1 > 0.50 AND</p> <p>RM5 > 0.35 AND</p> <p>BTM15 - BTM16 > threshold AND</p> <p>BTM15 > 270 K AND</p> <p>RM10 > (0.10 (-50 < lat < 50) OR 0.30 (elsewhere))</p>
Night/Water (-30 < lat < 30)	<p>0.58 K < BTM15 - BTM16 < 2.5 K AND</p> <p>1.0 < EMSM12 < 2.6</p>
Night/Water (lat < -30) or (lat > 30)	<p>0.58 K < BTM15 - BTM16 < 2.0 K AND</p> <p>1.0 < EMSM12 < 2.0</p>
Night/Land or Snow	<p>0.58 K < BTM15 - BTM16 < 2.0 K AND</p> <p>1.0 < EMSM12 < 2.0</p>

Condition	Logic
Night/desert	Same as land except test not applied over the Sahara desert $12 < \text{lat} < 32, -20 < \text{lon} < 45$

If no cloud overlap is found, cirrus detection is performed. Daytime cirrus tests include the $BT_{M15}-BT_{M16}$ and the R_{M9} combined with the R_{M12} . Another cirrus test is the R_{M9}/R_{M5} reflectance ratio (Roskovensky and Liou, 2003) which is employed as long as the overall visible reflectance (R_{M5}) is not too bright. $BT_{M15}-BT_{M16}$ and EMS_{M12} are used to classify cirrus at night.

Table 23. Cirrus cloud tests for cloud phase identification.

Condition	Logic
Day	$BT_{M15} - BT_{M16} > \text{threshold}$ AND $R_{M9} > 0.025$ AND $R_{M12} < 0.15$ OR $R_{M5} < 0.4$ AND $R_{M9}/R_{M5} > 0.17$
Day/Sahara Desert $12 < \text{lat} < 32, -20 < \text{lon} < 45$	$BT_{M15} - BT_{M16} > \text{threshold}$ AND $R_{M9} > 0.025$ AND $R_{M12} < 0.40$ OR $R_{M5} < 0.4$ AND $R_{M9}/R_{M5} > 0.17$
Night	$BT_{M15} - BT_{M16} > \text{threshold}$ AND $EMS_{M12} > 1.2$ OR $EMS_{M12} > 1.4$

If no overlap or no cirrus is detected, pixels with the lowest BT_{M15} (less than 233-K) are classified as opaque ice cloud. Other pixels are subjected to a final round of restoration tests described in Table 24. The $BT_{M14}-BT_{M15}$ value, good for detecting ice phase clouds, is the primary test. During the day, this test is combined with other reflectance tests. Pixels in the second BT_{M15} group undergo tests to detect mixed phase clouds. Lower $BT_{M14}-BT_{M15}$ and higher R_{M10}/R_{M5} values indicate the presence of liquid water. If liquid water is not sensed, the pixels are classified as opaque ice cloud. The opposite is done for the third BT_{M15} group. These are tested for opaque ice cloud characteristics. The added requirement that BT_{M15} fall below 263-K is made. Pixels in this grouping that do not pass the nighttime opaque ice tests are labeled as mixed phase clouds. Daytime pixels that fail the opaque ice tests are then tested for non-opaque cirrus using the tests under the *Further Cirrus Tests 2* label. To be classified as cirrus, they must have high $BT_{M14}-BT_{M15}$ values and must also possess moderate R_{M9} with lower R_{M12} , indicative of thin cirrus, otherwise they are characterized as mixed phase clouds. Pixels in the group with the highest BT_{M15} values are also tested similarly for thin cirrus cloud under the label *Further Cirrus*

Tests 1. If cirrus is not detected, these pixels are classified as water clouds since they possess high IR window brightness temperatures.

Table 24. Cloud phase reclassification tests.

Mixed Phase Tests	
Day	Night
BTM14 - BTM15 < threshold + 0.2 K OR RM10/RM5 > 1.0	BTM14 - BTM15 < threshold + 0.2 K
Opaque Ice Cloud Tests	
Day	Night
BTM14 - BTM15 \geq threshold AND BTM15 < 263 K AND RM10/RM5 < 1.0	BTM14 - BTM15 \geq threshold AND BTM15 < 263 K
Further Cirrus Tests 1	
Day	Night
BTM14 - BTM15 \geq 0.5 K AND RM9 > 0.01 AND (RM12 < 0.40 (Sahara => 12 < lat < 32, -20 < lon < 45) OR RM12 < 0.15 (elsewhere))	BTM14 - BTM15 \geq 0.5 K
Further Cirrus Tests 2	
Day	Night
BTM14 - BTM15 \geq threshold AND RM9 > 0.025 AND (RM12 < 0.40 (Sahara => 12 < lat < 32, -20 < lon < 45) OR RM12 < 0.15 (elsewhere))	N/A

The VIIRS cloud phase algorithm was applied to MODIS data collected 1 August 2001 and a cloud phase result was obtained (see Figure 26).

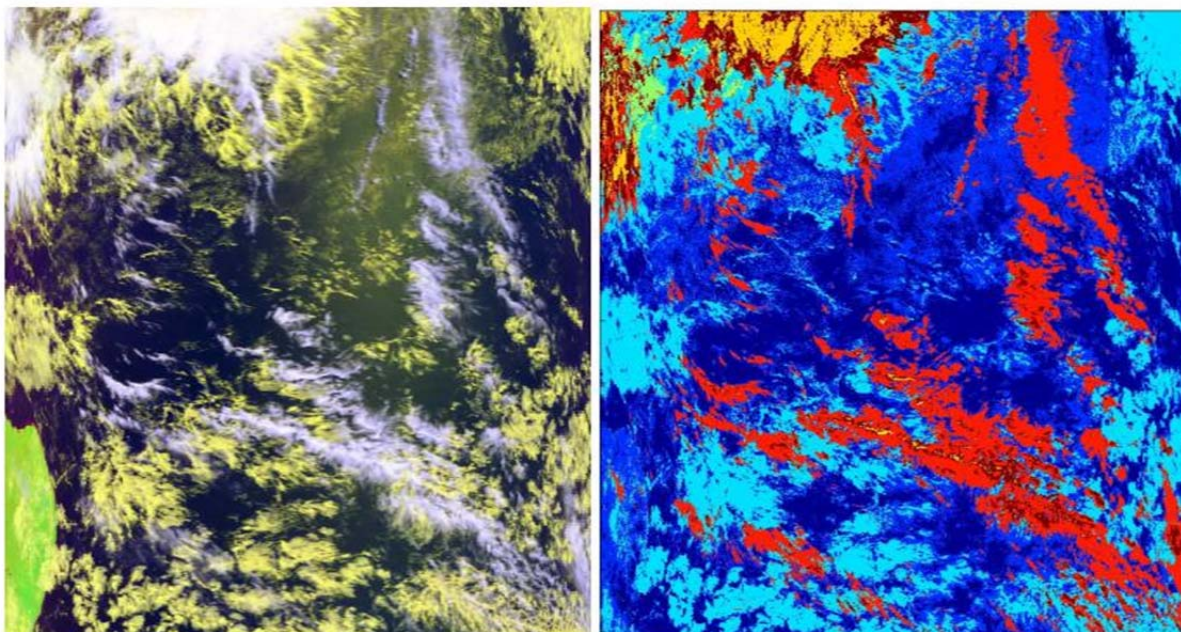


Figure 26. MODIS data collected 1 August 2001 from 1220 to 1225 UTC and the corresponding VCM Phase.

Left: RGB composite; Cold clouds are white, warm clouds are yellow, land is green and ocean is black. Right: Clear pixels are dark blue, partly cloudy are in blue, water clouds are in light blue, opaque ice clouds are in yellow, cirrus clouds are in red, and overlapping clouds are in dark red.

3.4.5 Differentiating Between Heavy Aerosols and Clouds

Pixels that contain aerosols with an optical depth that exceeds ~ 0.6 have typically been classified as confidently cloudy by VIIRS heritage cloud algorithms (Brennan et al., 2005) and similar performance has been noted with the most recent version of the VCM. Thus, the architecture of these cloud mask algorithms included logic that attempts to identify heavy aerosols after the cloud detection tests have been executed. If aerosol is indicated, a flag is set in the VCM output. Thus, users of the VCM, e.g. the aerosol module in particular, must read both the VCM cloud confidence and the heavy aerosol flag to understand whether a pixel is believed to contain clouds or aerosols.

Testing with the VCM and products from heritage algorithms demonstrated that these restoration tests were inadequate, i.e. they failed to provide the most rudimentary knowledge on the true presence of heavy aerosols (Hutchison et al., 2008). As a result, new procedures have been developed at NGST and are reported here. First, a brief discussion is provided of the heritage VCM procedures used for heavy aerosol detection. They included the following:

- Test 1 was based upon the fact that clouds have a high reflectance in both M5 and M11 bands but the reflectance of aerosols is negligible in the M11 band (Kaufman et al., 2002). The test was applied in to all pixels regardless of background and cloud confidence. While this test did in fact, detect these heavy aerosols, it also detected most clouds as will be shown in Figure 27 below (Hutchison et al., 2008). The inability of this test, as implemented, to distinguish between pixels that contained clouds from heavy

aerosols rendered a heavy aerosol flag based upon this test as useless to other VIIRS algorithms. Major modifications to this test have been, made as discussed below.

- Test 2 applied the reverse absorption technique (Prata, 1989a, 1989b; Prata et al., 2001) to test for volcanic ash. This test classified a pixel as heavy aerosol under the conditions that the brightness temperature difference between the 11.0- μm and 12.0- μm bands was less than a threshold, i.e. $T_{11.0} - T_{12.0} < -1.0$. The reverse absorption test was applied to all pixels except those classified as confidently cloudy. This test has been shown to be inadequate, typically failing to detect volcanic ash when present and misclassifying desert surfaces as volcanic ash.
- Test 3 set a flag to heavy aerosol if fire was detected in the pixel by examining the brightness temperature (BT) in the 3.7- μm (M12) band along with the (3.7- μm -10.76- μm) brightness temperature difference, i.e. $BT_{M12} - BT_{M15}$, over all land pixels. If the test was satisfied, the heavy aerosol flag was set in the VCM; however, this test has been replaced in the VCM, which now uses the VIIRS fire mask, generated by the Active Fire Algorithm (Hogan et al., 2003), as ancillary data. The heavy aerosol flag is no longer set for pixels classified as fire; since these are excluded from analysis in the aerosol module and the VCM typically fails to classify as cloudy pixels that contain fire in the Active Fire mask.

Results from the tests used to detect heavy aerosol in the original VCM and MODIS Cloud Mask (MCM) Collection 5 algorithms are shown in Figure 27, which contains in Panel (a) a false-color composite of a MODIS granule MODA2001.213.1210. This composite was constructed by placing the 0.65- μm , 1.6- μm , and 0.412- μm MODIS bands into the RGB of a CRT display. (These bands correspond closely to the VIIRS M5, M10, and M1 channels respectively.) The area shown in the scene covers the Eastern Atlantic Ocean centered on a region near the Canary Islands. An extensive area of sun-glint is evident in the right half of the image. Optically thick ice clouds appear purple in the color composite due to their low reflectance in the 1.6- μm band while water clouds are mostly white since their reflectivity is similar in all three bands. Regions with high aerosol concentrations have a greenish hue over the ocean, especially near Mauritania where the signature is similar to the desert surface, due to the relatively large reflectance in the 1.6- μm band. However, the aerosol feature takes on a purplish hue over the ocean regions near Morocco and the Iberian Peninsula, where the aerosol concentration decreases and the reflectance in the 1.6- μm band becomes smaller relative to that of the shorter wavelength bands. A manually-generated cloud mask for this scene is shown in Panel (b).

Cloud confidences from the VCM and MCM algorithms are shown in Panels (c) and (d) respectively. Maroon represents confidently cloudy, gold is probably cloudy, light-blue is probably clear and dark blue is confidently clear. It is evident from these analyses that both algorithms classify the airborne dust over the cloud-free ocean as confidently cloudy and a summary of the cloud detection PCT for each cloud mask is shown in Table 1 (Hutchison et al., 2008). The statistics show that using the 0.412- μm band with the VCM algorithm over desert surfaces, as discussed by Hutchison and Jackson (2003), helps reduce by about 50% the number of false alarms compared to the MCM. The PCT for the VCM and MCM binary cloud masks are 84.9% and 79.4% respectively. The large errors in these cloud masks, i.e. 15.1% and 20.6% respectively, result mainly from the misclassification of heavy aerosols as clouds. Panels (e) and

(f) of Figure 27 show the results for the VIIRS and MODIS heavy aerosol flags respectively. Comparisons between Panels (c) and (e) or Panels (d) and (f) reveal the inadequacy of the heavy aerosol tests in the VCM and MCM Collection 5 algorithms. Cirrus clouds are identified as heavy aerosols in the right side of the VCM analysis and in the upper-left corner. The optically thin dust, extending toward the Iberian Peninsula is classified as heavy aerosol in the VCM analysis; however, the very thick dust off the coast of Africa is not. Finally, numerous pixels toward the center of the VCM analysis are erroneously identified as heavy aerosols. The MODIS heavy aerosol flag identifies none of the heavy aerosol present in the scene.

Therefore a new set of procedures was developed at NGST to identify heavy aerosols in pixels classified as confidently cloudy by the VCM. The approach exploits the differences in spectral and textural signatures between clouds and heavy aerosols to identify “candidate” pixels that might contain heavy aerosols, including dust, smoke, volcanic ash, and industrial pollution. The term candidate is used to emphasize that these highly accurate, new spectral tests, developed to detect heavy aerosols over ocean surfaces using the 0.412- μm band, also detect some cloud edges. Therefore, these heavy aerosol candidates are analyzed using spatial tests to differentiate between heavy aerosols, which normally have more homogeneous signatures, compared to water cloud. Over land, variations in the cloud-free reflectance of different surfaces limit the value of these spectral tests; therefore, all water clouds are considered “candidate” heavy aerosols and are examined with the spatial tests. In addition, new procedures are used to detect volcanic ash.

3.4.5.1 Heavy Aerosols over Ocean Surfaces

Different spectral tests are used to identify candidates believed to contain dust and smoke over ocean surfaces. The M1/M5 Reflectance ratio and M1 reflectance tests are used to detect dust since heavy dust has its minimum reflectance in the M1 VIIRS band while both ice and water clouds are highly reflective in both bands. The thresholds established for these tests are based upon the principles of radiative transfer. Under cloudy conditions, the ratio between VIIRS M1 and M5 bands is nearly unity for ice clouds. For water clouds, this ratio is roughly proportional to the ratio of extinction coefficients in the M1 and M5 bands, i.e. $2.1042 / 2.1431$ or 0.98 for droplets with a particle radius of 6- μm . However, in cloud-free regions, the ratio of the extinction coefficients is inversely proportional to the 4th power of the wavelength ratio, i.e. $[(0.65/0.412)**4]$ or ~ 6.3 . Since airborne dust and blowing sand often occur at altitudes relatively near the Earth’s surface, it is expected that a significant number of air molecules are present above these non-cloud obscurations at higher levels in the atmosphere. Therefore, the threshold is set to 2.0. As a result, the threshold for the M1 reflectance test is set relatively low, i.e. to 0.3, in an attempt to avoid identifying pixels as heavy aerosols when they contain sub-pixel clouds. These procedures are more fully described by Hutchison et al., (2008).

To detect smoke over ocean surface, the VCM now employs the M11/M1 reflectance ratio test, since this ratio is nearly one for water clouds but very low in pixels containing smoke, e.g. ~ 0.1 . However, this test can also detect ice clouds since reflection for ice is smaller in the larger wavelength and reflectance in the M1 band is strongly affected by Rayleigh scattering. Thus, the test is only applied to pixels classified as water clouds in the VCM cloud phase analyses and the threshold for this test varies with scan angle to compensate for Rayleigh scattering.

Again, since the $2.1\text{-}\mu\text{m}/0.412\text{-}\mu\text{m}$ reflectance ratio test was found to accurately detect smoke but also misclassified water cloud edges, pixels detected by this spectral test are also considered heavy aerosol “candidates” and further tested with the spatial tests along with candidates identified by the dust test discussed in the previous section.

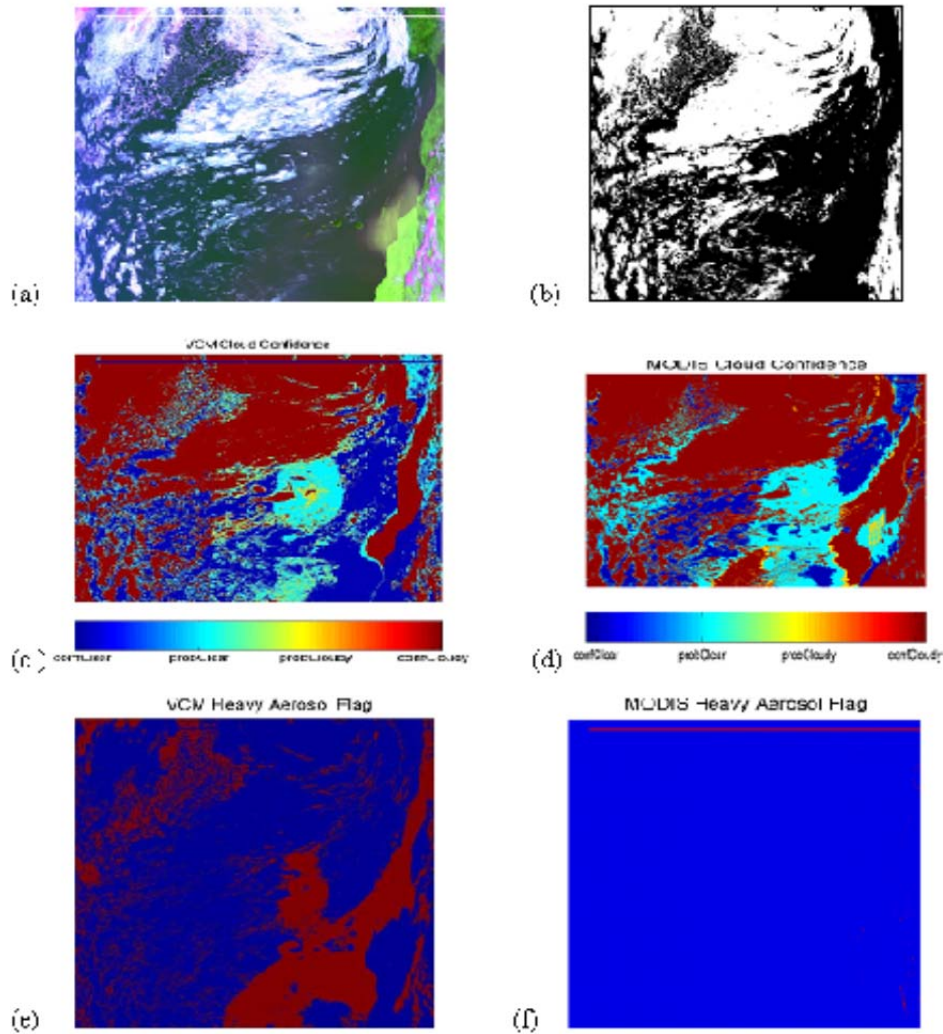


Figure 27. Analyses of MODIS granule MODA2001.213.1210 based upon the VCM using Tests 1-3 and the MODIS Collection 5 cloud mask algorithms. Panel (a) shows an RGB ($0.65\text{-}\mu\text{m}$, $1.6\text{-}\mu\text{m}$, $0.412\text{-}\mu\text{m}$) color composite of MODIS imagery and Panel (b) has a manually-generated cloud mask. VCM and MODIS results for cloud confidence are in Panels (c) and (d) respectively along with heavy aerosol flags in Panels (e) and (f).

These new spectral tests for heavy aerosols cannot be applied in sun glint regions, so initially there was no attempt made to differentiate between clouds and heavy aerosols in regions where the VCM sun glint flag was set. However, subsequent analyses were made using the criteria that all water clouds in sun glint areas be considered candidates. The results of further testing confirmed that heavy aerosols can be distinguished from clouds in sun glint regions using the condition that only water clouds be made heavy aerosol candidates and further tested with the spatial test (Hutchison et al., in press). However, sun glint may degrade the quality of the results

obtained with the VCM cloud confidence and cloud phase algorithms, which could then further impact the ability to differentiate between clouds and heavy aerosols using this logic.

The spatial test uses the 0.65- μm imagery (375-m) resolution band with a hopping window composed of all heavy aerosol candidates to distinguish between water clouds and aerosols, as shown in the next section. Noted that if the results of the 2.1- μm /0.412- μm reflectance ratio are less than 0.1 (nadir), the pixel is classified as heavy aerosol and this classification is not changed by results from the spatial test.

MODIS granule MODA2003.299.1840 is used to demonstrate the value of the 2.1- μm /0.412- μm reflectance ratio for discriminating between clouds and smoke. A color composite of these data, shown in Panel (a) of Figure 28, was constructed to enhance the signature of smoke along with different cloud types by putting the MODIS 0.412- μm , 1.6- μm , and the 11.0- μm – 12.0- μm brightness temperature difference ($T_{11} - T_{12}$) data into the RGB of a CRT display. (These bands equate to the reflectances in the VIIRS M1 and M10 channels and the brightness temperature differences between the M15-M16 channels respectively.) The data include much of coastal Southern California through the Baja Peninsula and the associated Eastern Pacific Ocean region. Smoke has a reddish hue as it streams off the Southern California coast in this composite since the main contribution comes from the 0.412- μm band. Water clouds are yellow due to their high reflectivity in both the 0.412- μm and 1.6- μm bands. Cirrus clouds range in color from blue (optically thin) to pink (optically thick) showing differences in the 1.6- μm reflectances and ($T_{11} - T_{12}$) thermal contrast. Middle-level water clouds (orange) are also present in the lower right corner of the image along with cirrus clouds.

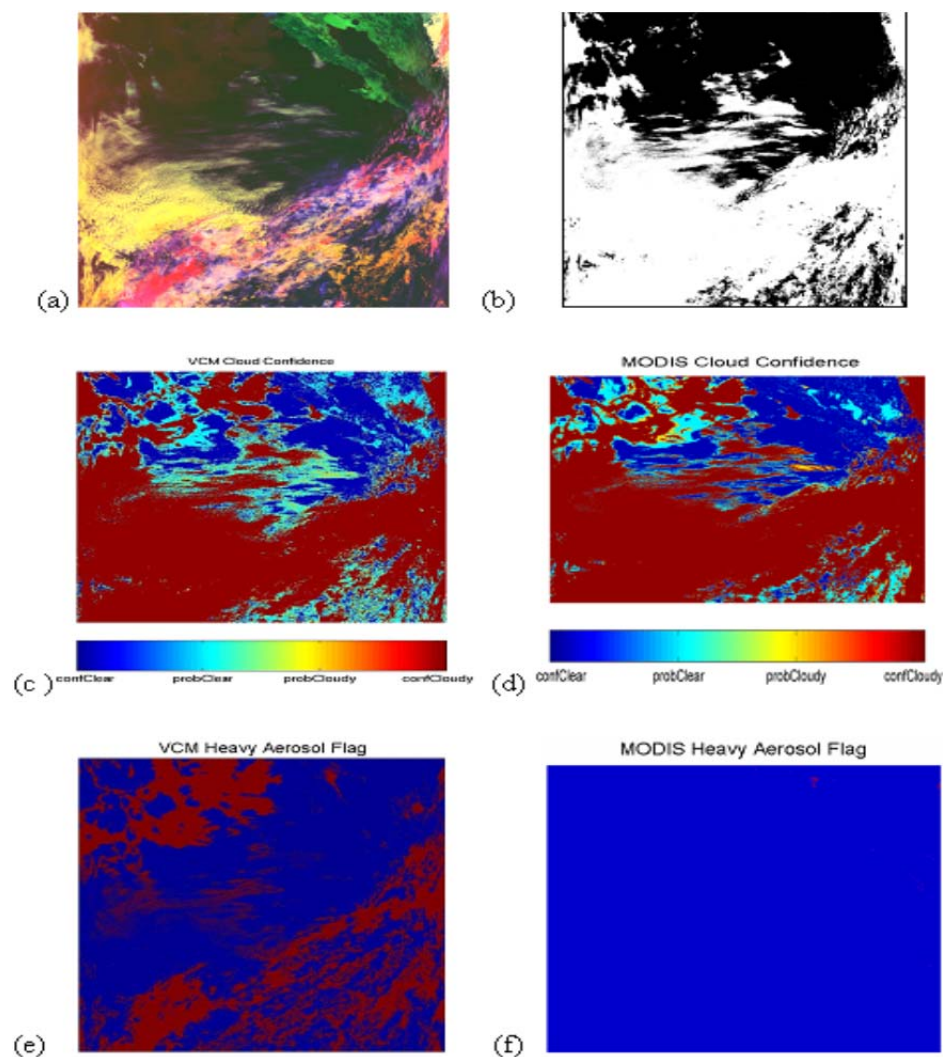


Figure 28. Analyses of MODIS granule MODA2003.299.1840 based upon the VCM using Tests 1-3 and MCM Collection 5 algorithms. Panel (a) shows an RGB [0.412- μm , 1.6- μm , (11- μm - 12- μm)] color composite of MODIS imagery and Panel (b) has a manually-generated cloud mask. VCM and MODIS results for cloud confidence are in Panels (c) and (d) respectively along with heavy aerosol flags in Panels (e) and (f).

A manually-generated cloud analysis is contained in Figure 28, Panel (b), where white again denotes clouds and black represents cloud-free pixels. In this manually-generated cloud analysis, water clouds that underlie the smoke have been classified as clouds and this was a conscious decision since ocean surface products, e.g. SST analyses, are generated when aerosols are present but not for pixels that contain clouds. Therefore, it is desirable that the cloud mask classify as confidently cloudy those pixels that contain both clouds and heavy aerosols to ensure minimal impact upon the SST product, which is one of the two highest priority NPOESS products generated from VIIRS data.

Cloud confidence analyses from the VCM and MCM algorithms are shown in Panels (c) and (d) of Figure 28 respectively. Hutchison et al., (2008) summarize the performance of both cloud masks against the manually-generated cloud analysis. Panels (c) and (d) show cloud confidences

that are very similar for both cloud masks, i.e. the PCT is 88.72% and 88.80% for the VCM and MCM respectively. However, results from the heavy aerosol flags, seen in panels (e) and (f), continue to show larger differences. The aerosol flag in the VCM includes many pixels that contain both ice clouds and water clouds along with the smoke. On the other hand, the MCM aerosol flag identifies very few pixels as heavy aerosol. The MCM Collection 5 algorithm does not classify as heavy aerosol any pixels that actually contain the heavy smoke.

Figure 29 demonstrates the impact of different cloud masks on the aerosol optical thickness (AOT) product. Panel (a) shows the retrieved VIIRS AOT product based solely upon the VCM cloud confidence, i.e. without aerosol restoral Tests 1-3 described in Section 2 above. These results show that AOT values can only be retrieved in the 0–0.6 τ range without the benefit of a heavy aerosol flag. Panel (b) shows a much improved AOT analysis with retrievals in the \sim 0-3 τ range. This analysis is the MODIS Collection 5 aerosol (MOD04) product, available through the EOS Data Gateway, which uses the cloud screening logic described by Martins et al. (2002). Note that pixels in the more dense smoke regions (highlighted area) are classified as cloudy with this algorithm so no retrievals were possible. Finally, Panel (c) shows the results extracted from the VIIRS aerosol module after the VCM cloud confidences have been combined with the new heavy aerosol tests. It is noteworthy that the cloud confidences of the heaviest smoke have been modified and retrievals are performed where AOT values than even exceed 3.0. Thus, these new procedures allow the aerosol product to be created across the full range of NPOESS operational requirements and well into the ranged needed for climate applications.

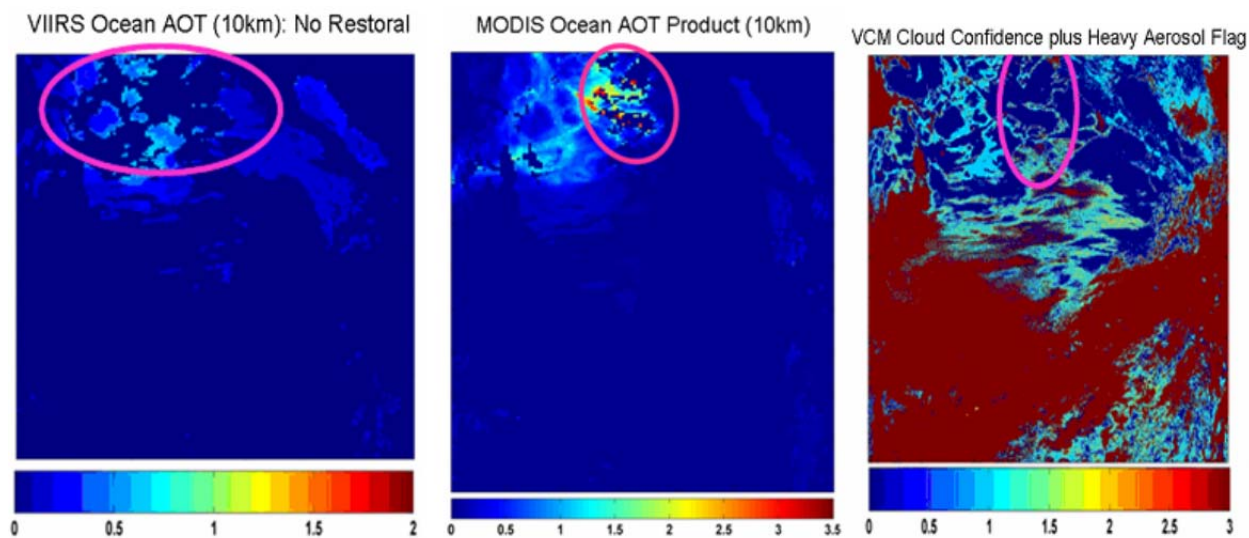


Figure 29. Panel (a) shows the VIIRS AOT retrievals without using the VCM heavy aerosol flags due to the large number of false alarms shown in Panel (e) of Figure 3 with Tests 1-3. Panel (b) shows the MODIS Collection 5 AOT results from the MOD04 product, and Panel (c) the cloud confidence in the VIIRS aerosol module after combining the cloud confidence and the heavy aerosol flag from the updated VCM procedures to identify heavy aerosols.

3.4.5.2 Heavy Aerosols over Land Surfaces

While spectral tests can be applied to identify heavy aerosol candidates over water backgrounds; variations in cloud-free surface reflectance negate using similar tests over land backgrounds, especially in the presence of more optically thin clouds. Therefore, all water clouds over land

surfaces are considered heavy aerosol candidates and are evaluated with the spatial tests alluded to in previous sections. In this section, the spatial test is described in detail and demonstrated through a complex scene, shown in Figure 30, which contains industrial pollution along with airborne dust in MODIS data collected over the Yellow Sea that includes much of mainland China, the Korean Peninsula, and parts of the Japanese Islands (Hutchison et al., 2008).

All candidates from spectral tests, discussed in Section 3.4.5.1, are integrated with all pixels over land that are classified by the VCM as confidently cloudy and containing water clouds. This group becomes the composite of heavy aerosol candidates. These candidates are then examined using a spatial test, based upon the 0.65- μm imagery resolution (375-m) data contained within a 2x2 array of moderate resolution pixels. Thus, the spatial test is applied to a nominal 1.5-km x 1.5-km analysis area. The standard deviation for all candidates with this 2x2 pixel array is calculated using a hopping window, as opposed to a sliding window, as follows:

- If only one candidate exists within the 2x2 array, it is assumed to be a cloud edge.
- Over ocean backgrounds, if at least two candidates exist in the 2x2 pixel array, the standard deviation is calculated using all imagery resolution pixels within these candidates. At least 8 but as many as 16 imagery resolution pixels are used in this calculation.
 - If the standard deviation $> 1\%$, all candidates are classified as water clouds. No heavy aerosol flag is set.
 - If the standard deviation is $\leq 1\%$, all moderate resolution pixels are defined to contain heavy aerosols.
- Over land backgrounds, if at least two candidates exist in the 2x2 pixel array and the TOC NDVI > 0.3 , the standard deviation is calculated.
 - If the standard deviation $> 2\%$, all candidates are classified as water clouds. No heavy aerosol flag is set.
 - If the standard deviation is $\leq 2\%$, all moderate resolution pixels are defined to contain heavy aerosols.

The thresholds used to define whether candidates contain cloud edges or heavy aerosols are larger than those used in the MODIS aerosol algorithm. The algorithm used to create the MOD04 product employs a threshold of 0.25% in a 3x3 array of MODIS 500-m pixels collected in the 0.55- μm band (Martins et al., 2002). The threshold used in the VIIRS cloud mask are quadrupled because the VCM provides a cloud mask that accurately defines cloudy pixels, including those with sub-pixel clouds (Hutchison et al., 2005), while the algorithm used to generate the MOD04 product must differentiate between clouds and cloud-free features including aerosols with this spatial test. There is no requirement for the VIIRS cloud mask to identify aerosol. The requirement is only for it not to classify as cloudy those pixels which contain heavy aerosols. Since candidates with water clouds have much large standard deviations across the 2x2 array, the heavy aerosol threshold can be larger and remain highly effective as shown in the following example.

Figure 30 shows in Panel (a) a true-color composite of NASA's Terra MODIS data center near the Yellow Sea at 0240 UTC on April 1, 2002. The granule identifier is MOD.2002.091.0240. An extensive area of industrial pollution is evident on the left portion of the image extending toward the lower left corner and also into the East China Sea. At the same time, airborne dust

extends across the northern part of the Yellow Sea into the Sea of Japan where it blankets lower-level clouds in the region.

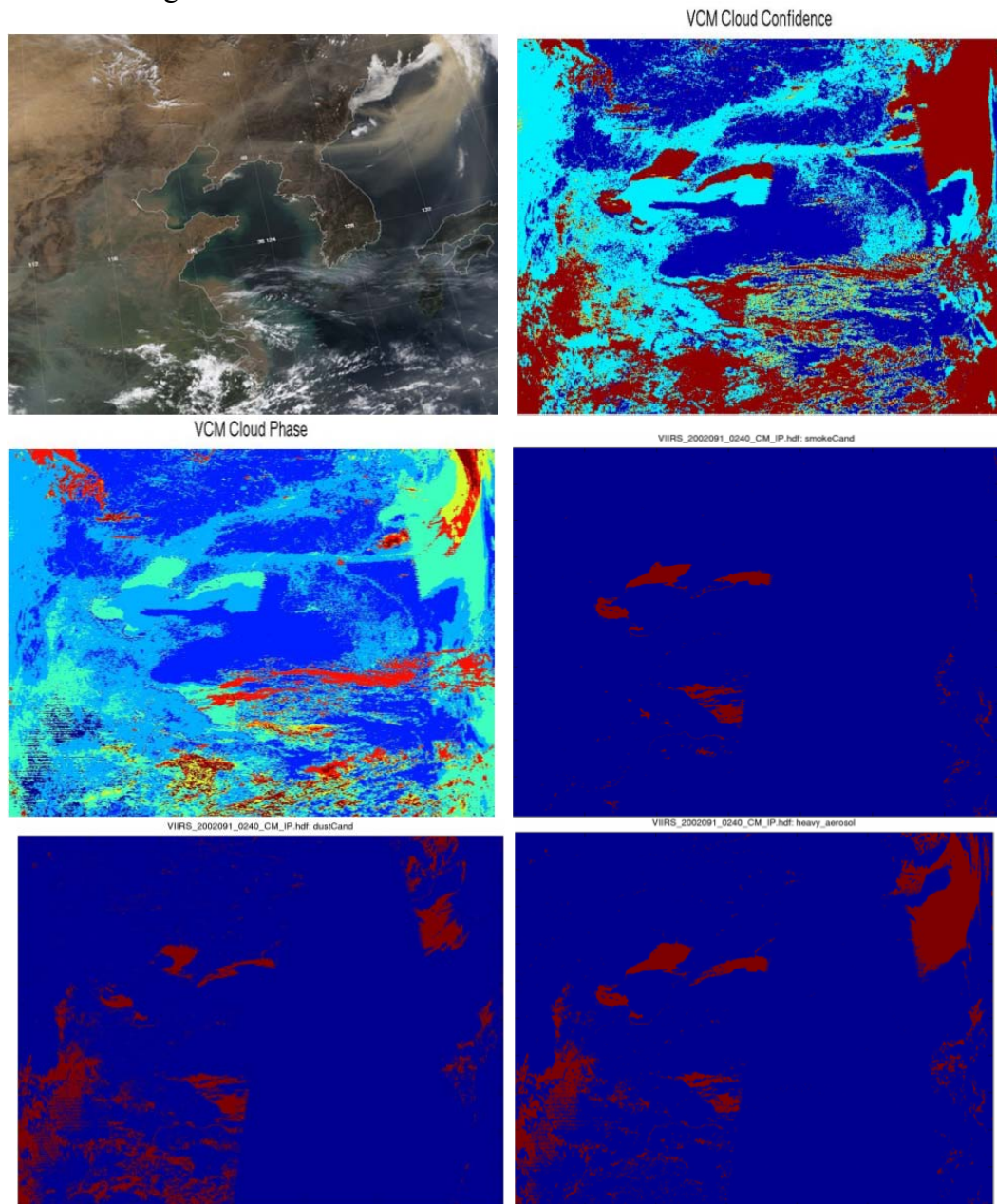


Figure 30. Analyses of heavy aerosols and clouds with the EVCN algorithms for MODIS granule MODA2002.091.0240. Panel (a) shows a true-color composite of MODIS imagery while Panel (b) has the automated cloud confidence and Panel (c) the cloud phase analyses. Candidate heavy aerosols detected by the smoke test are shown in Panel (d) along with dust candidates in Panel (e). The final heavy aerosol results are in Panel (f) after the spatial test has been applied to candidate heavy aerosols.

Panel (b) contains the results from the VIIRS cloud mask algorithm and shows the industrial pollution classified as confidently cloudy (dark red) over land and into the East China Sea, along with many regions of the heavy dust. (Dark blue means confidently clear while lighter blue is

probably clear. Yellow stands for probably cloudy.) The VIIRS cloud phase algorithm, shown in Panel (c) identifies these regions of heavy aerosols to be water cloud phase (light green). [Cirrus clouds are orange, red, or purple depending upon their classification as opaque, thin, or overlap (cirrus over lower-level water clouds in a single field-of-view) respectively.] Panel (d) contains results from the spectral test used to identify heavy aerosol candidates that contain smoke, and possibly water cloud edges, as discussed above. Panel (e) contains results from the spectral tests used to identify heavy aerosol candidates that contain dust, and possibly edges of water clouds. These candidates are combined and the standard deviation calculated, as discussed earlier in this section, to produce the final heavy aerosol analyses shown in Panel (f). Notice the reduction in heavy aerosols shown in the lower-left part of Panel (f), after the spatial test is applied, compared to the candidates detected by the dust test in Panel (e), which contained many water cloud edges. A comparison between Panel (a) and Panel (f) shows that almost all pixels identified as confidently cloudy but seen to contain heavy aerosols have been correctly identified by these new procedures and only a small region of water clouds has been misclassified, exactly in the lower-left corner.

The results shown in Figure 30 were based upon the initial version of these cloud-versus-heavy aerosol procedures that were not applied in regions of sun glint (Hutchison et al., 2008). However, subsequent analyses were conducted and it was determined that heavy aerosols can be distinguished from clouds in sun glint regions using the criteria that only water clouds be made heavy aerosol candidates for further testing with the spatial test (Hutchison et al., in press).

3.4.5.3 Volcanic Ash

Detection of aerosols composed of volcanic ash follows a modification of the approaches developed by Prata (1989a; 1989b) and Pavolonis et al. (2006). The VCM algorithm applies the “reverse absorption” method which is based upon the $T_{11} - T_{12}$ BTDF feature. The reverse absorption technique exploits the fact that $T_{11} - T_{12}$ is positive for cirrus clouds and cloud-free atmospheres (Inoue, 1985). The same is true for water clouds which typically have atmospheric water vapor between the cloud top and the satellite sensor. However, volcanic ash can produce a $T_{11} - T_{12}$ value that is generally negative; although this signature can be masked, e.g. by high levels of atmospheric water vapor (Prata et al., 2001). The VCM volcanic ash test is applied only to non-snow/ice covered ocean and land surfaces classified as confidently cloudy.

The threshold of the reverse absorption technique has also been modified. Originally, Prata recommended the threshold be set to 0.0 K but this leads to large numbers of false alarms, especially over desert regions and areas with persistent stratocumulus clouds as shown in Figure 31, which comes from Figure 10 of Pavolonis et al., (2006). The test was originally applied in the VCM with a threshold of -1.0K but this conservative threshold detected little volcanic ash. Subsequently, NGST modified the threshold to -0.25 K, to obtain useful information on dust, as shown in Figure 32, Figure 33, and Figure 34, where the threshold is changed incrementally from -0.5 K to 0.0 for the scene shown in Figure 27 above. This threshold also allows maximum detection of volcanic ash.

Over land surfaces, the VCM now employs Tier I and Tier II tests described by Pavolonis et al. (2006). These tests provide useful detection of volcanic ash with minimum false alarms. Results on the performance of these tests are available in Pavolonis et al (2006).

False Alarms – April 4, 2003 (Reverse Absorption)

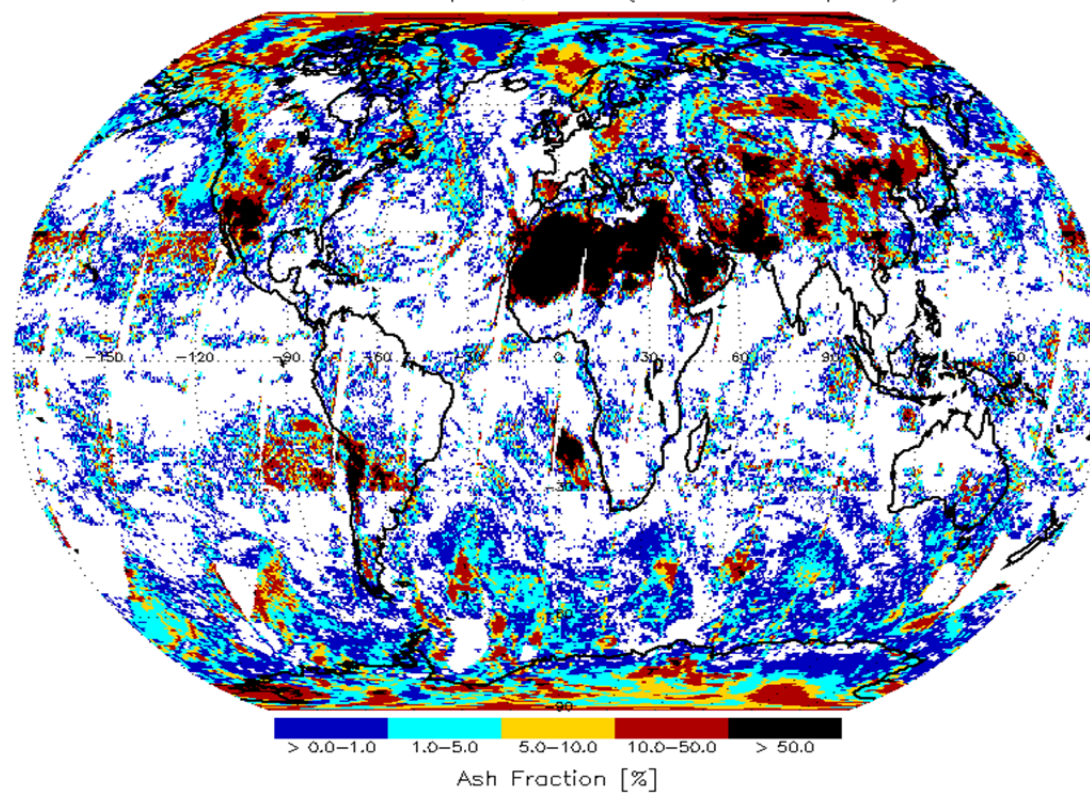


Figure 31. Frequency of occurrence for false alarms using reverse absorption technique with threshold of zero based upon global MODIS data (from Pavolonis et al., 2006)

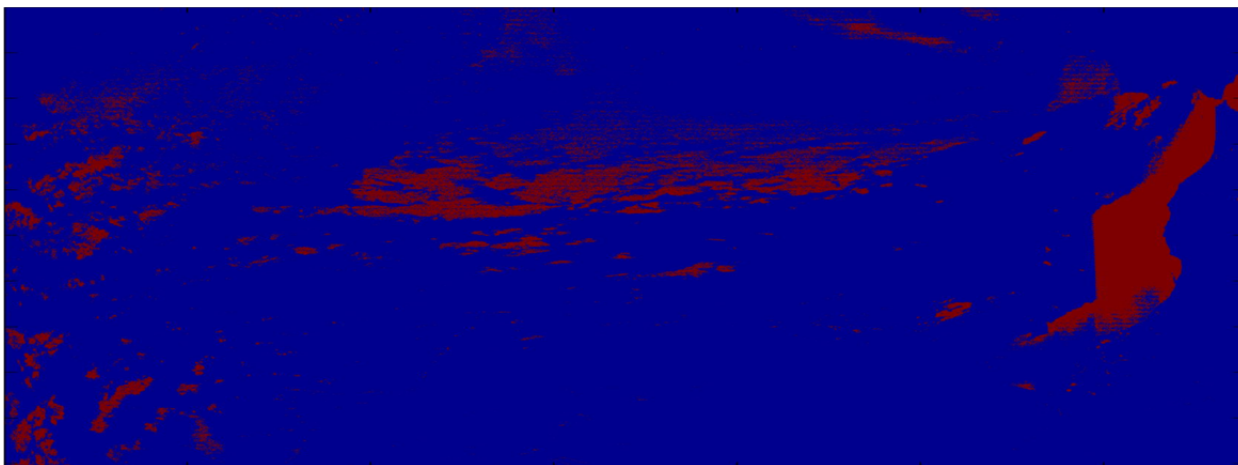


Figure 32. Misclassifications of clouds using reverse absorption test with Scene 1210 and thresholds = 0.0 K.



Figure 33. Misclassifications of clouds using reverse absorption test with Scene 1210 and thresholds = -0.25 K.



Figure 34. Misclassifications of clouds using reverse absorption test with Scene 1210 and thresholds = -0.5 K.

3.4.5.4 Impact of Cloud Phase Errors on Heavy Aerosols Identification

Initial testing of the procedures described above to identify heavy aerosols using numerous MODIS granules has demonstrated two potential difficulties. First, there exists a potential impact on these procedures due to errors in the cloud phase analysis. A second problem can arise from the implementation of the volcanic ash test as applied over ocean backgrounds.

Errors in cloud phase can seriously impact the heavy aerosol tests. As noted previously, the spectral test developed to detect heavy smoke is restricted from ice clouds since these particles have a depressed $2.1\text{-}\mu\text{m}/0.412\text{-}\mu\text{m}$ reflectance ratio that causes them to be classified as heavy aerosol candidates. In subsequent testing of many other MODIS granules, it was observed that the VCM cloud phase algorithm as described by Pavolonis and Heidinger (2004) too often classifies thin cirrus clouds as water clouds, especially in the humid tropics. When this occurs, the spatial test, based upon the $0.65\text{-}\mu\text{m}$ imagery band, is unable to distinguish these clouds from aerosols since the standard deviation may be very small ($\sim 0.1\%$), i.e. typically much smaller than the (1%) detection threshold used in these procedures as well as the 0.25% threshold used in the procedures used to create the NASA MOD04 product. It is possible that the smaller bandwidth of the VIIRS $1.38\text{-}\mu\text{m}$ channel (Hutchison and Cracknell, 2005) may reduce this problem; however more investigation will be needed to make that determination. The problem is demonstrated in the analyses that follow.

The top panels in Figure 35 are true-color images of the volcanic eruption in the Sangile Island north of Celebes in Indonesia on Julian day 268 of 2002. The left image is from Terra at 0155 UTC while the image on the right is from Aqua at 0450 UTC. Highlighted regions show the volcanic clouds associated with the eruption that started shortly before Terra overflew and increased throughout the afternoon. The VCM classified these volcanic clouds as “confidently cloudy” in both datasets and the results of the cloud phase are shown in the lower panels.

The heavy aerosol tests were applied as described above and the results for the smoke tests are shown in top panels of Figure 36. The spectral smoke tests, in both cases, detect a large number of heavy aerosol candidates towards both edges of scan. However, the spectral dust tests show many heavy aerosol candidates in the Terra scene, i.e. Panel (g), but few in the Aqua scene, i.e. Panel (h). Results from the dust tests are shown in the lower panels of this figure.

After combining the heavy aerosol candidates identified by the spectral tests, the spatial test is applied and the results are shown in the top panels of Figure 37. It is seen that large standard deviations are associated with the candidates identified by the dust test but very small values are associated with many candidates identified with the smoke test. Thus the smoke test erroneously identifies heavy aerosols.

False color composites for these images are shown in Figure 38. These images were generated specifically to emphasize thin cirrus clouds, which appear light blue in both images using 0.65- , 1.6- , and $3.7a\text{-}\mu\text{m}$ bands in the RGB with Terra data and 0.65- , 1.2- , and $3.7a\text{-}\mu\text{m}$ bands with Aqua since the $1.6\text{-}\mu\text{m}$ band is badly degraded in this sensor. Upon inspection it is seen that thin cirrus clouds in both images have been misclassified as water clouds by the cloud phase algorithm (see highlighted areas). These misclassifications result in ice clouds being detected as heavy aerosol candidates by the smoke tests. Since the standard deviations of ice clouds can be very small in the I1 band, their values are below the heavy aerosol threshold of 1% used in the

VCM. In fact, the values are even less than the 0.25% used in the MOD04 product. The conclusion is that failure of the VCM to accurately classify the phase of thin cirrus clouds can impact the heavy aerosol detection tests. Thus, these problems occur not because of poor tests for heavy aerosols but because of errors in the cloud phase logic in the VCM. The issue should be evaluated more closely in the future. For example, all thin cirrus should be better screened using the more narrow (10-nm) VIIRS 1.38- μm band than is possible with the more broad (30-nm) MODIS bandpass.

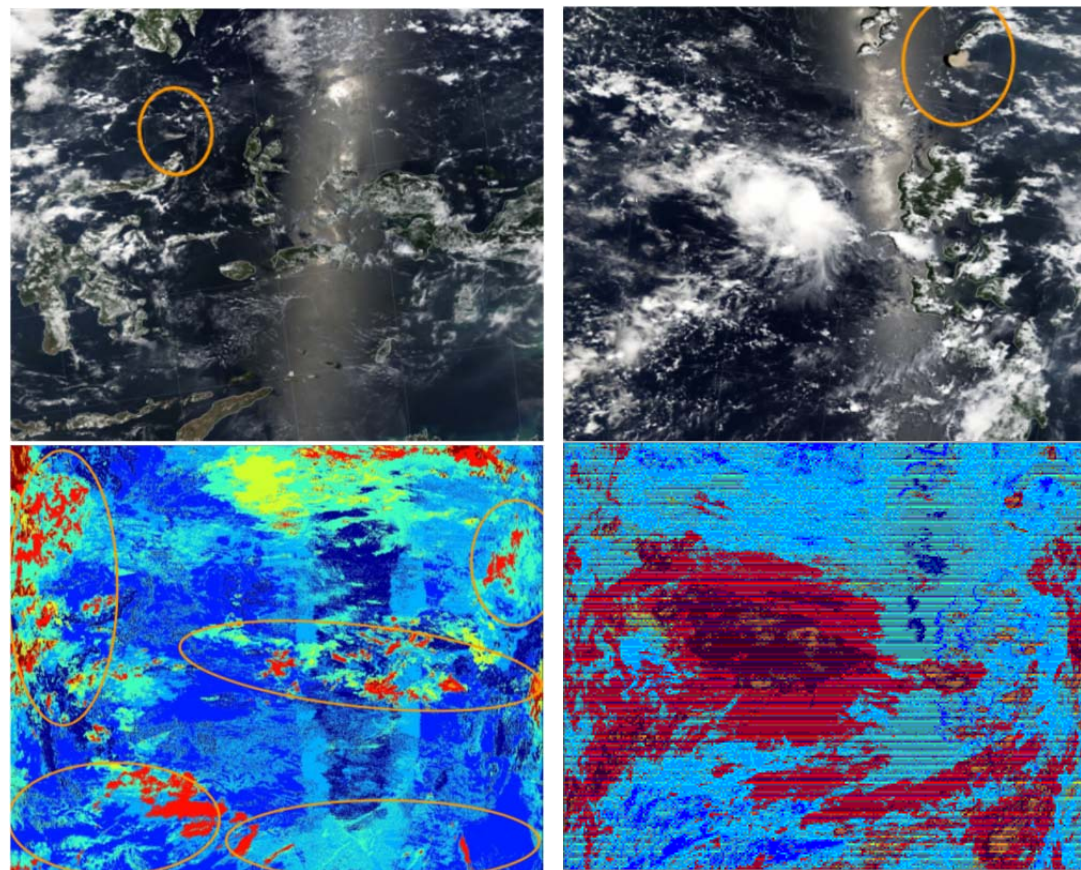


Figure 35. True color images of volcanic eruptions caught by MODIS Terra (0155 UTC in upper left) and Aqua (0450 UTC in upper right) granules on Julian day 268 in 2002. VCM cloud phases analyses shown in lower panels.

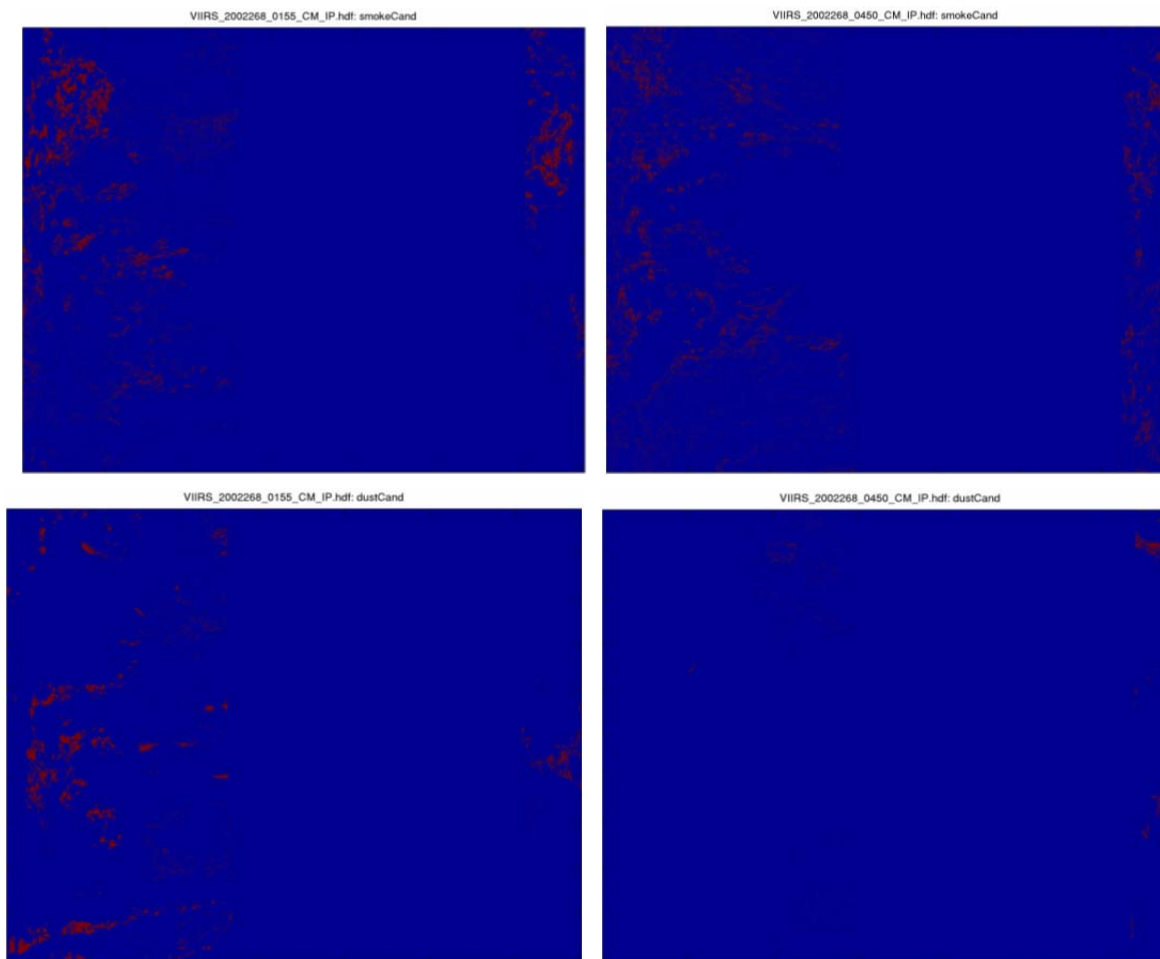


Figure 36. Heavy aerosol candidates identified by application of the new VCM smoke test (upper panels) and new dust test (lower panels) for granules shown in Figure 35.

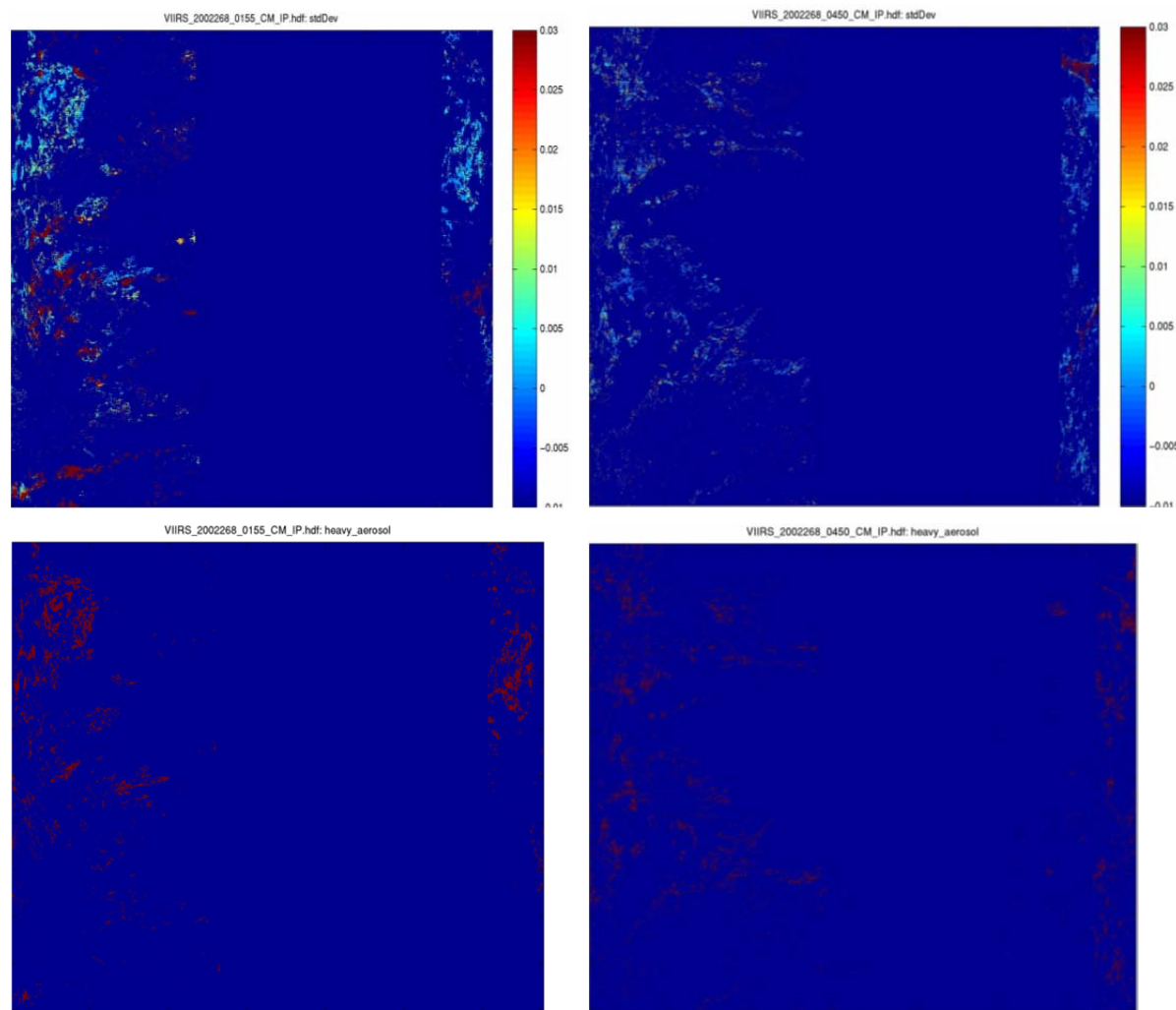


Figure 37. Results from the new VCM spatial test of heavy aerosol candidates (upper panels) and final heavy aerosol flags (lower panels) for granules shown in Figure 35.

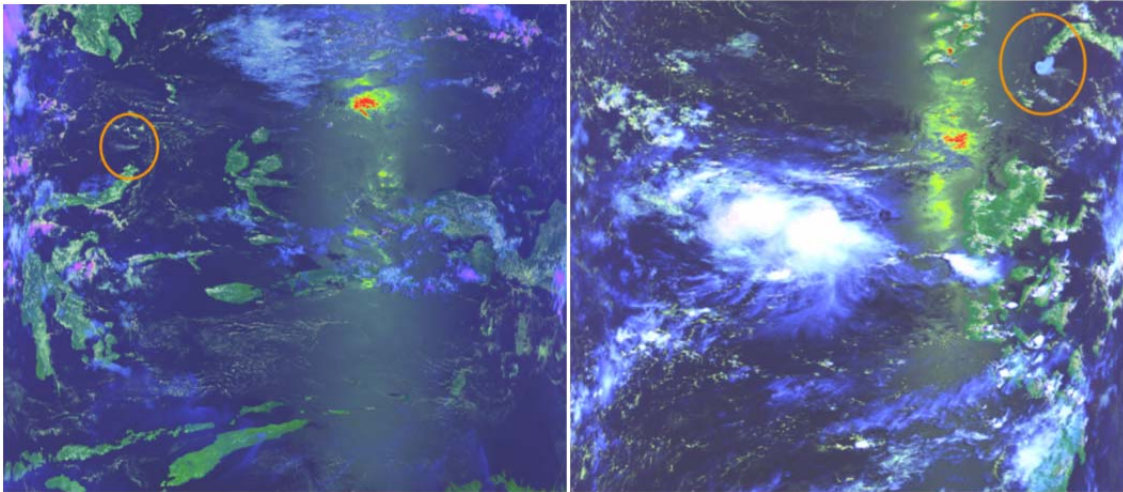


Figure 38. Color composites of MODIS data shown in Figure 35 reveal misclassifications by new heavy aerosol procedures occur because thin cirrus in misclassified as water clouds in the cloud phase analyses.

A second problem can arise from the implementation of the volcanic ash test as applied over ocean backgrounds. As noted above, this test can detect water cloud edges especially over regions that contain semi-permanent fields of stratocumulus which are associated with cold ocean currents. Use of the current $-0.25K$ shows very few of these clouds are detected as heavy aerosols. If further testing determines that these number are too large, results of the volcanic ash test might also be examined with the spatial test to remove unwanted cloud edges. However, this represents a minor modification to the procedures described herein.

3.4.6 The Geometric-Based Cloud Shadow Algorithm

Some VIIRS algorithms are as sensitive to the presence of shadows as they are to contamination by thin clouds; thus, the VIIRS Cloud Mask algorithm checks for the presence of shadows cast onto cloud-free surfaces. Shadows tests are executed under daytime conditions for confidently cloudy pixels casting shadows on to confidently clear and probably clear pixels based on sun to cloud geometry computations (Hutchison et al., 2009). Alternatively, probably cloudy pixels can also be included in the analysis, however, at the expense of an increase in latency. An optional run mode can be set to include probably cloudy pixels in the determination of cloud shadows; however, this option is not currently used due to the increase in latency.

The VCM cloud shadow algorithm follows an approach originally developed for the NASA MOD09 (land surface) products. However, initial testing with this algorithm showed that it increased VCM execution time by more than an order of magnitude. Therefore, it was re-engineered solely to reduce system latency. The logic is as follows: M15 derived brightness temperatures are used to assign cloud top temperatures of confidently cloudy pixels. Clear-sky, mean NCEP surface air temperatures are computed for sub-regions defined by a hopping $m \times m$ pixel window, which has historically been set to a 20×20 window but can be tuned. A mask indicating whether at least one confidently clear pixel exists in each sub-region is also determined. Water cloud top and base heights are then computed using a standard atmospheric

lapse rate and the difference between the mean, clear sky NCEP surface air temperature and the cloud top temperature. While this approach follows the MOD09 implementation, one major change is that the VCM cloud phase information is also used to set cloud base and cloud top heights for thick ice, cirrus and mixed phased clouds to predetermined ice cloud limits. Testing suggests this approach provides improved performance in cloud shadows cast by the VCM over those from the MOD09 algorithm. The VCM thin cirrus flag is used to set cloud base and heights to predetermined limits for thin cirrus clouds. The minimum and maximum cloud height levels are constrained by tunable parameters in two ways in order to further reduce algorithm latency. This is a second major difference between the VCM implementation and that of the MOD09 algorithm. First, computed cloud top heights are constrained not to exceed a mean tropopause height limit that is internally computed as function of latitude (linear interpolation between tunable equatorial and polar tropopause height limits). Furthermore, cloud top and base heights are limited by tunable overall cloud base and cloud top height limits. The algorithm will iterate over the cloud boundary to compute a line-of-sight cloud shadow geometry at each height interval, using at most four iterations. The MOD09 approach allows 32 iterations per pixel. Shadow target latitude/longitude coordinates are converted to granule row and column coordinates. The shadow flag is set for confidently clear and probably clear pixels within an adjustable-sized "local shadow cast neighborhood" window, currently set to a 3x3 pixel group, centered about the computed shadow target location. This local window has the effect of spreading the shadow beyond that of just the computed shadow target location pixel. The extent of a computed shadow is determined by the computed cloud top height, cloud base height and the local neighborhood window size. Algorithm latency is controlled by tunable parameter settings that constrain the cloud base and top heights and the height iteration step size for line of sight geometry computations. The algorithm logic is summarized and described in further detail below:

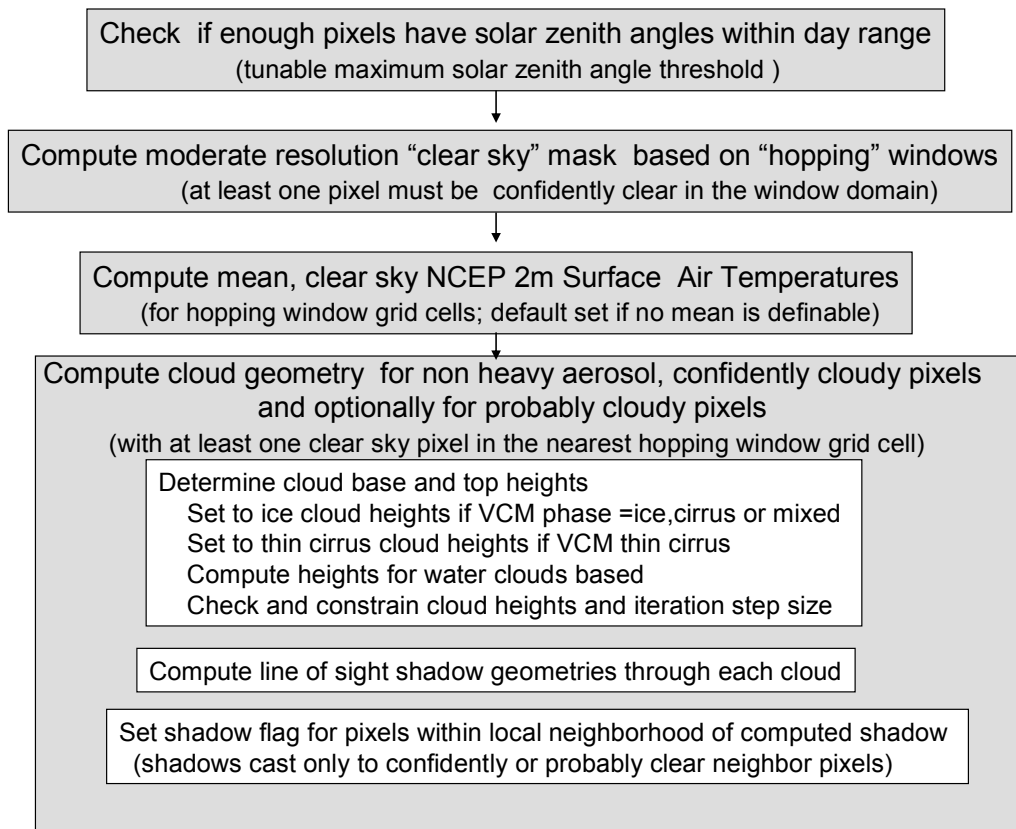


Figure 39. Cloud Shadow Algorithm Logic.

Cloud top and cloud base heights are set to predetermined "ice cloud" tunable limits for confidently cloudy moderate resolution pixels with the VCM cloud phase flags indicating presence of an opaque ice cloud, cirrus, or mixed phase cloud.

$$Z_{upper} = Z_{upper_ice_cloud}$$

$$Z_{lower} = Z_{lower_ice_cloud}$$

Cloud top and cloud base heights are set to predetermined "thin cirrus cloud" tunable limits for confidently cloudy moderate resolution pixels with the VCM thin cirrus flag indicating presence of thin cirrus.

$$Z_{upper} = Z_{upper_thin_cirrus}$$

$$Z_{lower} = Z_{lower_thin_cirrus}$$

Cloud top and cloud base heights for water clouds are computed based on the temperature difference between the mean, clear sky NCEP 2 meter surface air temperature (for the nearest

neighbor hopping window) and the cloud top temperature of a cloudy pixel divided by an assumed lapse rate.

$$\Delta T = \bar{T}_{NCEP} - T_{M15}$$

$$ZZ = \Delta T / \Gamma$$

$$Z_{upper} = (1 + \alpha)ZZ + \beta$$

$$Z_{lower} = (1 - \alpha)ZZ - \beta$$

where:

\bar{T}_{NCEP} is the mean, clear sky NCEP 2m surface air temperature in a hopping window

T_{M15} is the VIIRS M15 brightness temperature for a confidently cloudy pixel

Γ is a tunable mean atmospheric lapse rate in deg K/km

α is a cloud height or thickness fractional factor

β is a height offset factor (km)

Computed and predetermined cloud top heights are constrained such that they may not exceed a latitude dependent mean tropopause height limit (km):

$$Z_{Tropo_limit} = (Z_{Tropo_polar} - Z_{Tropo_equator}) \cdot \frac{\text{abs}(\text{latitude})}{90.0} + Z_{Tropo_equator}$$

Cloud top and base heights may be limited further by overall tunable maximum and minimum height limits. Line of sight sun-cloud-earth line shadow geometries are computed by iterating over the cloud thickness using a tunable default height step size. If the number of iterations for a given cloud thickness and step size exceeds a tunable maximum number of iterations limit then the step size is computed such that the number of height iterations does not exceed the limit.

For each height iteration (from cloud base to cloud top), a line-of-sight geometry is computed using the zenith and azimuth angles for the sun and sensor view and the iterated cloud height. Shadow distances are computed as projected displacements from the cloud pixel along the zonal and meridional axis. A spherical mean earth radius (6378.137 km) is used to compute the displacement in terms of latitude and longitude displacements from the pixel location and the shadow target coordinate is determined. The target coordinates are converted to granule row and column coordinates:

- Determine displacements along latitude (meridional) and longitude (zonal) directions for the satellite-cloud-earth line of sight and computed view direction target:

$$dx_{view} = \cos(2\pi - \phi) * \tan \theta * z$$

$$dy_{view} = \sin(2\pi - \phi) * \tan \theta * z$$

$$dlon_{view} = dy_{view} / (R_{earth} * \cos(\text{latitude}))$$

$$dlat_{view} = dx_{view} / (R_{earth})$$

$$lat_{view} = lat + dlat_{view}$$

$$lon_{view} = lon - dlon_{view}$$

- Determine displacements along latitude (meridional) and longitude (zonal) directions for the sun-cloud-earth line of sight and computed shadow direction target:

$$dx_{shadow} = \cos(2\pi - \phi_0) * \tan \theta_0 * z \quad dy_{shadow} = \sin(2\pi - \phi_0) * \tan \theta_0 * z$$

$$dlon_{shadow} = dy_{shadow} / (R_{earth} * \cos(lat_{view})) \quad dlat_{shadow} = dx_{shadow} / (R_{earth})$$

$$lat_{shadow} = lat_{view} - dlat_{shadow}$$

$$lon_{shadow} = lon_{view} + dlon_{shadow}$$

The algorithm computes the row and column granule coordinates for the shadow target and examines pixels within a local "shadow-cast" neighborhood window, currently set as a 3x3 pixel group, centered on the shadow target and sets the shadow flag for those pixels in the window that are confidently or probably clear.

3.5 PRACTICAL CONSIDERATIONS

3.5.1 Numerical Computation Considerations

Bispectral cloud detection tests are computationally inexpensive. All possible cloud detection tests will be applied for a given pixel. Tests for aerosols, fire and shadows are made only after all cloud tests have been applied and pixels identified as cloud-contaminated have been flagged. Cloud phase is also determined after cloud confidence has been defined by the cloud tests. Geometric cloud shadow computation scheme has been adapted to reduce latency via a set of tunable constraint parameters.

3.5.2 Programming and Procedural Considerations

The procedural outline has been described in Section 3.1 Processing Outline.

3.5.3 Configuration of Retrievals

To avoid "hard-wiring" specific values into the operational software, a retrieval configuration file can be adopted. The file would store numerical values of adjustable parameters used within the retrievals, such as the thresholds establishing whether a successful retrieval occurs.

3.5.4 Quality Assessment and Diagnostics

The first 4 bits of the VIIRS Cloud Mask output make up a quality indicator. Additional information regarding the VIIRS Cloud Mask quality can be found in Section 3.3.1 Cloud Mask Quality.

3.5.5 Exception Handling

VIIRS will produce a cloud mask under all circumstances. If a band is bad, the tests that use that band will not be used. This will be reflected in the Cloud Mask Quality flag.

3.6 ALGORITHM VALIDATION

The VIIRS cloud mask algorithm will continue to be verified pre-launch using proxy data from MODIS and global synthetic data generated by NGST. Results with these datasets have shown remarkable similarities when using synthetic TOA radiance convolved with MODIS bandpasses, as described in the NPOESS document D44199, VCM Chain Testing Report. The results with these synthetic data also demonstrate their value for pre-launch algorithm tuning of cloud detection thresholds, as shown in this report, e.g. Figure 10. This pre-launch algorithm tuning is essential since most VCM threshold have been tuned for MODIS bandpass and results of chain testing showed several cloud detection tests must be re-tuned before the NPP launch. A demonstration of the procedures used for pre-launch tuning is planned using MODIS global synthetic TOA SDR data. The approach is to adjust some VCM cloud detection thresholds, as noted above and throughout this document. Then, the revised thresholds will be used to re-analyze the 40+ scenes of MODIS proxy data available during chain testing. This allows the impact of the updated thresholds to be examined in detail, especially with the first 14 scenes for which a manually-generated cloud mask exists. Once the process of updating VCM thresholds has been demonstrated with MODIS data, the VIIRS global synthetic SDRs will be used for pre-launch tuning of the cloud detection thresholds to analyze VIIRS NPP data.

Results shown in this document also demonstrate the need to focus more attention upon pre-launch testing of the VCM cloud phase algorithm, especially those shown in Section 3.4.5 Differentiating Between Heavy Aerosols and Clouds. The topic of cloud phase validation has not been addressed in the literature for any heritage algorithm. Additionally, an accurate cloud phase analysis is a key component in the generation of all downstream VIIRS cloud EDRs. The performance of the VCM cloud phase algorithm can be assessed as described above using global synthetic data. However, in this case, there may be less value in first using the MODIS global synthetic SDR data, since there is no truth data for MODIS proxy datasets. The exercise might be useful for the VIIRS Imagery/VCM Cal/Val team as a pre-launch activity.

Post-launch verification as described in documents under development by the VIIRS cal/val cloud team. These activities are expected to involve qualitative comparisons between VCM products and VIIRS imagery; quantitative intercomparisons between VIIRS and heritage cloud mask products with Cloudsat and Calipso data, if available; qualitative evaluations of derived products, such as sea surface temperature and cloud EDRs, that utilize the VCM; and quantitative comparisons between the VCM products and manually-generated cloud masks which will serve as truth for the VCM.

4.0 ASSUMPTIONS AND LIMITATIONS

4.1 ASSUMPTIONS

- (1) Cloud Mask receives an image of VIIRS calibrated and geolocated TOA reflectances and TOA BT's in the bands used by the Cloud Mask, including any Imagery bands used.
- (2) Quality flags accompany all input data into the Cloud Mask Module indicating if the data is good or questionable.
- (3) Cloud Mask receives Geolocated Latitudes and Longitudes of all pixels in the region being masked.
- (4) Cloud Mask receives an entire image of the region being masked.
- (5) Cloud Mask needs a Land/Water reference database.
- (6) Cloud Mask needs an Ecosystem reference database.
- (7) Values received from granulated Land/Water Mask – Quarterly Surface Type have no “unknown” types.
- (8) Cloud Mask receives Sun Sensor geometry.
- (9) Cloud Mask receives a database of recent snow/ice knowledge.
- (10) Cloud Mask receives a database of recent TOC NDVI values with no values filled.
- (11) Cloud Mask receives Total Precipitable Water data.
- (12) Cloud Mask received Near Surface Temperature data.
- (13) Cloud Mask receives sea surface wind speed data in region being masked for determination of Sun Glint Flag.
- (14) Output mask results will have 4 levels of confidence: Confident Cloudy, Probably Cloudy, Probably Clear, and Confident Clear.

4.2 LIMITATIONS

- (1) Can only produce Cloud Mask if BT and Reflectance data are available.
- (2) Can only produce Cloud Mask if underlying surface type is known.
- (3) The full logic update for execution of the VCM in the NPOESS 1730 L orbit awaits the collection of on-orbit data with the launch of the NPP system. The accuracy of radiative transfer models decreases at high solar zenith angles and MODIS currently provides data with substantially different spatial resolution from VIIRS. Thus, datasets needed to evaluate cloud tests in the terminator regions will be collected after NPP cal/val and used to update the VCM performance in the 1730 L orbit.

5.0 REFERENCES

- Ackerman, S. A., W. L. Smith and H. E. Revercomb (1990). The 27-28 October 1986 FIRE IFO Cirrus Case Study: Spectral Properties of Cirrus Clouds in the 8-12 Micron Window. *Mon. Wea. Rev.*, **118**, 2377-2388.
- Ackerman, S. A., K. Strabala, P. Menzel, R. Frey, C. Moeller, L. Gumley, B. Baum, C. Schaaf, and G. Riggs (1997). Discriminating Clear-Sky From Cloud With MODIS Algorithm Theoretical Basis Document (MOD35). Version 3.2
- Baum, B.A., P.F. Soulen, K.I. Strabala, M.D. King, S.A. Ackerman, W.P. Menzel, and P. Yang, (2000). Remote Sensing of Cloud Properties Using MODIS Airborne Simulator Imagery During SUCCESS. II. Cloud Thermodynamic Phase, *J. Geophys. Res.*, **9**, 11781-11792, 2000.
- Ben-Dor, E., (1994). A precaution regarding cirrus cloud detection from airborne imaging spectrometer data using the 1.38 μm water vapor band. *Remote Sens. Environ.*, **50**, 346-350.
- Berk, A., L. S. Bernstein, and D. C. Roberson (1989). MODTRAN: A Moderate Resolution Model for LOWTRAN7, Report AFGL-TR-89-0122 (Air Force Geophysics Laboratory), Hanscom, AFB, MA 01731.
- Brennan, J. I., Kaufman, Y. J., Koren, H., and R. R. Li, 2005: Aerosol-cloud interaction – Misclassification of MODIS clouds in heavy aerosol, *IEEE Transactions on Geoscience and Remote Sensing*, **43**, 911-915.
- Gao, B. C., A. F. H. Goetz, and W. J. Wiscombe (1993). Cirrus Cloud Detection From Airborne Spectrometer Data Using the 1.38 Micron Water Vapor Band, *Geophys. Res. Lett.*, **20**, 301-304.
- Gustafson, G. B., R. G. Isaacs, R. P. d'Entremont, J. M. Sparrow, T. M. Hamill, C. Grasotti, D. W. Johnson, C. P. Sarkisian, D. C. Peduzzi, B. T. Pearson, V. D. Jakabhazy, J. S. Belfiore, and A. S. Lisa (1994). Support of Environmental Requirements for Cloud Analysis and Archive (SERCAA): algorithm descriptions, PL-TR-94-2114, Phillips Laboratory, AFMC, Hanscom AFB, MA.
- Hall, D. K., G. A. Riggs, and V. V. Solomonson (1995). Development of Methods for Mapping Global Snow Cover Using Moderate Resolution Imaging Spectroradiometer Data. *Remote Sens. Env.*, **54**, 127-140.
- Hall, D. K., G. A. Riggs, and V. V. Solomonson (1996). Algorithm Theoretical Basis Document (ATBD) for the MODIS Snow-, Lake Ice-, and Sea Ice-Mapping Algorithms. Version 3.0.
- Hogan, D., Zaccheo, S. Kennelly, T., and Y. He, 2003: Visible Infrared Imaging Radiometer Suite (VIIRS) Active Fire Mask, Active Fires: Fire Mask, Algorithm Theoretical Basis Document, Version 1.0.2, Atmospheric Environmental Research, Inc., 55 pp.
- Hutchison, K. D., and K. Hardy (1995). Threshold functions for automated cloud analyses of global meteorological satellite imagery. *International Journal of Remote Sensing*, **16**, 3665-3680.

- Hutchison, K.D., Mahoney, R., Vermote, E. F., Kopp, T. J., Jackson, J. M., Sei, A., and B. D. Iisager, 2009: "A Geometry-based Approach for Identifying Cloud Shadows in the VIIRS Cloud Mask Algorithm for NPOESS," *J. Atmospheric and Oceanic Technnology*, **26**, 1388–1397.
- Hutchison, K. D., Hauss, B., Iisager, B., Agravante, H., Mahoney, R., Sei, A. and J. M. Jackson, 2010, Differentiating between clouds and heavy aerosols in sunglint regions, *Journal of Atmospheric and Oceanic Technology*, **27**, 1085-1094.
- Hutchison, K.D., Iisager, B. D., Kopp., T. J., and J. M. Jackson, (2008): "Discriminating between Clouds and Aerosols in the VIIRS Cloud Mask Algorithms," *J. Atmospheric & Oceanic Technology*, **25**, 501-518.
- Hutchison, K. D., and A. P. Cracknell, 2005: "*VIIRS - A New Operational Cloud Imager*," CRC Press, 218 pp.
- Hutchison, K.D., Roskovensky, J.K., Jackson, J.M., Heidinger, A.K., Kopp, T. J., Pavolonis, M.J, and R. Frey, 2005: "Automated Cloud Detection and Typing of Data Collected by the Visible Infrared Imager Radiometer Suite (VIIRS)," *International Journal of Remote Sensing*, **20**, 4681 - 4706.
- Hutchison, K. D. and J. M. Jackson, 2003: "Cloud detection over desert regions using the 412 nanometer MODIS channel, *Geophysical Research Letters*, **30**, 2187-2191
- Hutchison, K. D., and N. Choe (1996). Application of 1.38 μm imagery for thin cirrus detection in daytime imagery collected over land surfaces. *International Journal of Remote Sensing*, **17**, 3325-3342.
- Hutchison, K. D., K. Hardy, and B. C. Gao (1995). Improved detection of optically-thin cirrus clouds in nighttime multispectral meteorological satellite imagery using total integrated water vapor information. *Journal of Applied Meteorology*, **34**, 1161-1168.
- Inoue, T., (1987). A cloud type classification with NOAA 7 split window measurements. *J. Geophys. Res.*, **92**, 3991-4000.
- Inoue, T., 1985: On the Temperature and effective emissivity determination of semi-transparent cirrus clouds by bi-spectral measurements in the 10- μm window region, *J. Meteorological Society of Japan*, **63**, 88-99.
- Kaufman, Y. A., Tanre', D., and O. Boucher, 2002: A satellite view of aerosols in the climate system, *Nature*, **419**, 215-223.
- King, M. D., W. P. Menzel, P. S. Grant, J. S. Myers, G. T. Arnold, S. E. Platnick, L. E. Gumley, S. C. Tsay, C. C. Moeller, M. Fitzgerald, K. S. Brown, and F. G. Osterwisch (1996). Airborne Scanning Spectrometer for Remote Sensing of Cloud, Aerosol, Water Vapor, and Surface Properties. *J. Atmos. Oceanic Technol.*, **13**, 777-794.
- Kriebel, K. T., and R. W. Saunders (1988). An Improved Method for Detecting Clear Sky and Cloudy Radiances from AVHRR Data. *Int. J. Remote Sens.*, **9**, 123-150.
- Kriebel, K. T., Gesell, G., Kaestner, M. and H. Mannstein, 2003: The cloud analysis tool APOLLO: Improvements and validations, *Journal of Remote Sensing*, **24**, 2389-2408.

- Martins, J.V., D. Tanré, L.A. Remer, Y.J. Kaufman, Mattoo, S., and R. Levy, 2002: MODIS Cloud screening for remote sensing of aerosol over oceans using spatial variability. *Geophys. Res. Lett.*, **29**, 10.1029/2001GL013252.
- McClain, C. R. and Yeh, E.-N. (1994). Sun Glint Flag Sensitivity Study, SeaWiFS Technical Report Series, 13, Case Studies for SeaWiFS Calibration and Validation, Part 1, 46-47.
- Pavolonis, M. J. and A. K. Heidinger (2004). Daytime Cloud Overlap Detection from AVHRR and VIIRS. *J. Appl. Meteor.*, **43**, 762-778.
- Pavolonis, M. J., A. K. Heidinger and T. Uttal (2004). Daytime Global Cloud Typing from AVHRR and VIIRS: Algorithm Description, Validation, and Comparisons. Accepted by *J. of Appl. Meteor.*
- Pavolonis, M. J. and A. K. Heidinger (2005). *Advancements in identifying cirrus and multilayered cloud systems from operational satellite imagers at night*. Proc. SPIE, **5658**, 225 (2005); DOI:10.1117/12.57764
- Pavolonis, M. J.; Feltz, W. F.; Heidinger, A. K., and G. M. Gallina, 2006: A daytime complement to the reverse absorption technique for improved automated detection of volcanic ash, *J. Atmos. Ocea. Technol.*, **23**, 1422-1444.
- Pinty, B. and Verstraete, M. (1992). GEMI: a non-linear index to monitor global vegetation from satellites, *Vegetatio* Vol 101, 15-20.
- Prata, A. J., 1989a: Observations of volcanic ash clouds in the 10-12-micron window using AVHRR/2 data, *International Journal of Remote Sensing*, **10**, 751-761.
- Prata, A. J., 1989b: Radiative transfer calculations for volcanic ash clouds, *Geophysical Research Letters*, **16**, 1293-1296.
- Prata, A. J., Bluth, G., Rose, B., Schneider, D., and A. Tupper, 2001: Failures in detecting volcanic ash from a satellite-based technique – Comments, *Remote Sensing of the Environment*, **78**, 341-346.
- Rogers, R. R., 1976: "*A Short Course in Cloud Physics*," Pergamon Press, 227 pp.
- Roskovensky, J. K. and K. N. Liou, (2003). Detection of thin cirrus from 1.38 μm /0.65 μm reflectance ratio combine with 8.6 – 11 μm brightness temperature difference. *Geophys. Res. Lett.*, **30**, doi:10.1029/2003GL018135.
- Saunders, R. W. and K. T. Kriebel, (1988). An improved method for detecting clear sky and cloudy radiances from AVHRR data, *International Journal of Remote Sensing*, **9**, 123-150.
- Stowe, L. L., P. Davis, and E. P. McClain (1995). Evaluating CLAVR (Clouds from AVHRR) Phase I Cloud Cover Experimental Product. *Adv. in Space Res.*, **16**, 21-24.
- Stowe, L. L., P. Davis, and E. P. McClain (1998). Scientific Basis and Initial Evaluation of the CLAVR-I Global Clear/Cloud Classification Algorithm for the Advanced Very High Resolution Radiometer, *J. Atmos. and Oceanic Technology*, submitted May 1st.
- Strabala, K. I., S. A. Ackerman, and W. P. Menzel (1994). Cloud Properties Inferred from 12 micron Data, *J. Appl. Meteor.*, **33**, 212-229.

- Valvocin, F. R. (1978). Spectral radiance of snow and clouds in the near infrared spectral region. *Tech Report No. 78-0289*, Air Force Geophysics Laboratory, Hanscom Air Force Base, MA.
- Wylie, D. P., and W. P. Menzel, 1999: Eight years of high cloud statistics using HIRS. *J. Climate*, **12**, 170–184.
- Yamanouchi, T., K. Suzuki, and S. Kawaguci, (1987). Detection of clouds in Antarctica from infrared multispectral data of AVHRR. *J. Meteor. Soc. Japan*, 65, 949-962.